Properties of spontaneous and evoked discharges in the human subiculum

Dr. Fabó Dániel

Semmelweis University, Doctoral School,
Clinical Neurosciences

Instructors: Prof. Dr. Halász, Péter DSc.
Dr. Ulbert, István Ph.D.

Opponents: Prof. Dr. Kamondi, Anita Ph.D.
Prof. Dr. Szente, Magdolna DSc.

Qualifying exam committee, chair: Prof. Dr. Szirmai Imre DSc.
Qualifying exam committee: Dr. Arányi Zsuzsanna Ph.D.
Dr. Kondákor István Ph.D.

Budapest
2008

Abbreviations

AMPA	alpha-Amino-3-hydroxy-5-Methyl-4-isoxasole Propionic Acid
AV	Antero-Ventral nucleus of thalamus
Br	Brodmann
BFNC	Benign Focal Neonatal Convulsions
CA 1,2,3	Cornu Ammonis region 1,2,3 of the hippocampus
CSD	Current Source Density
Ctx	Cortex
DC	Direct Current
DG	Dentate Gyrus
dME	deep laminar Multi-contact Electrode
EC	Entorhinal Cortex
ECoG	Electrocorticogram
EEG	Electroencephalogram
EP	Evoked Potential
(i) ERSP	(individual) Event Related Spectral Perturbation
FLAIR	Fluid Attenuation Inverse Recovery sequence
FFT	Fast Fourier Transform
FPG	Field Potential Gradient
FR	Fast Ripple
GABA	Gamma Amino Butyric Acid
GEFS +	Generalized Epilepsy Febrile Seizures plus
IIS	Interictal Spike
ILAE	International League Against Epilepsy
Hc	Hippocampus
HcF	Hippocampal Formation
HFO	High-Frequency Oscillation
(s/m) HS	(severe/mild) Hippocampal Sclerosis
HW	Half amplitude duration (Width)
KCC-2	Potassium-Chloride cotransporter - 2
LFP	Local Field Potential
ME	laminar Multi-contact Electrode
MRI	Magnetic Resonance Imaging
MUA	Multiple Unit Activity
MTA-KOKI	Institute of Experimental Medicine of Hungarian Academy of Sciences
MTA-PKI	Institute for Psychology of Hungarian Academy of Sciences
NMDA	N-methyl-D-aspartate
NKCC	Sodium-Potassium-Chloride cotransporter
OITI	National Institute for Neurosurgery
OPNI †	National Institute of Psychiatry and Neurology
OR	Operating Room
mTLE	mesial Temporal Lobe Epilepsy
nucl.	nucleus
PreS	Presubiculum
RMS	Root Mean Square
sATL	standard anterior temporal lobectomy
SC	Subicular Complex
Str.	stratum
Sub	Subiculum
SWS	Slow Wave Sleep
T1, T2, T3	Superior, medial, inferior temporal gyri

Table of content

Introduction

In recent decades in parallel with the exponential development of information technology, our knowledge on the anatomical and functional changes of the human brain in different pathological states reached a formerly inconceivable amount. The widespread use of high field — 1.5 Tesla or higher — magnetic resonance imaging (MRI) combined with functional MRI for clinical and scientific purposes resulted detailed structural and functional information even in diseases affecting hidden structures in the brain (Barsi et al., 2000; Janszky et al., 2004). Meantime the electroencephalography (EEG) techniques progressed also substantially under the age of digital EEG and the possibility of high frequency data sampling (Swartz, 1998; Vanhatalo et al., 2005). Despite these developments the extra-cranial EEG with scalp electrodes remained ineffective, or provided only smattering of signals in those cases where pathology lied deep in the brain. Another EEG approach, the intracranial EEG, developed parallel with scalp recordings mainly for those epilepsy patients that the scalp recordings did not provide enough data for localizing the seizure focus. Multiple electrode types, with different insertion methods made the deep, or even mesial temporal, structures accessible for the electro-physiologists working hand in hand with neurosurgeons (Bancaud et al., 1970; Penfield and Jasper, 1954; Van Roost et al., 1998; Wieser et al., 1985). These techniques were fine enough to sample deep brain activity but were too robust to record the electrical activity of local neural networks, or single neurons, which would require sub-millimetre or micrometer spatial resolution.

The circumstance that the patient's skull becomes opened for electrophysiological recordings, gave the opportunity for scientists to attach smaller electrodes to the clinical ones that are capable to go beneath the millimetre scale, and to get data that were unreachable by any other techniques.

In the collaboration of Institute for Psychology of Hungarian Academy of Sciences (MTA-PKI) and several clinics in the United States, Ulbert and his colleagues approved and standardized microelectrodes appropriate for human intra-cortical laminar recordings (Ulbert et al., 2001a). Using this technique they were able to record extra-cellular Action Potentials (AP), Multiple Unit Activity (MUA), and Local Field Potentials (LFP) from the neocortex of patients undergoing epilepsy surgery. With small modification of the electrode the system became capable to record from deep structures

of the brain (Halgren et al., 2006). In the later case however it was not possible to coregistrate the histologically verified cortical layers and the electrical findings, that possibility in turn had been a big advantage when they applied the electrode in more superficial positions.

This pitfall seemed to be even higher when the possibility of recording from the hippocampus (Hc) was taken into account. This become clear if we consider the fact, that functionally highly different regions are separated by only several millimetres from each other in the hippocampal, and parahippocampal structures because of the unusual and complex folding of their layers.

Whereas there is a big need for detailed electrophysiological data from the human hippocampus. The most common and unfortunately the most refractory form of focal epilepsy affect the hippocampus in humans (Semah et al., 1998). The examinations of either healthy or epileptically transformed rodents have provided a abundant information from the function (Buzsaki, 2002; Geisler et al., 2007) and malfunction (Ben-Ari and Cossart, 2000; Bragin et al., 1997; Buhl et al., 1996; Sloviter, 1991) of the hippocampus, but very little is known about the activity of neuronal circuits in the human hippocampus, which gap can be linked to the big technical demand of human investigations.

The hypothetic possibility to perform such an invasive examination is given. Those therapy resistant patients whose hippocampus at one side had been proven to be epileptogenic may undergo temporal lobectomy in order to remove the seizure generating focus. In 1953 Falconer developed the “en bloc” resection technique that allowed the histological analysis of these epileptic hippocampi (Falconer et al., 1955). Using this technique the recorded electrical activities can be hypothetically linked to the anatomical locations, cell layers or laminas found in the histology thus conclusions on the activity of the microcircuits might be drawn.

In this dissertation I describe the first successful approach of human hippocampus with laminar multielectrodes (ME) in vivo. We succeeded to match the electrical activity with the cell layers of a specific subregion of the hippocampus verified by histological reconstruction of the electrode trajectory in patents undergoing temporal lobectomy for intractable epilepsy. We modified and used the recording system that was applied previously for animal and human intracortical recording (Mehta et al., 2000; Ulbert et

al., 2001a; Ulbert et al., 2004; Ulbert et al., 2001b). The modified electrodes, and micromanipulators were designed, and fabricated in Hungary in the MTA-PKI. The intra-hippocampal recording system was set in the National Institute for Neurosurgery (OITI), Budapest, Hungary and in the MÁV Central Hospital, Budapest, Hungary. The patient selection and presurgical evaluation was done in the National Institute of Psychiatry and Neurology (OPNI †), Budapest, Hungary, except one patient, who was examined in the "Szent István" Central Hospital, Budapest, Hungary. The histological processing of the tissue was done in the Institute of Experimental Medicine of Hungarian Academy of Sciences (MTA-KOKI), Budapest, Hungary.

The document contains the details on the special deep laminar multi-electrode (dME) and the micromanipulator system capable to position the electrodes into deep brain structures, and the description of the co-registration technique. We developed also a data analysis system to remove the artefacts generated by the unusual application of the MEs. The main issue is focused on different types of interictal spikes (IIS) recorded in vivo in the human subiculum of eleven patients, and we provide data on electrically evoked potentials (EP) in five, and recurring afterdischarges (AD) in three patients.

Specific aims

Recording and data analysis techniques

Our major aim was to update the existing technique designed for intracortical recording and to fabricate deep laminar multielectrodes (dME) suitable for human intrahippocampal use. With the updated system we aimed to record IISs from the seizure generating hippocampal formation (HcF) in vivo. After the histological procedure of the "en bloc" removed hippocampus we aimed to co-registrate the histologically verified cell layers with the electrophysiological activity.

There are multiple techniques to verify the position of MEs in the tissue. Townsend et al. reported a precise method used in rats (Townsend et al., 2002). They applied strong direct current (DC) pulse through an adjacent contact pair of the ME, which harmed the tissue marking the electrode trajectory and the position of the selected electrodes along it. Later, on the histological section, they were able to locate the damage in the tissue. We regarded this method for human application as unethical since we did not know the

long term effect of harmful DC pulse even if it was applied on tissue to be removed. Instead of marking the electrode trajectory we looked for a technique that allowed us to follow visually the electrode insertion point from the time that the electrode penetrated the tissue until the histology was performed to avoid missed localization of the trajectory.

The only condition we found to be suitable for these criteria was, if we tried to insert the electrode right before the removal of the hippocampus during the surgery. This technique had the advance to position the dME under visual control, and after the removal of the electrodes the insertion point could be recorded relative to the surface vascularisation.

In order to perform the special intraoperative recoding we constructed an electrode positioning system that fits the special conditions in the operating room (OR).

The build-up of the recording system in the OR required additional activity by the surgeon and needed time while the patient was anaesthetized. Basic requirement was to reduce this additional time, and make the assembly procedure as easy as possible. To overcome this problem we designed a “sterile kit” that contained the semi-assembled microelectrode on the electrode holder, and made possible to move and sterilize it together.

The IISs used to be recorded during the surgery via electrocorticography (ECoG). The spontaneous IISs on the ECoG provides further evidence on the epileptogenic nature of the tissue, and helps to determine the border of the resection (Alarcon et al., 1997; Gloor, 1975). During the operation we used ECoG meantime the experimental recording to study the interaction of the activity recorded on the ECoG and in the Hc.

Internal (Vida et al., 1995), or external (Ylinen et al., 1995) functional afferents of the Hc were investigated by multielectrodes via current source density (CSD) analysis. The position of the first inward current corresponded to the fastest excitation reaching the hippocampus. In order to investigate the functional connections between the cortical and hippocampal area in the temporal lobe we applied electrical stimuli through the adjacent contacts of the strip. Functional pathways were investigated by single electrical stimuli, and evoked potentials (EP) were analyzed.

We aimed to evoke ictal like afterdischarges (AD) by bipolar train stimuli according to the traditional method (Ojemann et al., 1992).

The IIS generation in the human Hc was examined in vitro in slice preparations that were obtained from surgically removed hippocampi of mTLE patients (Cohen et al., 2002). The slice preparation technique yields functionally active tissue, in which some of the original intrinsic connections are maintained but all of the extrinsic afferents are lost. Under these circumstances the IISs were generated solely by the Sub. These events resembled the IISs that had been previously measured in the same patients with intracranial electrodes.

Based on these observations we focused our attention to the Sub and aimed to characterize the IISs generated by the intact Sub in vivo.

An additional aim was to develop a data analysis system that is able to run all the algorithms needed for the appropriate interpretation of our data.

Qualifying intrasubicular activity

Our aim was to describe the laminar characteristics of the IISs, EPs and ADs in the Sub. Current source density (CSD), multiple unit activity (MUA), and spectral analysis was applied on the recorded data. With the aid of these transformations our aim was to determine the spatiotemporal properties of the excitatory and inhibitory processes of subicular neural networks. More precisely we aimed to characterize

- the overall IIS activity of Sub in anaesthetized condition;
- the types of IISs based on the spatiotemporal distribution of their CSD, MUA and spectral content;
- the intrasubicular synchrony of spontaneous IIS using dual dME recording;
- the CSD, MUA and high frequency content of the EPs and ADs in the Sub;
- the variability of EPs relative to the position and strength of the electrical stimulus.

Background

Epilepsy

Epilepsy is a devastating disease affecting about 1% of the population worldwide. The incidence is age dependent with higher occurrence in children and elderly. The cumulative incidence is higher than prevalence indicating spontaneous remissions (Hauser, 1997; Hauser et al., 1993). Epilepsies are multi-casual chronic diseases with the common feature of recurrent spontaneous seizures. The loss of quality of life is mainly caused by the unpredictable occurrence of the seizures with transient loss of consciousness, behavioural alterations, involuntary motor actions or convulsions. The epileptic patients are usually stigmatized resulting social isolation and unemployment. Between seizures the patients can be free of symptoms but a subgroup of patients can suffer from cognitive impairment, neurological deficits, or psychiatric symptoms due to epilepsy, the underlying etiological factor, or caused by the treatment. The lifetime expectancy of patients is worsened by 2-10 years, and there is a 2-3 fold increase in mortality ratio depending upon the syndrome, aetiology, seizure status, and numerous factors like gender, age etc. (Gaitatzis et al., 2004; Lhatoo et al., 2001).

The socially isolated, undereducated patients with recurring seizures cause a multi-disciplinary challenge and refer a difficult to treat condition. More than twenty different compounds are available worldwide for medical treatments (Rogawski and Loscher, 2004), and about sixteen in Hungary, but only 60-70% of the patients can achieve seizure freedom. The remaining 30-40 % can benefit from surgical treatment, or alternative treating strategies e.g. special diets, or neuromodulation, but app. 30% of the patients must live with seizures for long time (Kwan and Brodie, 2000).

The epilepsies were classified by the ILAE (International League Against Epilepsy) in 1989 and 2001 (Engel, 2001b; Roger et al., 1989). In spite the former classification that had two axes, one spanning from focal to generalized and the other from idiopathic to symptomatic epilepsies, the later classification uses a multiaxial approach. The third axis refer the syndromatology in which the mesial temporal lobe epilepsy (mTLE) with and without hippocampal sclerosis (HS) are separated from the other epilepsy syndromes.

Pathophysiology of epilepsy

For the first time Hughlings Jackson set the hypothesis in 1873 that the common background of epilepsies is the "occasional, sudden, excessive, rapid, and local discharges of grey matter" (Jackson, 1873). This statement has been referred as the "electrical theory" of epilepsies (Reynolds, 2001).

Under healthy conditions the neural excitation is controlled by various inhibitory machineries. Different neuronal changes can lead to hyperexcitability and the brake-down of inhibition at different levels of neural networks.

At the very basic level of ion channels the neural excitability is determined by voltage gated Na^+, K^+, and Ca^{2+} channels. The sodium and potassium channels are enrolled in action potential genesis. The termination of the action potential, which is one key moment that prevents neurons from hyperexcitation, depends on two steps. These are the fast inactivation of sodium channels, and the activation of potassium channels. Inherited defects of both can lead to epilepsies in the early life. The slowing of inactivation time lead to GEFS+ (generalized epilepsy febrile seizure plus) syndrome (Wallace et al., 1998). The loss-of-function mutation of brain specific potassium channel KCNQ2 and 3 leads to in BFNC (benign neonatal focal convulsions) (Lerche et al., 2001).

With one step further to the neuronal and synaptic level we can find again that changes of both excitatory and inhibitory mechanisms can lead to epileptogenic transformations. In human epileptic tissue increased AMPA (alpha-amino-3-hydroxy-5-methyl-4-isoxasole propionic acid) and altered NMDA (N-methyl-D-aspartate) receptor expression was measured (Zilles et al., 1999). Changes in the GABA (gamma-amino-butyric-acid) signalling can lead to hyperexcitability also. Normally GABA-A receptors act through increasing hyperpolarizing inward Cl^- conductance in the cell leading to inhibition of cell firing. The Cl^- concentration gradient required for this inhibitory current is maintained by KCC-2 (potassium-cloride-cotransporter-2) activity driven by the electro-chemical driving force of potassium. The increase of extracellular K^+ concentration (Dudek et al., 1998; Lux and Heinemann, 1978), or reduction of KCC-2 activity (Zhu et al., 2005) can lead to a consequent intracellular accumulation of Cl^-, that can reach such an amount that might change the direction of Cl^- channels. Under these conditions the opening of GABA-A receptors result outward Cl^- current and

depolarizes the membrane that resembles the similar properties of immature neurons (Rivera et al., 1999). More details can be found in section “Epileptic transformations in the subiculum”.

Considering the local neuronal networks a lot of complex changes are present under epileptic conditions. Like in the previous paragraphs, both excitatory and inhibitory mechanisms can be changed. The sprouting of excitatory connections was shown in the hippocampus and the neocortex in animal models and humans (Babb, 1999; Marco and DeFelipe, 1997 39; Salin et al., 1995). The sprouting and reorganization of inhibitory terminals can be also demonstrated by detailed morphological analysis (Maglóczky and Freund, 2005; Wittner et al., 2002).

The baffling variety and richness of potential epileptogenic neuronal changes can be increased if we consider that the “excessive, rapid and local discharges of grey matter” in the electrical theory require some synchronizing mechanisms in the affected region. Cobb et al. demonstrated that synchrony can be mediated by solely inhibitory actions (Cobb et al., 1995). This observation served explanation for the findings, that even increased, instead of decreased inhibition persists under different epileptic conditions (Babb et al., 1989; Isokawa-Akesson et al., 1989; Nusser et al., 1998; Wu and Leung, 2001).

Temporal lobe epilepsy

In humans the temporal lobe epilepsy (TLE) is the most common form of focal epilepsy, and gives the approximately 40% of adulthood focal epilepsies (Engel, 2001a; Semah et al., 1998).

Based on electroclinical categorization the TLE can be dissected into two separate syndromes called lateral (lTLE), and mesial temporal lobe epilepsies (mTLE) (Pfander et al., 2002). In the former case the seizures arise in the neocortical part of the temporal lobe, while in the later case in the limbic regions — including the hippocampus (Hc). Majority of TLE patients fall under mTLE syndrome (Engel Jr. et al., 1997).

The typical mTLE seizures are dysmnestic, psychomotor, automotor seizures, often accompanied by loss of consciousness, and long term recovery.

The seizures of mTLE syndrome is highly resistant to pharmacotherapy, but well treatable by surgery (Janszky et al., 2005; Kelemen et al., 2006; McIntosh et al., 2001;

Semah et al., 1998; Spencer and Spencer, 1985; Wieser et al., 2003). This condition resulted the consensus, that typical mTLE patients must be evaluated for surgery after the first or second failed drug regime (Engel Jr. et al., 1997).

Human temporal lobe spikes

The hallmark of human mTLE syndrome in the EEG is the well known temporal lobe interictal spikes (IIS) recorded on scalp (Jasper, 1951; Rose et al., 1987). These are commonly present on fronto-temporal electrodes (F3/F7, T4/F8) and consist of a spike that usually ends up in a slow wave (de Curtis and Avanzini, 2001; Wieser, 2004). The spike component lasts 50-70 ms, and the wave several hundreds of milliseconds (de Curtis and Avanzini, 2001). These relatively blunt and long duration spikes are called sharp waves by definition (Chatrian et al., 1974).

There has been a continuous effort to understand the mechanism of generation and to localize the origin of human mTLE spikes. It has been already proven that the source of scalp recorded IISs is different from the mesial temporal structures and rather involves the neocortical part of the temporal lobe. With intracranial electrodes the deep structures were demonstrated to be more active than the cortex, and the coupling between them varied with stages of vigilance (Clemens et al., 2003; Lange et al., 1983; Sammaritano et al., 1991; Wieser, 1991). Early studies that used intracranial microelectrodes focused on single or multiple unit activity and they found neuronal activation in the hippocampus and parahippocampal structures during mTLE spikes (Babb et al., 1973; Ward and Schmidt, 1961). When digital EEG was available more detailed studies were done both in awake and anaesthetised state (Alarcon et al., 1997; Bartolomei et al., 2001). These examinations explored multiple foci that appeared both within one patient or between cases based on which several subcategories of patients could be set. The most common focus that produced the largest amplitude and usually leading spikes was the hippocampus that showed a close functional ensemble with the subtemporal neocortical areas (Alarcon et al., 1997). In 2002 Cohen et al. done a detailed in vitro examination (Cohen et al., 2002). They studied ex vivo transversal hippocampal slice preparation, and found that the intrahippocampal spikes were originated in the subiculum (Sub). For more details see section: “Epileptic transformations in the subiculum”.

High frequency oscillations

In recent years increasing evidences refer, that not the IIS itself but the high frequency content of them is related to epileptogenic process. In slices of ex vivo rat pup's hippocampi, the kainate induced seizures transformed the contralateral side to an independent seizure focus. This process was related to the presence of high frequency oscillations (HFOs) in the contralateral side (Khalilov et al., 2005).

It was proven that HFOs are associated to IISs and seizures both in animal and human TLE (Worrell et al., 2004). Two distinct HFO frequency band was reported from humans, one at 96+/-14 Hz, another at 262+/- 52Hz. (Staba et al., 2002). Since these oscillations shows waxing and waning patterns they are called ripples, and fast ripple (FR) respectively. The occurrence of FR well predicted seizure generation both in animal and humans (Bragin et al., 2004; Rampp and Stefan, 2006; Staba et al., 2004). Ripples and FR usually appear in natural slow wave sleep (SWS) (Staba et al., 2004). The underlying mechanism of HFO generation was hypothesized to be mainly excitatory in the adult brain (Le Van Quyen et al., 2006).

The ripple oscillations can be detected in humans by clinical depth electrodes (Urrestarazu et al., 2006), or foramen ovale electrodes. Clemens et al. provided evidences that the ripples in parahippocampal region are linked to IISs and are modulated by thalamo-cortical oscillations (Clemens et al., 2007).

Structure of the human hippocampal formation

The hippocampal formation (HcF) is located in the medial part of the temporal lobes. Based on its 3 layered cytoarchitectonic structure the HcF represents the most primordial cortex of the mammalian brain, the archicortex (Lopes da Silva et al., 1990).

The human hippocampus can be divided into three different regions longitudinally: 1) the head or anterior segment, containing the digitationes hippocampi and the uncus, 2) the body or middle segment, and 3) the tail, or posterior segment. (Figure 10.) The hippocampal formation is composed of three parts: the dentate gyrus including the hilus (DG), the Ammon's horn (cornu Ammonis, CA) and the subiculum (Sub) listed from proximal to distal (Duvernoy, 1998). While describing the structure of the human hippocampal formation, the nomenclature of Lorente de No (Lorente de Nó, 1934) will be used with the modifications of Amaral and Seress (Amaral, 1978; Seress, 1988).

Based on these descriptions, the Ammon's horn can be further divided into three regions: CA1, CA2 and CA3 regions. (Figure 1. / A)

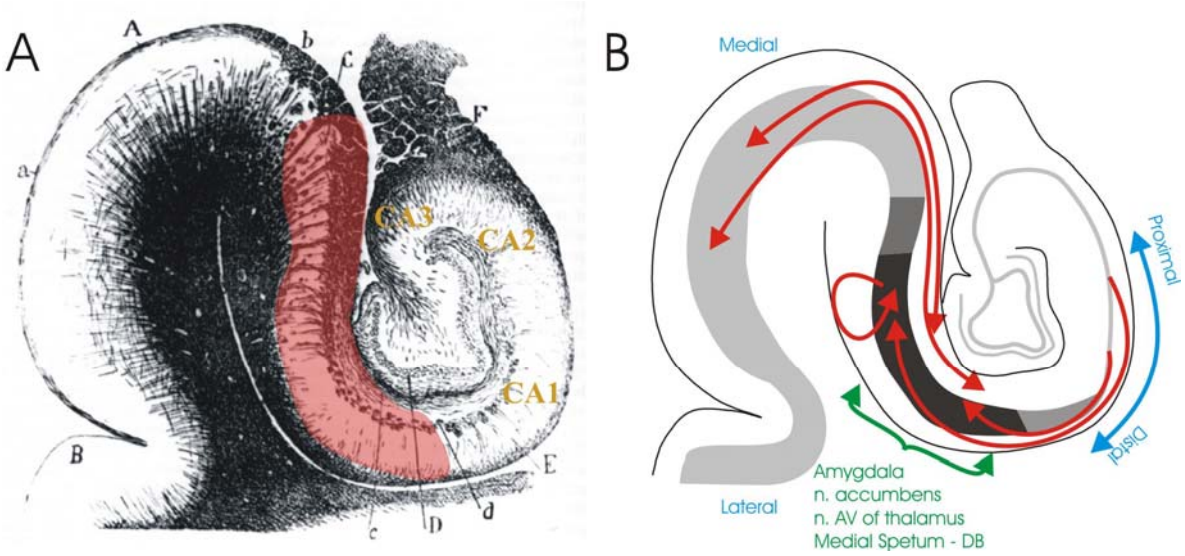

Figure 1.

Anatomy of hippocampal and parahippocampal regions in humans A) Drawing of S. Ramon y Cajal in 1901.* The original marks indicate the following structures A: parahippocampal gyrus, B: sulcus collateralis, C: subicular complex (shaded red), D: dentate gyrus, E cornu ammonis region 1 (CA1), F: Fornix, a: entorhinal cortex (EC), b: presubiculum, c: fissura hippocampi, d: str. moleculare (myelinated fibers). Braun marks indicate cornu ammonis regions (CA 1, 2, 3)
B) Schematic drawing of major connections of the subiculum. Cell rich layers are shaded grey. Light grey: parahippocampal regions; medium grey: presubiculum (close to EC) prosubiculum (close to CA1); dark grey: subiculum. Red lines: hippocampal and parahippocampal connections. The routes, and the target layers (apical dendritic, or somatic) are schematically indicated. The bidirectional arrows indicate reciprocal connections. The existence of 2 parallel information processing route is visible involving the proximal (close to CA1) and distal part (close to EC) separately. Green arrows show subcortical afferents. Blue arrows and marks indicate conventional orientation.
n.: nucleus; AV: anteroventralis; DB: diagonal bundle
* Downloaded from http://faculty.washington.edu/rhevner/HumanHippo.jpg

Principal cells of the dentate gyrus are the excitatory granule cells, whereas in the cornu Ammonis and the Sub pyramidal cells give the majority of the excitatory principal neurons. Principal cells are densely packed in a narrow layer, named granular layer in the DG, and pyramidal layer in the CA regions. In the Sub the pyramidal layer gets thicker and the neurons are arranged more loosely (Insausti and Amaral, 1990). Inhibitory cells are present in all regions of the hippocampal formation, and are relatively small in number (10-15%), but heterogeneous in their functions (for review see (Freund and Buzsaki, 1996)).

Intrahippocampal connections are described mostly in animals (Lorente de Nó, 1934; Ramón y Cajal, 1909-1911; Ramón y Cajal, 1968). This connection system is called the 'trisynaptic loop' of the Hc. The major input of the dentate granule cells is the perforant path arriving from the entorhinal cortex (EC). Granule cells project their axons towards the Ammon's horn and innervate CA3 pyramidal cells. CA3 pyramidal cells possess large number of recurrent collaterals terminating on other CA3 neurons, as well as the so called Schaffer collaterals, forming synaptic contacts in the CA1 region. CA1 pyramidal cells send their axons to the subiculum and terminate on subicular pyramidal cells, which in turn project their axons back to the EC.

The basic connectivity of human HcF is thought to be similar to the animals, but substantial differences are reported to be present (Lim et al., 1997).

By means of these connections the hippocampal formation is a part of a larger, structurally heterogeneous, but functionally highly synergistic network, the so called parahippocampal-hippocampal system. It includes at least nine domains: the DG, CA3 and CA1 fields, the subiculum, pre- and parasubiculum, the entorhinal, perirhinal, and parahippocampal cortices (Witter, 2006). This network plays a significant role in learning and memory processes. As a consequence of hippocampal damage, cognitive abilities and information processing are disturbed (Gabrieli et al., 1997; Hampson and Deadwyler, 2003; Hermann et al., 1992; Scoville and Milner, 1957; Zola-Morgan et al., 1986).

Anatomy and electrophysiology of the subiculum

The subicular complex (SC) is positioned between CA1 field of Hc and the entorhinal cortex (EC). On the Figure 1. / B the location and the basic connectivity of Subiculum are visible. The SC consists 3 main parts, the subiculum (Sub) the presubiculum (PreS) and parasubiculum. The Sub is also an archicortical structure built of tree layers similar to Hc, whereas the PreS contains an additional cell layer, above the pyramidal layer with densely packed neurons arranged in islands (Insausti and Amaral, 1990). The existence of the transition area between the CA1 region and the Sub, called prosubiculum (ProS) is controversial (Duvernoy, 1998; Insausti and Amaral, 1990; Stafstrom, 2005). As in the case of the hippocampus, the connections of Subiculum is studied in rat (Naber and Witter, 1998; Witter and Groenewegen, 1990) cat (Van Groen

et al., 1986), and monkey (Aggleton et al., 2005; Van Hoesen et al., 1979), but that of the human subiculum is still under debate.

The Sub give rise to the vast majority of fibers travelling through the fornix toward subcortical structures like lateral septum and the mammillary bodies (Swanson and Cowan, 1977). Via the angular bundle Sub is reciprocally interconnected with the nucleus accumbens and the amygdala (Canteras and Swanson, 1992) and the Sub projects back also to the EC via the perforant pathway as mentioned in the previous section. It sends fibers to several further subcortical structures like the lateral hypothalamus, anterior olfactory nucleus, bed nucleus of stria terminalis, endopiriform nucleus, and nucl. reuniens, nucl. interanterolateralis, and nucl. paraventricularis of the thalamus. It reaches also some cortical structures like the medial - and lateral orbitofrontal, pre- and infralimbic, agranular insular, retrosplenial and anterior cingulate cortices (Amaral and Witter, 1985; Witter, 2006).

The Sub's most important afferent come from the CA1 region of the Hc. The CA1 – Sub projection is topographically organized in the proximo-distal extent (Amaral et al., 1991; Stafstrom, 2005). (Figure 1. / B.) This connection is mostly unidirectional however minor reverse order fibers from the Sub to CA1 were reported (Harris and Stewart, 2001b). Further afferents invades Sub from medial septum-nucl. diagonal bundle complex, supramammillary nucleus, and topographically arranged inputs come from the amygdala and nucl. reuniens and paraventricularis of the thalamus. It receives modulatory fibers from the histaminergic premammillary nucleus, the noradrenergic locus coeruleus the dopaminergic ventral tegmental area, and substantia nigra, and the serotoninergic medial and dorsal raphe (Witter, 2006).

Based on these observations, as a general rule, the Subiculum can be considered as the most important output structure of hippocampal formation driven by the CA1 region (Rosene and Van Hoesen, 1977). In this peculiar position the Sub can develop a gating function on the hippocampus (Benini and Avoli, 2005; O'Mara, 2006), and through its widespread connections it can integrate the information of the limbic network and redistribute it to other brain structures (de la Prida et al., 2006).

It is functionally highly relevant also that the Subiculum is massively innervated by the EC similar to the Hc thus contributing to multiple re-entrant pathways in the temporal lobe (Kloosterman et al., 2004). These pathways run parallel to each other since the

columnar topography involves multiple domains of parahippocampal-hippocampal network, illustrated on (Figure 1. / B) Two main streams are present mimicking a cog-wheel like topography. The first follows the route proximal CA1 — distal Sub — medial (proximal) EC, and the second distal CA1 — proximal Sub — lateral (distal) EC (Amaral et al., 1991; O'Mara et al., 2001; Witter, 2006).

Beside the topographic columnar-like organization, laminar arrangement is either present in the Sub forming functionally different layers in the pyramidal layer (Ishizuka, 2001). However this concept is debated by others (Witter, 2006) it is accepted, that the Subicular projection, express a rather parallel pattern, than a collateral based projection unlike the hippocampus proper (Naber and Witter, 1998).

The laminar arrangement of the afferent pathways in the Sub was tested in several studies. It was shown that CA1 input reaches the proximal dendrites in the pyramidal layer of the Sub (Bartesaghi and Gessi, 1986; Stafstrom, 2005; Taube, 1993). This projection topography was strengthened by anatomical data (Tamamaki et al., 1987). The input from the EC reaches the outer two third (Behr et al., 1998; Gigg et al., 2000; Tamamaki and Nojyo, 1993), while perirhinal cortex innervates the inner one third of molecular layer (Kosel et al., 1983; Van Groen et al., 1986; Van Hoesen et al., 1979). Some of these findings are illustrated on Figure 1. Comparing data from different species substantial differences were measured. In guinea pig the strongest hippocampal afferent arises from CA3 while in rat from the CA1 (O'Mara et al., 2001). This discrepancy emphasizes the necessity of direct human data for conclusions appropriate for clinical purposes.

The laminar segregation of the afferents to the Sub might underlie the finding that the stimulation of cingulate cortex evoked positive potential deflection in the pyramidal layer, while the CA1 stimulation evoked negative going response (O'Mara et al., 2001).

One of the most pronounced properties of the Sub is the effectiveness of the feedback inhibition. Stimuli applied both orthodromically or antidromically evoked 50-500 ms lasting inhibition in the Sub (Colino and Fernandez de Molina, 1986; Finch and Babb, 1980; Finch et al., 1988; Gigg et al., 2000). One important function of this inhibition was that it held the burst firing neurons under strong and effective inhibitory control (Menendez de la Prida, 2003 124).

Hippocampal Sclerosis

Hippocampal sclerosis (HS) is an anatomical phenomenon in close relationship with TLE. The HS can be visualized on MRI that shows reduction in size and enhanced signal in T2 and FLAIR sequences on the affected side (Berkovic et al., 1991). Examination of a large series of TLE patients revealed that HS can be visualized by MRI in 55% (Lehericy et al., 1997). The validity of MRI was reviewed recently in a consensus report and stated that in the pathologically affected tissue the MRI shows atrophy in 90-95%, loss of internal architecture in 60-95%, T2 signal increase in 80-85%, and T1 signal decrease in 10-95% (Wieser, 2004).

The HS is a combined neuroanatomical damage and reorganization of both excitatory and inhibitory circuits of the Hc. HS consists of a shrunken hippocampus with a characteristic cell death and gliosis pattern in the hippocampal formation (Babb, 1999; Margerison and Corsellis, 1966; Meencke and Veith, 1991; Sommer, 1880). Pyramidal cells of the CA1 region, as well as neurons of the hilus of the dentate gyrus are selectively lost in HS, whereas dentate granule cells and CA2 pyramidal cells are known as resistant cell types. The Subiculum is also relatively well preserved (Dawodu and Thom, 2005; Fisher et al., 1998), whereas the vulnerability of the CA3 region is variable, different stages from the severe atrophy to the less affected CA3 region can be found among TLE patients. Beside the selective cell loss and gliosis, very intense synaptic reorganization and axonal sprouting has been demonstrated affecting both excitatory and inhibitory circuits of the hippocampus (Lehmann et al., 2001; Lehmann et al., 2000; Toth et al., 2007), for review see (Magloczky and Freund, 2005). The synaptic reorganization possibly precedes hippocampal atrophy, since axonal sprouting and changes in synaptic connections have been shown in the hippocampus of TLE patients without HS (Wittner et al., 2002; Wittner et al., 2001).

The severity of HS was staged by different authors (Blumcke et al., 2007; de Lanerolle et al., 2003; Magloczky et al., 2000; Wittner et al., 2005), based on the cell loss pattern and changes in synaptic reorganization. Our classification – established by Zsófia Maglóczky and described in details in (Wittner et al., 2005)– consists of four groups of patients. Type 1 HS is similar to the control; Type 2 shows patchy cell loss in the CA1 region; Type 3 hippocampus shows the typical HS; Type 4 hippocampus is shrunken and gliotic, with cell loss in every region.

Epileptic transformations in the subiculum

It was suggested that Subiculum plays an important role in mTLE (Behr and Heinemann, 1996) (Arellano et al., 2004; Cohen et al., 2002; Huberfeld et al., 2007; Wozny et al., 2005) and reviewed by others (de la Prida et al., 2006; Stafstrom, 2005).

Following the previous apparition, many changes were detected in the Sub at very different levels of neural networks. Right at the level of ionic currents Vreugdenhil et al. demonstrated enormous amount of persistent sodium currents in the Sub in animal model (Vreugdenhil et al., 2004). The hyper-excitability of this region was also linked to the relatively high proportion, more that 50 %, of bursting cells even in normal conditions (Greene and Totterdell, 1997) which can be further enhanced in response to epileptogenic transformations (Wellmer et al., 2002). De la Prida et al. demonstrated that the intrinsically bursting neurons can initiate interictal transients. In the background of this finding they found unaltered synaptic currents but changed intrinsic properties, like lowered firing threshold, and increased synaptic inputs at distal dendrites (Menendez de la Prida, 2003; Menendez de la Prida and Gal, 2004), and enhanced after-depolarization currents were found in epileptically transformed rats (Wellmer et al., 2002).

Cohen et al. measured the activity of surgically removed human epileptic Hc slices in vitro, and demonstrated that only the Sub produced spontaneously recurring IISs, but the other sub-regions of HcF did not (Cohen et al., 2002). The excitatory action of GABA was hypothesized in this preparation based on such property of a sub-population of subicular cells. The underlying changes of the most important Cl^- transporters, the previously mentioned KCC2 and the NKCC (sodium-potassium-chloride-cotransporter), were demonstrated recently in rodent (de Guzman et al., 2006) and in human epileptic Sub (Palma et al., 2006).

The intrinsic and extrinsic connections are also changed in the epileptic Sub. In animal model of epilepsy enhanced projection was observed from CA1 to Subiculum (Cavazos et al., 2004; Cross and Cavazos, 2007). However it was also demonstrated that Subiculum can produce IISs without detectable sprouting in the region (Knopp et al., 2005).

Surgical treatment of temporal lobe epilepsy

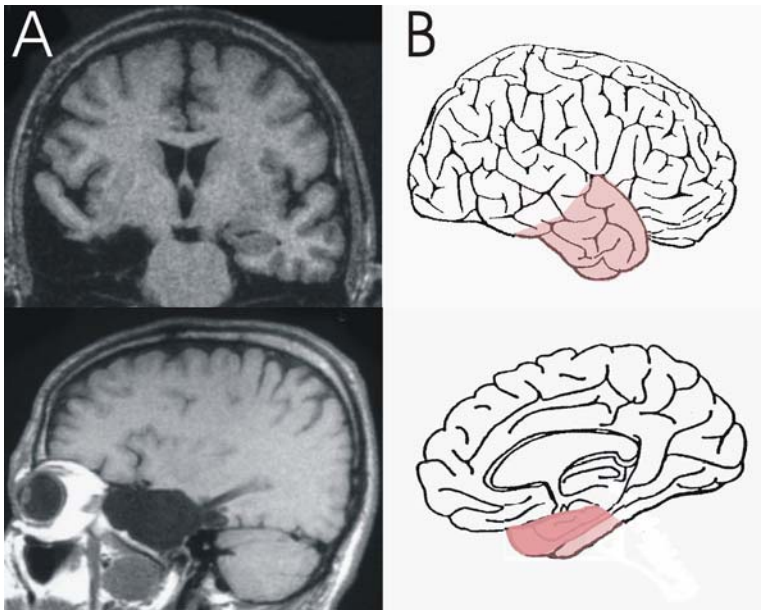

Figure 2.
Surgical techniques for temporal lobe epilepsy

(A) Post-operative MRI image of sATL patent.
(B) Schematic drawing of resected part in the brain. Selective amygdalo-hippocampectomy shaded dark pink; sATL shaded light pink.

sATL: standard anterior temporal lobectomy

As mentioned earlier, the mTLE patients are early candidates for epilepsy surgery. There are first line evidences for the effectiveness of surgery in mTLE syndrome (Wiebe et al., 2001). Three types of surgery are used worldwide. The selective amygdalo-hippocampectomy (Yasargil et al., 1993), the standard anterior temporal lobectomy (sATL), and the so called "tailored" surgery (Halasz et al., 2004; Spencer and Spencer, 1985). In the selective resection the Hc, Sub, EC - parahippocampal cortices, the uncus, and the amygdala are removed. In the sATL in addition the anterior 1/3 of the temporal lobe is removed including the temporal pole, the anterior half of the T2, T3 gyri, and the anterior third of the T1 gyrus (Sperling and Schnur, 2002) (Figure 2.) The tailored surgery reflects patient by patient varying resections based on imaging or electrophysiological data.

The bigger resections result in slightly better epileptological, with worse cognitive outcome, while more selective resections result in better neuropsychological but slightly worse in seizure outcome (Helmstaedter, 2004).

In Hungary at OPNI † - OITI Epilepsy Centrum the sATL is done since more than 15 years with excellent results (Kelemen et al., 2006).

Methods

Hippocampal recording technique

Intrahippocampal recordings were performed during the standard anterior temporal lobectomy of medically intractable mTLE patients in general anaesthesia (Propofol and N_2O or Isofluran and N_2O). Eleven patients were enrolled into this study. All of them underwent MR imaging, video-EEG monitoring as a part of standard presurgical evaluation procedure before the operation for localizing the seizure onset zone. The diagnostic workup was done in the OPNI † Epilepsy Centre (10 cases), or in "Szent István" Central Hospital, Department of Neurology (1 case). On the ground of the presurgical examinations all of the patients were diagnosed as mTLEs having unilateral seizure onset. The surgery and the electrode implantations were done in the OITI.

Each subject was fully informed and consented under the auspices of the Hungarian Medical Research Council, in accordance with the Declaration of Helsinki. The recordings were done only in the hippocampus to be resected, thus no additional risk that may stem from the invasive nature of our investigation were anticipated.

Electrode

Laminar multi-contact electrodes (ME) were previously developed to record the layer specific electrical activity of the neocortex (Heit et al., 1999; Ulbert et al., 2001a; Ulbert et al., 2004; Ulbert et al., 2001b). The original electrode for neocortical recording had a thumb-tack like shape with a short shaft ending in a small flat silicone head. (Figure 3. / A.) These MEs were not suitable for hippocampal recording, so we designed deep-multielectrodes (dMEs) to reach deep structures in an easy and fast way during the surgery. Two types of dMEs were made. Type 1 dME (100 µm dME) had better spatial resolution but worse spatial extent. This dME had a 10cm long, 350µm diameter, stainless steel needle shaft, with 24 contacts presenting on the shaft near the tip. The contacts were formed by the cut ends of linearly arranged 25µm diameter Pt/Ir wires with 100µm centre to centre distance. The first contact was positioned 5 mm far from the tip. (Figure 3. / B.) So the 100 µm dME covered 2.4 mm recording length. The resistance for each contact was around 500kohms at 1 kHz. Type 2 dME was similar to the previous, but its inter-contact distance was increased to 200 µm to reach 4.8 mm

coverage at the expense of worsened spatial resolution. The numbering of the contacts was started at the shaft with increasing numbers toward the tip.

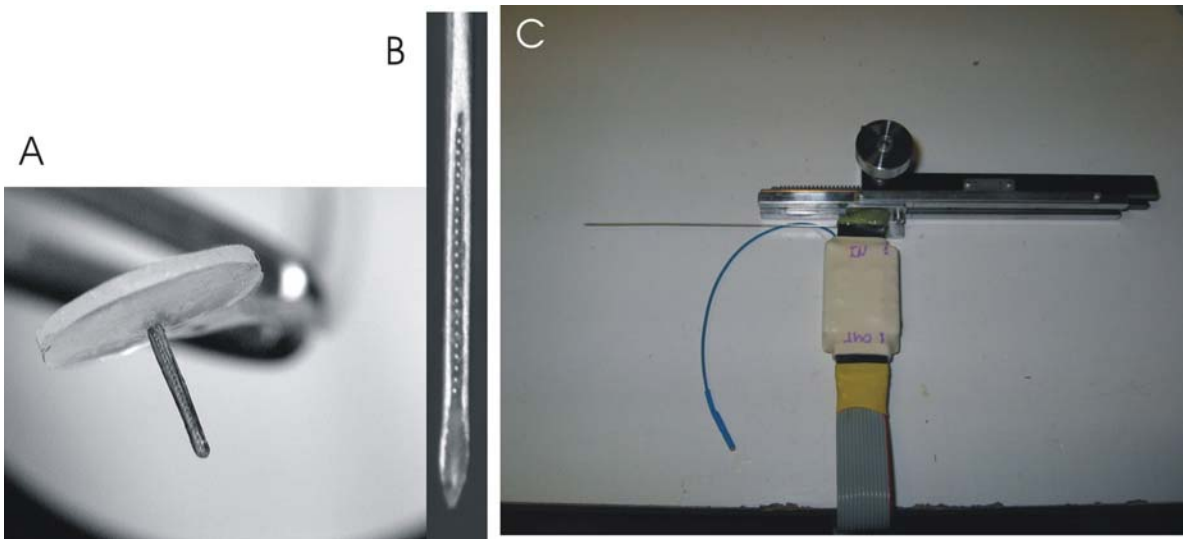

Figure 3.

Electrodes (A) Thumbtack multi-contact electrode **(B)** deep multi-contact electrode (dME) **(C)** dME mounted on early type positioning device.

Electrode positioning, surgery and cortical stimulation

The positioning of the dMEs was done by different micromanipulators. The early device was constructed of a manual micromanipulator, which led us to set the electrode position in app. 3-500µm precision. (Figure 3. / C.) Later we improved the system and changed to a 10µm precision hydraulic micro-manipulator. The following advances could be achieved by means of the new device. The positioning precision increased app. 5 times. The traumatic effect of the dME could have been lowered because of reducing the insertion speed to app. 200µm/sec. The positioning of the dME could be done by the electro-physiologist instead of the surgeon, thus better control and documentation of invasion depth could be conducted.

One or two dME were mounted on the micromanipulator together with the attached high impedance preamplifiers. In the case of dual laminar recordings, the electrodes were separated by 6mm.

All the equipment going into the surgical field was sterilized in ethylene-oxide. A sterile pack was constructed to keep all the devices to be sterilized together. (Figure 4.)

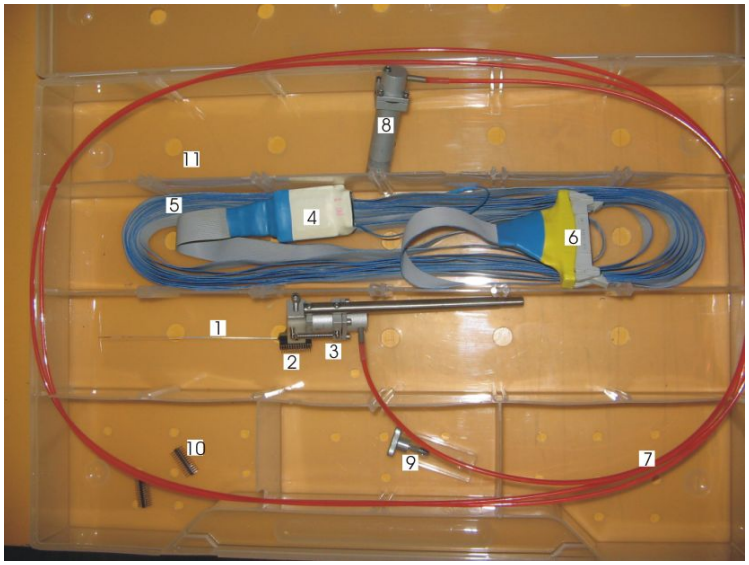

Figure 4.

Steril kit. The content of the steril box. 1: dME, 2: electrode connector with interface, 3: piston of the hydraulic microdrive at the electrode's side, 4: preamplifier, 5: electrode cable, 6: main amplifier connector, 7: oil cable, 8: piston of the hydraulic microdrive at the manipulator's side, 9: clamp for the electrode holder, 10: supplementary interfaces, 11: perforated plastic box appropriate for ethylen oxide sterilisation. dME: deep laminar multi-contact electrode

The sterile pack contained the dMEs mounted on the micro-manipulator, the hydraulic cabling, the preamplifiers, and the cabling that links the preamplifiers to the main amplifier.

The manipulator with the mounted multielectrodes and preamplifiers was attached to a medical instrument holder at the beginning of the recording, which allowed the surgeon to aim towards the hippocampus under visual control using an operating microscope. The intraoperative electrode setup is illustrated in (Figure 5./ A-B.) In order to conserve medial-lateral temporal pathways, the lateral ventricle was opened from a small incision involving the deep aspect of the superior temporal sulcus to reveal the head and body of the hippocampus. (Figure 5./ C.) Under visual control, the multielectrode tip was positioned onto the ependymal surface of the Hc through the incision. After the initial positioning, the electrodes were advanced into the tissue with 2-4mm increments using the hydraulic manipulator. At each step, the signal was recorded for 3-5 minutes continuously.

Using this approach the most probably hit region was the Subicular complex, and the dentate-gyrus-hilus-CA3c regions. The possible position of the electrode could vary in a wide angle. The most proximal insertion point was in the CA2, and the most distal in the Prosubiculum. (Figure 5. / D.)

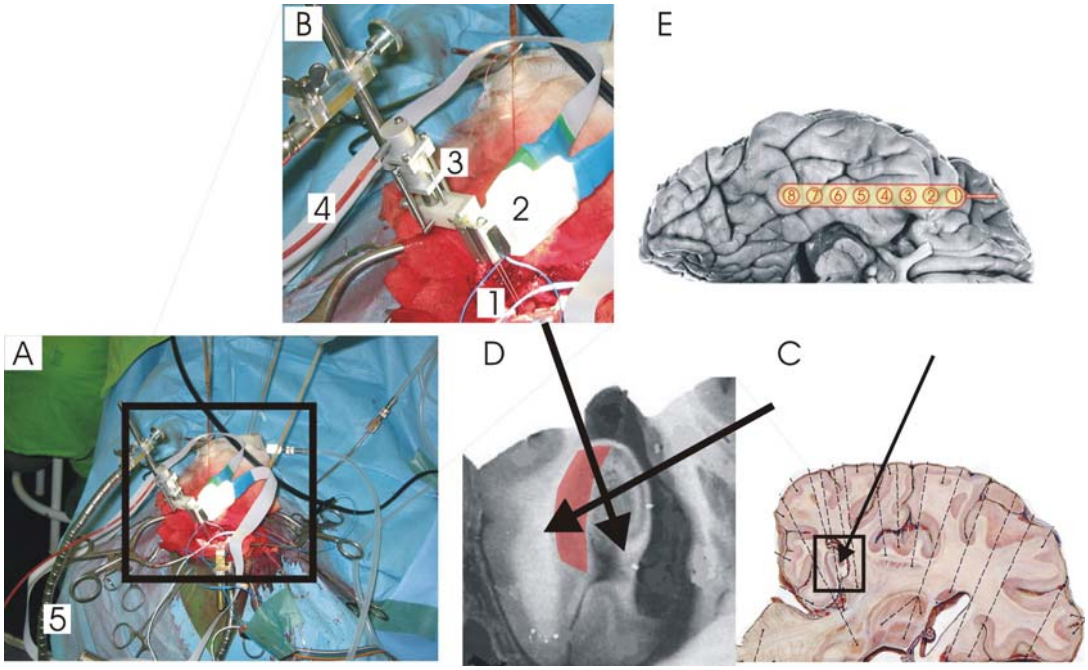

Figure 5.
Intraoperative setting. (A) and **(B)** intraoperative photo of dual dME setup with hydraulic micro-drive. **(C)** Approximate position of the brain during the recording. The arrow indicates the insertion position of the electrode between the T1 and T2 gyrus. **(D)** High resolution MRI image of the hippocampus and parahippocamal regions indicated in C. Arrows show the possible angle of electrode position relative to hippocampal surface. Note that both extremes and almost every trajectory cross the Subicular complex shaded red. **(E)** The approximate position of the clinical strip electrode under the temporo-basal surface. 1: Electrodes, 2: Preamplifiers, 3: Hydraulic microdrive, 4: Oil cable, and Electrode cable, 5: Screw lock ("Leila") device; dME: deep laminar multi-contact electrode

In addition to the dMEs, as a part of the standard ECoG procedure, an 8 point clinical strip electrode (Ad-Tech Medical Instrument Corporation, Racine, USA) was placed in 8 cases onto the tempo-lateral and the temporo-basal regions to explore the temporal neocortical spiking activity. The temporo-basal areas were approached from the anterior part sliding the strip around the temporal pole. The strip was left in the later position throughout the experimental recording. Based on the angle and visual inspection of the strip, it reached the temporo-polar (Brodmann, Br. 38), perirhinal (Br. 35-36) and inferotemporal (Br. 20) areas, but not the entorhinal (Br. 28) area.

Through the adjacent electrode contact sites of the strip, which were separated by 1 cm, we applied different electrical stimuli to the cortex. Two type of stimulation was used. 1.) Single electrical stimuli were used to elicit evoked potentials (EP). The stimulation parameters were 5-10-15mA in strength, 0.2ms pulse duration, 2 sec repetition time, 25 or 50 stimuli per trial. 2.) Train electrical stimuli were applied to provoke after-discharges (AD). In this paradigm the stimulus parameters were 10-15mA in strength,

0.2ms pulse duration, 50Hz stimulus frequency and 2 sec (100 stimuli) trial length. If ADs were elicited 3 min. restitution time was left afterwards.
At the end of the recording the HcF and the EC was removed “en-bloc” for histological processing (Falconer et al., 1955).
After tissue removal, the neurosurgeon and the histologist confirmed and recorded the region and angle of the dME insertion based on the surface vascularisation of the hippocampus, because the entrance point of the dME was sometimes not apparent. Digital photograph was taken of the removed hippocampal part, and then the block was cut into 4-5mm thick slabs in the operating room, parallel with the dME trajectory.

Amplifiers, data sampling

The dMEs were attached to high impedance preamplifiers. To reduce the external noise in the operating room, we used spatial differential amplifier to record the field potential gradient (FPG) in the tissue. It gives the first spatial derivative of local field potentials (Eq. 1.). The differentiation was done using the adjacent (1-2, 2-3, 3-4, etc.) electrode sites of dMEs with 10 to 50 output amplification.
Eq. 1. $FPG(z,t)= dU(z,t)/dz$,

where ‘z’ is space, ‘t’ is time, ‘U’ is the extra-cellular local field potential (LFP).

The FPG signal was split into two bands. One to sample the EEG, in this case the signal was filtered between 0.1-500 Hz, sampled at 2kHz/channel with 16 bit precision; and the other for multiple unit activity (MUA) and action potentials, filtered between 150Hz-5000Hz, 20kHz/channel, 12 bit. The gain of the main amplifier could vary from 200 to 2000, resulting 2000 – 20000 overall amplification. Both bands were digitalized using PCI bus analogue to digital converter cards (PCI-6071E for EEG, and PCI-6033E for MUA, National Instrument Inc.). ECoG was filtered (0.1-1000Hz), digitized at 5kHz with 16bit resolution and stored for off-line analysis (Brainvision Recorder, Brain Products GmbH., Gilching, Germany). Laminar and strip recordings were coregistered using a common trigger line.
We used a Pentium based PC as an acquisition machine with 128Mbyte memory, and two 120Gbyte hard disk drive (Samsung HD120HJ) one of which was put into a

removable rack. LabView 4.0 software (National Instruments Inc.) was used to write data acquisition virtual instrument (VI) software. The VI included high speed on-line displaying, data sampling and data storing modules. The precise technical details of this system were published earlier (Ulbert, 2002; Ulbert et al., 2001a). The initial archiving was done by copying the data onto the removable drive after the recording, and this drive was used later for off-line analysis.

Off-line data analysis

We analyzed the data in Neuroscan Edit and Stats module (Neuroscan Inc.), and in Matlab (Mathworks Inc.) scripts modified from EEGLAB (Delorme and Makeig, 2004) and self written data-editor program called NSWIEW (see section "NSWIEW data reviewing and analysis program").

Current Source Density

Using the Current Source Density (CSD) the summed transmembrane currents can be estimated from the extracellular field potentials. The derivation results in sinks and sources that correspond to the inward and outward currents through the cell membrane respectively. (Figure 6.)

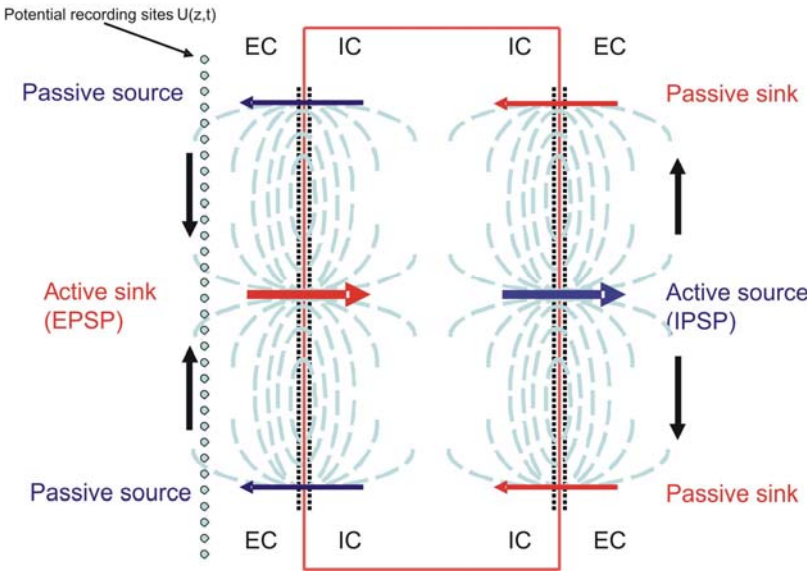

Figure 6.

Current Source Density
Schematic drawing of the extracellular and intracellular currents during an active sink: left; and an active source: right. Black arrows indicate the extracellular currents along the recording electrode. Red and blue arrows indicate the sinks and sources respectively.
EPSP: excitatory postsynaptic potential. IPSP: inhibitory postsynaptic potential, EC: extracellular, IC intracellular.

Methodologically the CSD is the second spatial derivative of the extracellular field potentials (Eq. 2).

Eq. 2. $CSD(z,t)=-k*d^2U(z,t)/dz^2$,

where U(z,t) is the extracellular LFP in the function of space and time, 'k' is a linear coefficient that is proportional to local extra-cellular resistance of the tissue.

This equation can be split into two steps if the extracellular currents are calculated first. (Eq. 3 and 4.).

Eq. 3. $I_{ex}(z,t)= -k*dU(z,t)/dz$,
Eq. 4. $CSD(z,t) = dI_{ex}(z,t)/dz$,

where I_{ex} equals to extracellular currents.

Our CSD method was different from the method reported by (Freeman and Nicholson, 1975; Nicholson and Freeman, 1975) since our first spatial derivative was already done in an analogue fashion in the differential preamplifier resulting that our system measured directly the FPG. (See the "Amplifiers, data sampling" section.) The combination of Eq.1. and Eq.3. lead to the equation that describes the linear correlation between extracellular currents and the FPG.(Eq 5.).

Eq. 5. $I_{ex}(z,t)= -k * FPG(z,t)$,

Combining Eq. 4. and Eq. 5, we can derived the CSD from the FPG signal directly (Eq. 6.).

Eq. 6. $CSD(z,t) = -k * dFPG(z,t)/dz$,

The computation is illustrated in Figure 7. / B. A Gaussian was used to model an ideal extracellular LFP signal (blue). First (FPG, red) and second (CSD, green) spatial

derivative is calculated and plotted. The calculation resulted a sink (in the middle) surrounded by "return" sources (see later in this section).

Before calculating the CSD, a Hamming window based spatial filter was applied to the signal to avoid spatial disturbances that affect CSD (Rappelsberger et al., 1981).

There are four conditions required to calculate adequate CSD. 1) The distance of recording sites on the electrode shaft should be equal, 2) the resistance of the tissue near the electrode must be constant, 3) the ME must be put into laminar structure, where the waste majority of the cells are arranged into the same direction, and 4) the ME must be parallel with the long dendrites of the cells. The ideal arrangement is illustrated on Figure 7. / A.

Inhomogeneous conductivity and electrode distance was not taken into account, thus the first and the second condition were considered to be true. The third condition is true for the allocortex, since the majority of cells are the pyramidal cells arranged into the same direction. For details see the Introduction: "Structure of the human hippocampal formation". The forth condition can be achieved by putting the electrode in an appropriate angle into structure.

In extracellular electrophysiology always closed current-loops are measured. So an active current e.g. a sink is always snuggled by passive, so called, return currents. (Figure 6.) So an active current e.g. a sink is always snuggled by passive, so called, return currents. (Figure 6.) These are passive phenomena that do not depend on specific ionic mechanisms, but only on the passive properties of the membrane, like the input resistance or leakage currents.

However in real conditions more complex spatial distribution can be present and usually distorted CSD can be obtained instead of the ideal profile. (Figure 7./ B, C)

Figure 7. / C illustrates the distortion of the CSD due to the different dendrite orientation relative to the ME. Those currents that flow perpendicular to the ME (grey arrow upward) result in less accurate CSD, only those that flow parallel to the electrode (black arrow downward) produce well detectable CSD profile.

Multiple Unit Activity

The multiple unit activity (MUA) represents the background high frequency noise in the signal, which corresponds to the summed extracellular action potentials of neurons surrounding the electrodes in an app. 300 μm radius (Wang et al., 2005). The highest

frequency field potential oscillations that have been reported in humans were 600 Hz (Staba et al., 2002). Therefore we used 500-5000 Hz third order zero-phase-shift Butterworth digital filter with rectification to calculate MUA that was not affected by HFOs in the sampled tissue.

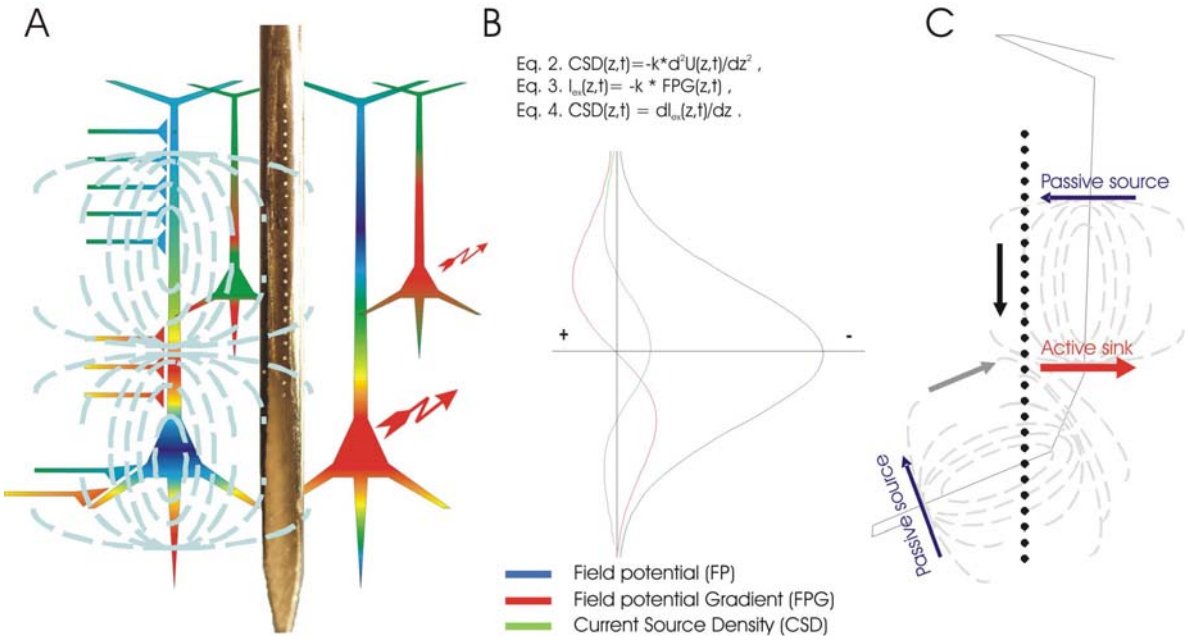

Figure 7.

An active sink (A) Schematic drawing of transmembrane currents beside the ideal electrode position. **(B)** Step by step derivation of an ideal CSD profile from a potential curve modelled by a Gaussian. Positive FPG means downward current, negative FPG means upward current (red curve). Positivity and sources are plotted leftward; negativity and sinks rightward. The amplitude relationship can be also observed. See equations in the text. **(C)** The distortion of CSD signal on basal dendrites. Black arrow indicate downward current parallel with the electrode and enhances by adjacent dendrites, grey arrow indicate upward current partially perpendicular to the electrode, and weekend by adjacent dendrites.

Time-Frequency analysis

The classic spectral analysis, the Fourier transformation, converts the signal to frequency domain while the time domain information is lost. This drawback becomes important when transient oscillations are inspected. To resolve this problem several time-frequency analysis (TFR) methods, like wavelets were developed (Samar et al., 1999).

The measurement of the spectral content of IISs means obviously the measurement of transient oscillations. We used individual trial event related spectral perturbation (iERSP). Dividing the resultant values with the baseline (-500ms to -50ms) activation in

each frequency band gives the relative change of spectral activity. Statistical significance ($p<0.01$) of the iERSP was assessed using bootstrap analysis (Delorme and Makeig, 2004). We applied iERSP on single sweep FPG traces first, and averaged TFR maps were calculated thereafter. Significant spectral activity changes were plotted in dB values, and warm (red) colours were used to mark increase and cold (blue) colours to decrease.

Histology

Before histological procedure photographs were taken of the removed tissue. The blocks were measured to allow subsequent estimation of shrinkage, finally all of them were immersed separately into fixative containing 4% paraformaldehyde, 0.1% glutaraldehyde and 0.2% picric acid in 0.1 M phosphate buffer (PB, pH 7.4), as described earlier (Magloczky et al., 1997). The fixative was changed every hour to a fresh solution during constant agitation for 6h, and then the blocks were post-fixed in the same fixative overnight. Vibratome sections (60μm thick) were cut from the blocks, and photographs were taken from the electrode tracks (Figure 10 / B). Following washing in PB, sections were immersed in 30% saccharose for 1–2 days then frozen three times over liquid nitrogen. Sections containing the electrode track were either stained with cresyl violet, or processed for immunostaining against glutamate receptor subunit 2 and 3 (GluR2/3), as follows. Sections were transferred to Tris-buffered saline (TBS, pH 7.4), then endogenous peroxidase was blocked by 1% H_2O_2 in TBS for 10min. TBS was used for all the washes (3x3-10min between each sample) and dilution of the antisera. Non-specific immunostaining was blocked by 5% milk powder and 2% bovine serum albumin. A polyclonal rabbit antibody against GluR2/3 (1:100, Chemicon, Temecula) was used for 2 days at 4°C. The specificity of the antibody has been thoroughly tested by the manufacturer. For visualization of immunopositive elements, biotinylated anti-rabbit immunoglobulin G (1:300, Vector) was applied as secondary antiserum followed by avidin-biotinylated horseradish peroxidase complex (ABC; 1:300, Vector). The immunoperoxidase reaction was developed by 3,3'-diaminobenzidine tetrahydrochloride (DAB; Sigma) dissolved in Tris buffer (TB, pH 7.6) as a chromogen. Sections were then osmicated (1% OsO_4 in PB, 40min) and

dehydrated in ethanol (1% uranyl acetate was added at the 70% ethanol stage for 40min) and mounted in Durcupan (ACM, Fluka).

The location of the electrode tracks were defined based on light microscopic examination. Only cases were included in this study, where the electrode passed through the subicular complex (including the subiculum, pre- and prosubiculum). In the cases without HS, the border between the CA1 region and the Sub was determined by the enlargement of the pyramidal cell layer, with clearly distinguishable two sublayers, and the presence of islands of small cells (Insausti and Amaral, 1990). In the sclerotic cases, the CA1-Sub border was determined by the absence or presence of pyramidal cells, respectively. The entorhinal cortex was distinguished based on the presence of six cortical layers, and islands of large modified pyramidal cells (Insausti and Amaral, 1990).

Co-registration of the signal with anatomical layers

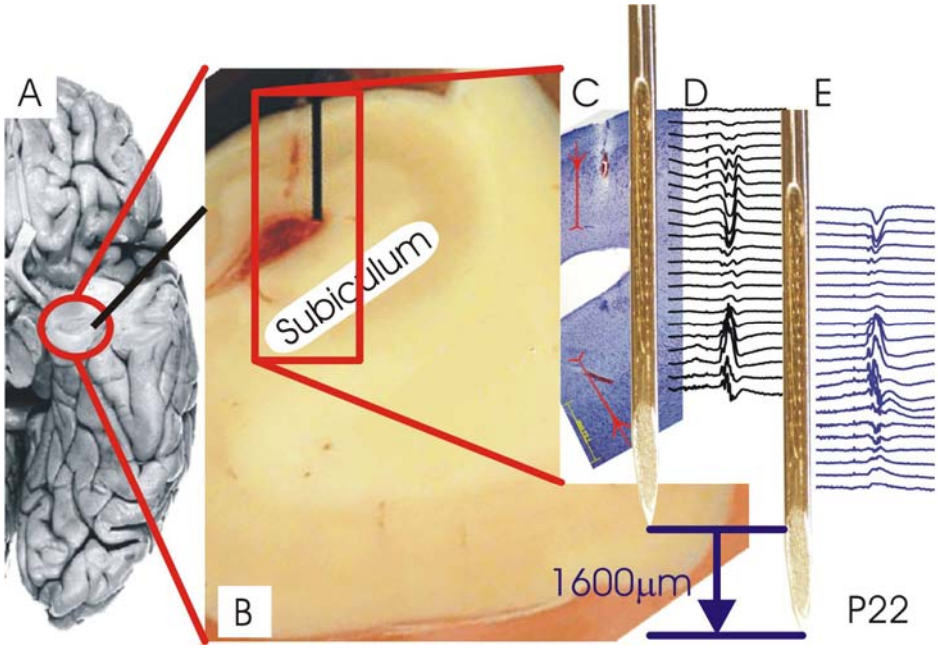

Figure 8.

Histological procedure and coregistration of electrophysiology with histology
(A) Position of the electrode (black line). **(B)** Photo of the "en block" resected hippocampus (block photo) at the level of digitationes hippocampi. The red injury in the middle is the entrance of the electrode signed by black line beside. **(C) –(E)** The co-registration procedure. **(C)** Nissl stained section with the injury of electrode entrance in the middle. The red schematic neurons indicate the direction of apical dendrites of pyramidal cells. **(D)** Field-potential profile in the first electrode depth, and **(E)** in the second depth. The scalebar for the B, C, D, E are the same.

The Figure 8. illustrates the co-registration procedure of the signal with the anatomical findings. The trajectory of the electrode was reconstructed from multiple stained sections. The resulted image was digitized at high resolution with distance calibration and transferred into CorelDraw (Corel Inc., Dallas, TX), an accurate vector graphics software, to reconstruct the electrode tract and potential profile corresponding to the individual recording sites and epochs. Using the shrinkage value of the tissue, the readings from the micromanipulator and additional information from the height of the first penetration (tracked by the operating microscope), all the spatial positions of the recording epochs were marked on the digitized slide. We acquired separate files for each movement of the dME. Based on the FPG phase reversals and amplitude maximums of IISs or EPs, the waveform profiles from different but overlapping depths were fitted to get the reconstructed FPG signal (Figure 8.D, E). The electrodes that were positioned outside the tissue were selected based on progressive decay of the signal. Finally the reconstructed FPG signal and the electrode trajectory on the digitized slide were suited. Additional information was obtained from MUA distribution. Because MUA is generated by the discharge of neurons surrounding the electrode contacts, it is most pronounced around the cell body layer, and decays rapidly with distance. Thus, comparing the depth of the maximal spiking activity with the location of the cell layers gave us a good measure to verify the graphical co-registration procedure.

NSWIEW data reviewing and analysis program

NSWIEW is Matlab based software developed by our laboratory for adequate data analysis, and to measure IIS parameters. (Figure 9.)

The program is designed for data reviewing and processing. The following file formats of different EEG platforms are importable (the file extensions are indicated in brackets): Neuroscan (.cnt, .avg), Brainquick (.trc), Windaqui (.wdq), Brain Vision (.vhdr), self generated continuous, and averaged file formats (.mat and _avg.mat), generic header (.txt), and ASCII format (.prn).

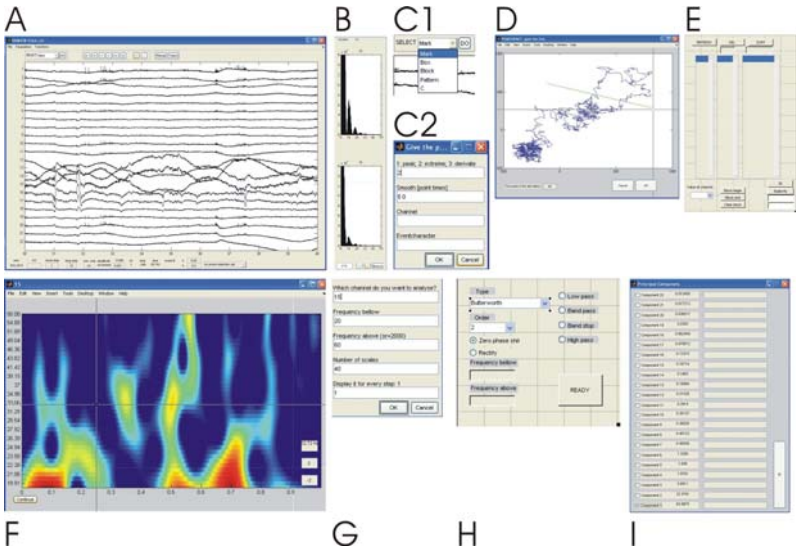

Figure 9.
(A) Main window, **(B)** FFT windows for selected channels, **(C)** event selection "pull-down" menu, and GUI **(D)** GUI for phase space based event selection, **(E)** GUI for browsing events, **(F)** continuous wavelet window, **(G)** menu for wavelet parameter setting, **(H)** GUI for custom filter definition, **(I)** GUI for principal component analysis

FFT: fast Fourier transform, GUI: graphical user interface

Powerful event selection possibilities are available both by manual selection and different threshold based algorithms. Events can be defined by the slope, waveform patterns, ongoing phase (Hilbert transform), or based on multi-dimensional embedding (phase space) as well. The selected events can be reviewed manually using graphical event editor, or the program is capable to scroll through them automatically.

During reviewing or automatic scrolling various tasks can be defined that are performed in each step thereafter. These tasks may be cumulated, and the result can be exported into file. Using this possibility multiple digital filters, smoothing, and linear derivation (linear transformation throughout the channels, like CSD) can be combined. Event triggered averages and peri-event time histograms (PETH) can also be calculated.

Graphical user interfaces are included for filter design, Fourier transform (fast-Fourier transform, FFT), continuous wavelet transformation, and principal component analysis.

The variance and skewness of the plotted data can also be calculated.

Single unit discharges can be selected and discriminated based on multiple channel distribution patterns, and K-means clustering algorithm with graphical user interface is available.

There are additional transformations in the scroll mode. Beside artefact rejection, signal to noise ratio calculation, wavelet scale-averaging and frequency domain averaging are available. In this mode the linear shifting coefficient that corresponds to the relative movement of the signal throughout the channels due to the passive displacement of the electrode in the tissue can be automatically determined, and corrected averages can be

calculated. The description of this algorithm is found later in section “Complex CSD, MUA and spectral characterization”. Based on this correction algorithm event by event half amplitude duration (half width, HW) and area under curve can be obtained that are not affected by the electrode displacement and suitable for statistical processing.

Results

Spontaneous interictal discharges

We have recorded subicular laminar electrical activity from eleven patients in sixteen multielectrode penetrations under general anaesthesia. Hippocampus was removed “en bloc” after the implantation containing the electrode track. In seven cases we have found direct histological evidence, that the electrodes reached the target and recorded subicular activity. In four cases the Sub was damaged and lost during the removal. Reconstructions - based on the remnant tissue and the general anatomy - by expert morphologist, revealed that it is highly likely, that in the remaining four cases, the electrodes also reached the target and recorded subicular activity. All available tissue was analyzed with respect to cell loss and reorganization with immunohistochemical methods.

In seven patients we observed severe cell loss in the CA1 region, (severe HS, sHS) in four patients relatively mild cell loss was detected (mild HS, mHS). Nine out of the eleven patients (n=6 with sHS, n=3 with mHS) showed at least one spike exceeding the ±2SD threshold for spike detection in the Sub during the entire recording session (10-25min). Overall spike frequency in six (P3, P10, P21, P22, P25 and P33) patients (n=4 with sHS, n=2 with mHS) exceeded the 1spike/min value and yielded enough events, which we determined as the minimum criteria for adequate FPG, CSD, MUA and spectral measurements. Data from these six patients were analyzed in details. In five of the six patients the complete histology of the electrode track was available. In two of the six patients, ECoG was obtained concurrently from strip electrodes placed on the pial surface of the temporal lobe in addition to the subicular recordings. All of the six patients were anesthetized by the combination of Propofol and N_2O. Table 1. summarizes the patient data and Figure 10. shows the reconstructed trajectories and some sample histology of the electrode penetrations.

Patient	Included in detailed analysis	Age (years)	Impl. side	Gend.	Duration of epilepsy (years)	MRI finding	Hc damage	Elec. 1 loc.	Elec. 2 loc.	Anesth	Outcome
P3	Yes	47	Left	F	36	Bilateral HS	sHS	body	NA	Prop.	3A
P4	No	35	Left	F	30	Left HS	sHS	head	NA	Iso.	1A
P10	Yes	24	Left	F	20	Left HS	sHS	body	body	Prop.	1A
P17	No	31	Right	M	22	Right HS	sHS	body	head	Iso.	1A
P20	No	56	Left	F	7	TU (left temporo-polar)	mHS	body	digit.	Prop.	1A
P21	Yes	26	Right	F	7	Right HS	mHS	body	body	Prop.	4B
P22	Yes	46	Left	F	10	Bilateral HS	sHS	head	digit.	Prop.	1A
P25	Yes	36	Left	F	6	Left HS	sHS	*body	*head	Prop.	1A
P26	No	40	Right	F	26	Bilateral HS	sHS	body	body	Iso.	2B
P30	No	40	Right	F	15	TU (right temporo-lateral)	mHS	head	head	Prop.	1A
P33	Yes	51	Left	F	32	TU (left amygdala)	mHS	*head	*head	Prop.	2B

Table 1.

Summary of patient characteristics. Abbreviations: Impl. side: implantation and resection side, Gend.: gender, F: female, M: male, MRI: Magnetic Resonance Imaging, HS: hippocampal sclerosis, TU: tumor, Hc.: hippocampal, sHS: severe cell loss and reorganization of hippocampus (severe hippocampal sclerosis), mHS: mild cell loss and reorganization of hippocampus (mild hippocampal sclerosis), Elec. loc.: electrode location, digit.: hippocampal digitations, according to (Duvernoy, 1998). NA: not applicable, Anesth.: anesthesia, Prop.: Propofol, Iso.: Isofluran. Dual electrode experiments, where both electrodes were implanted to and recorded successfully from the Sub are marked by an asterisk. Outcome: 1 year outcome (Engel classification (Engel et al., 1993): 1A: Aura and seizure free; 2B: Rare seizures; Often seizure with worthwhile reduction; 4B: No change.

Subicular discharge morphology was differentiated based on single sweep FPG and CSD waveforms and their spatial relationship to the anatomy of the region, as follows.

Overall, 347 spikes were analyzed from the six patients, and two clusters were distinguished. Type 1 spike (marked by triangle on Figure 11. and Figure 12.) was characterized by a positive, while Type 2 (marked by diamond) was characterized by a negative initial sharp FPG peak located in the somatic layer. In a fraction of the cases, visual inspection revealed biphasic activation; these were manually assigned to the second type.

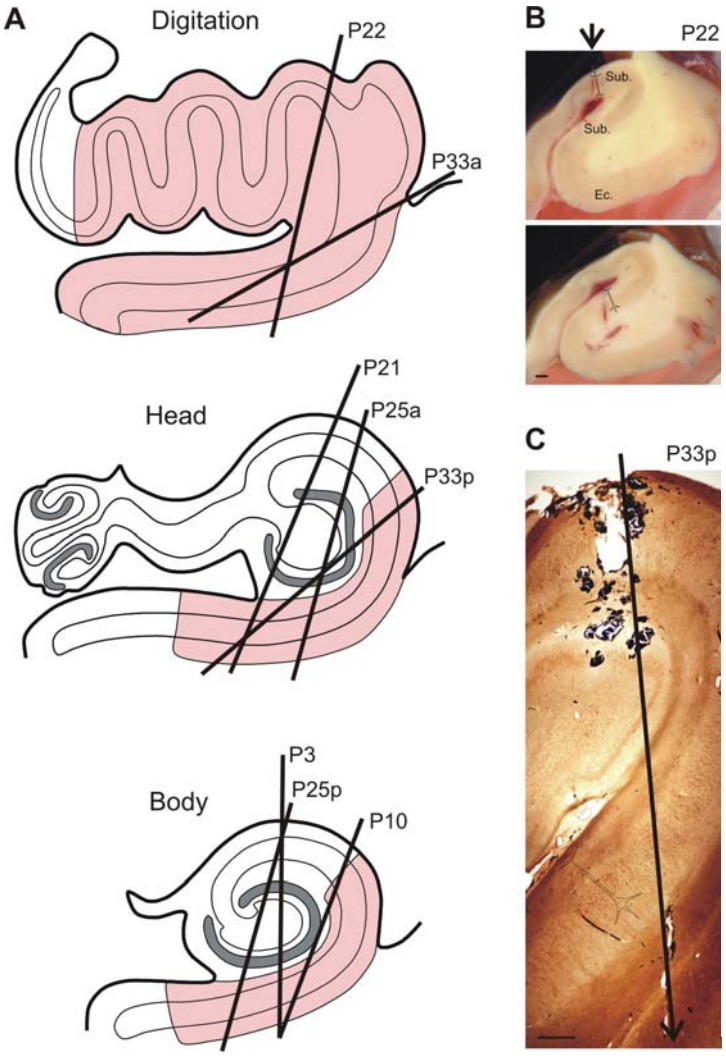

Figure 10.

A) Schematic drawings showing the location of the electrodes for the six patients included in the detailed analysis (P3, P10, P21, P22, P25 and P33). In two of these cases we inserted two electrodes, 6 mm apart from each other. The anterior traces are marked with *a*, while the posterior traces are marked with *p*. The Sub is indicated with pink color, modified from Duvernoy (Duvernoy, 1998) B) Photographs showing the electrode track in patient 22 (arrow), taken during sectioning of the resected block. The exact location of the electrode was determined after light microscopic examination. Ec.: entorhinal cortex. Schematic neuron illustrates principal cell orientation and approximate location of the pyramidal and apical dendritic layer. C) Light micrograph of a GluR2/3-immunostained section containing the posterior electrode track (arrow) in patient 33. A bleeding (black patches in the proximal Sub) occurred after the removal of the electrode. Scale bars: 1 mm.

Spike classification

In general, the detected subicular events closely resembled to the well known interictal discharges frequently recorded from the temporal lobe of epileptic patients: the early sharp spike component was followed by a late slow wave component (de Curtis and Avanzini, 2001). Detection, assignment of discharges into different subtypes and time zero definition for event triggered averages was established in all cases selected for detailed signal analysis.

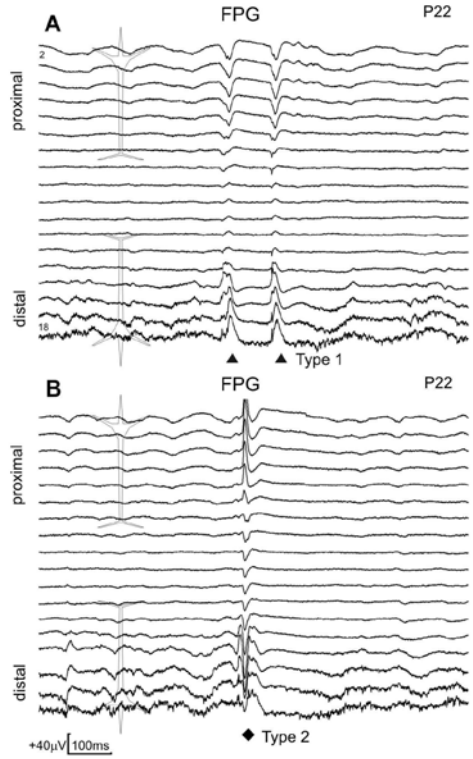

Figure 11.

Simultaneous FPG recordings of different types of interictal spikes from the proximal and distal Sub of patient 22. Continuous, non averaged data. The multielectrode crossed both the proximal and the distal part of the Sub in one penetration. Upper traces (channel 2) are close to the base of the multielectrode; lower traces (channel 18) are close to the tip. Spatial separation between traces is 200μm. Schematic neuron illustrates principal cell orientation and approximate location of the pyramidal and apical dendritic layers. Calibration: +40μV, 100ms, positivity upwards. The spikes appeared in a close temporal relationship to each other at both subicular locations. **(A)** Type 1 spikes (marked by triangles) with the major FPG deflection being positive in the distal and negative in the proximal Sub. **(B)** Type 2 spike (marked by a diamond) with the major negative deflection in the distal Sub. In the proximal Sub, the corresponding component is positive. Of note, a smaller positive peak (preceding the major negative deflection) was observed in the distal recordings, which was much less pronounced in the proximal traces, indicating the variability of Type 2 spikes

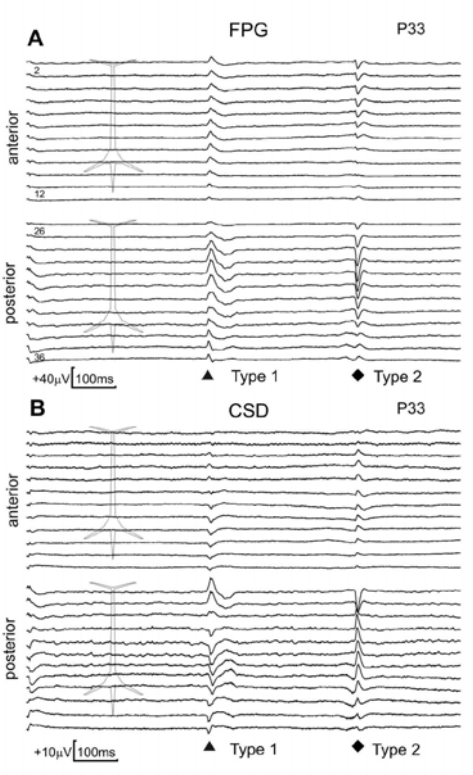

Figure 12.

Dual multielectrode, simultaneous FPG and CSD recordings from the anterior and posterior part of the Sub indicating successively appearing Type 1 (triangle) and Type 2 (diamond) spikes in a somatically oriented penetration. Continuous, non averaged data. As in the previous figure, the spikes appeared in a close temporal relationship to each other at both subicular locations. **(A)** FPG traces, eleven channels are shown from the anterior (channels 1-12) and from the posterior (channels 25-36) multielectrodes, recorded simultaneously. Spatial separation between traces on a given multielectrode is 200μm. Schematic neuron illustrates principal cell orientation and approximate location of the pyramidal and apical dendritic layers. Calibration: +40μV, 100ms, positivity upwards. **(B)** Continuous non averaged CSD traces from the anterior and posterior multielectrodes computed from the corresponding FPG. Calibration: +10μV, 100ms. Positive deflections indicate sources (outward currents), negative deflections indicate sink (inward currents). Since the tissue conductivity and electrode spacing were not taken into account, the CSD measurement unit is expressed in μV. Type 1 spike initial component is associated with brief somatic sink, inward, presumably depolarizing current complemented by sources from the dendritic region. Type 2 spike initial component shows an inverted sink-source pattern indicating a possible initial apical dendritic depolarizing mechanism.

Type 1 (n=255, 73.5%) spike was detected in all six, while Type 2 (n=92, 26.5%) was detected in four subjects. Patients with sHS showed significantly (Fisher exact test, $p>0.05$) greater number of Type 2 spikes than patients with mHS. Average spike frequency in sHS was 9.59spike/min (Type 1: 7.71spike/min, Type 2: 1.88spike/min), in mHS it was 9.14spike/min (Type 1: 8.93spike/min, Type 1: 0.43spike/min). Occasional epochs of rhythmic spiking activity (0.3-1Hz) were observed in four patients. To define time zero in each spike cluster for accurate analysis, single sweep CSD traces were further investigated. As a result, time zero was arbitrarily assigned to the peak of the initial CSD activation after threshold crossing.

The scenario, when a single electrode penetrated both the proximal (to CA1) and distal segments of the Sub in one track (P22, P33) are illustrated on Figure 11. In the majority of the spikes, the proximal part of the Sub showed initial sharp negative FPG peak around the somatic layer while the distal segment of the Sub produced positive FPG peak (Figure 11. / A). The minority of the spikes were characterized by inverted polarity FPG peaks with more complex morphology (Figure 11. / B). We have to note that FPG in our setup is a directional measurement, since the calculation is done in the preamplifier attached permanently to the electrode. If the tip of the electrode aims towards the soma, the resulting FPG at the same spatial location is minus one times of the case if the tip aims towards the dendrites, assuming similar current flow on the membranes. By careful co-registration of electrophysiology and anatomy, the localization of the electrode contacts with respect to the soma-dendritic axis was revealed, thus FPG readings were adequately interpreted.

Dual electrode recording experiments were made in two patients (P25, P33). The activity was simultaneously recorded from the anterior and posterior part of the Sub separated by 6mm. An example of typical single sweep FPG and corresponding CSD traces are shown from a dual electrode experiment on Figure 12. For simplicity, only twelve channels are shown.

Complex CSD, MUA and spectral characterization

When we tried to measure and statistically compare the average CSD waveforms, we faced a problem needed to be solved. During the experiment the dMEs shifted toward the deeper structures caused by the weight of the electrode holder and the preamplifiers.

The speed of this shift was 0 - 2,6 μm/sec (median 0.53) in the six patients selected for detailed analysis. This velocity meant that the median shift of the 200 μm dME was 1.53 electrodes (range 0-7.8) during the app. 10 min recording time. The shift leads to a continuously varying waveform in one particular channel, causing an artificial variability of the spike length and amplitude. This shift was corrected based on the assumption that the speed did not differ in time. Linear shifting coefficient was calculated by interpolating 100 virtual channels using spline fit method between the adjacent CSD channels. We determined the peak of the major deflection of the spike, and looked for the zero crossing electrodes between the largest sink and source. The linear shifting coefficient was approximated by fitting a line on the time curse of the zero channel position through the interpolated channels. Before the analysis every IIS was corrected in depth using the coefficient.

We calculated the CSD peak amplitudes and half amplitude duration (HW) for each individual spikes and we used Kruskal-Wallis ANOVA and Mann-Whitney U tests for statistical analysis. Alpha was set to 0.05.

Event triggered CSD, MUA and spectral averages for separate discharge classes were constructed for all the selected patients. Type 1 discharge revealed brief initial CSD sink (range: 47-78 ms, mean: 61 ms and HW: 25 ±7ms) in the somatic layer (Figure 13.), while the late wave component was associated with longer lasting (range: 50-300ms, mean: 187 ms) source current in the same location (Figure 14.). Both the early somatic sinks and late sources were complemented by early sources and late sinks respectively in the dendritic layer (Figure 14.).

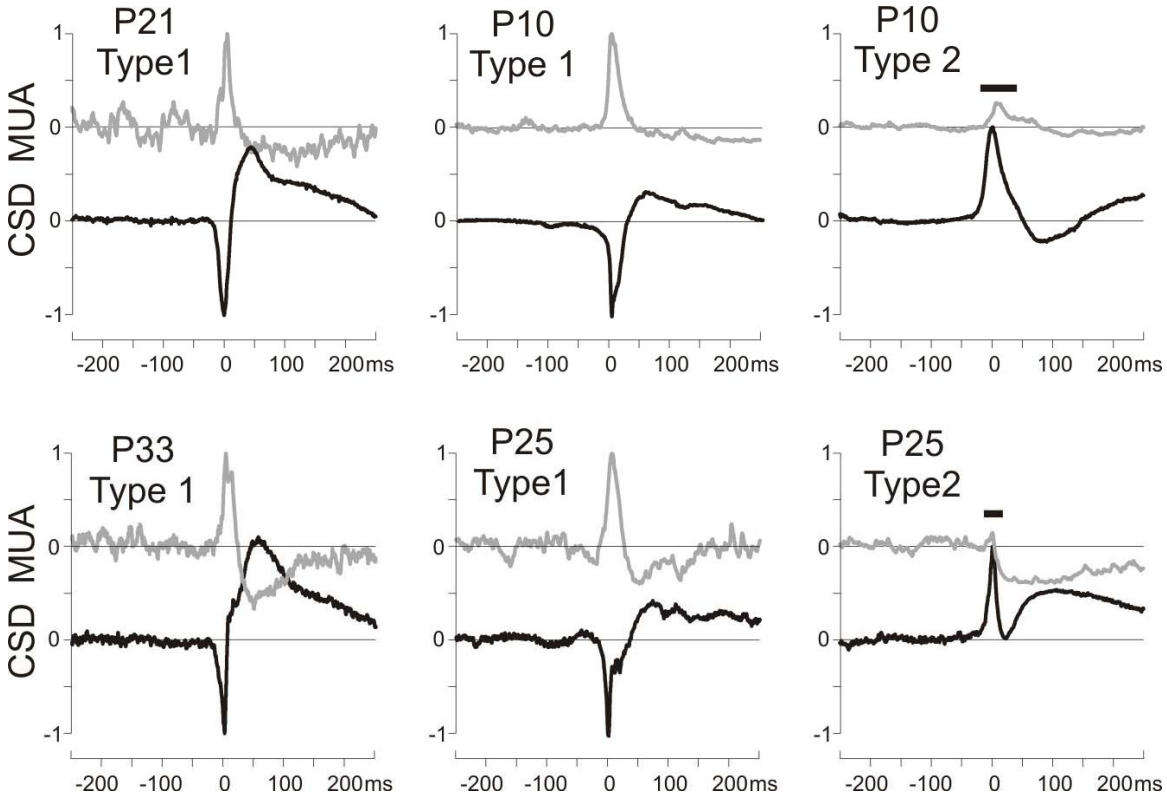

Figure 13.

Averaged CSD and MUA traces recorded from the pyramidal layer. Representative data from four patients indicating Type 1 (P10, P21, P25, P33: left two columns) and Type 2 (P10, P25: right column) spikes. In order to compare the time course of Type 1 spikes between patients, CSD and MUA averages (P10, P21, P25, P33: left two columns) were scaled to 1 using the peak values of the initial activation. In the right column, indicating Type 2 spike, only the CSD peak was scaled to 1, while MUA was scaled with the value derived from the Type 1 peak. This permits comparison of the MUA amplitude ratio between Type 1 and Type 2 spikes recorded from two patients (P10 and P25). For Type 1 spikes, the CSD and MUA time courses show remarkable similarities between patients. The shape and timing of the initial sink and MUA increase nearly overlap, while the late source and MUA decrease are also similar in appearance. The CSD and MUA time courses of Type 2 spikes show less correspondence between patients, but the main characteristics are similar: the initial source is followed by a developing sink and concludes with a slow source. MUA recordings revealed an initial small firing rate increase followed by a variable firing rate decrease during the late part of Type 2 spike. Comparison of Type 1 (middle column) and Type 2 (right column) spikes in the same patient (P10, P25) revealed inverted initial CSD activation pattern, while the late wave component appeared to be quite similar. MUA during the initial part of Type 1 spikes was significantly larger (indicated by the thick line above the plot) than in Type 2 spikes (t-test, $p<0.01$) in both cases.

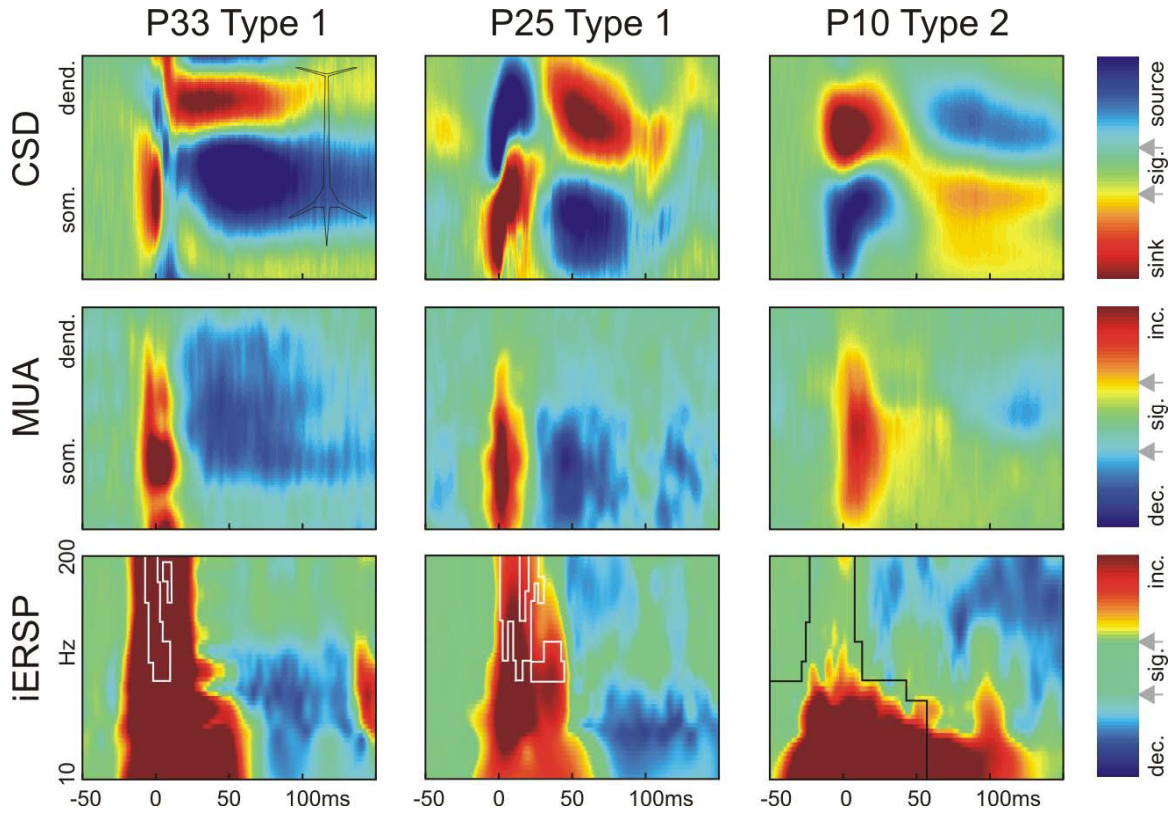

Figure 14.

CSD, MUA and iERSP maps of Type 1 and Type 2 spikes in different patients (P10, P25 and P33). X axis indicates time: from -50ms to 150ms, Y axis indicates depth: covering 2mm of the Sub. Approximate locations of somatic and apical dendritic layers are abbreviated on the figure. Small schematic pyramidal cell shows the orientation of the recording. Cold (blue) colors indicate activity decrease (dec.) compared to baseline, while warm (red) colors indicate activity increase (inc.) compared to baseline for MUA and iERSP. CSD sink is depicted in red, source in blue. Color range was adjusted so that both increases and decreases were visible. iERSP is shown from one channel located in the pyramidal layer. Statistical comparison to baseline was performed using a t-test for CSD and MUA, and bootstrap analysis for iERSP. Significance level (bootstrap: $p<0.01$, t-test: $p<0.01$) is indicated on the side color bar by arrows. Statistically non-significant activity in iERSP is shaded green. Type 1 spike is initiated by an inward current and firing rate increase in the pyramidal layer, accompanied by a presumably passive source in the dendritic region. iERSP during this period revealed a significant wide band oscillatory power increase up to 200Hz. The wave component was accompanied by a source and firing rate decrease in the pyramidal layer, accompanied by a presumably passive current sink in the apical dendritic region. iERSP during the wave component showed a significant oscillatory power decrease. Type 2 spikes showed an inverted initial CSD pattern with an MUA increase in the pyramidal layer and accompanying spectral activity increase up to 100Hz. The wave component was associated with later CSD inversion, as well as firing rate and spectral activity decreases. Significant differences (Kruskal-Wallis ANOVA, $p<0.05$) between Type 1 and Type 2 spikes are indicated by the inclusion area of white (Type 1 activity is significantly higher than Type 2 activity) and black (Type 2 activity is significantly smaller than Type 1 activity) lines in the iERSP color map for the initial spike component.

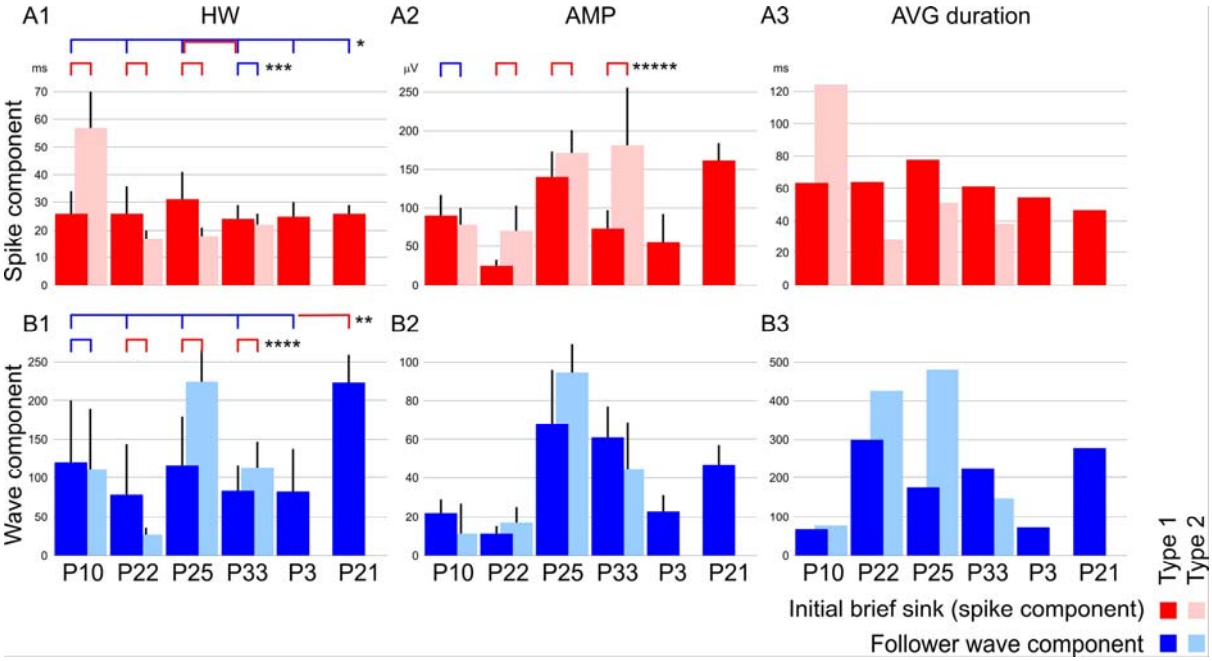

Figure 15.

Statistical comparison of type 1 and type 2 spikes. (A1 and B1): HW (half amplitude duration) of the active CSD component that means the sink for the initial brief transients (red and pink colors, "spike component") or the source for the wave components. Note clips signed by *: type 1 spike's initial sinks did not differ significantly between cases, except the longest (P25) and the shortest (P33) case. The same relation can be found for type 1 waves signed by **. The only outlier was the longest P21 case. Whereas there was significant differences between type 1 and type 2 spikes with a few exceptions. Note marks *** and ****. The spike component for type 1 spike was usually longer. **(A2 and B2)**: Amplitudes of the same active CSD components. The sign ***** marks the case by case comparison of spike components. Note that the amplitude of type 2 spike was usually higher. **(A3 and B3)**: Total average duration of the previous CSD components. The low variability of type 1 spike's initial brief component and the superiority above type 2 spike components can be observed.

Red and pink bars (A1-3) show initial sink ("spike component"), blue and light blue bars (B1-3) show wave components. Dark colors depict type 1, light colors type 2 spikes.
Statistical analysis (Blue clips indicate non significant $p>0.05$, red clips significant $p< 0.01$ differences; Kruskal-Wallis ANOVA)

Figure 15. shows the case by case comparison of these variables. The Kruskal-Wallis ANOVA analysis of the duration of initial sinks did not show significant differences ($p<0.01$), except the longest (P25) and the shortest (P33) durations. The same was found for the duration of the waves. Only the wave in one case (P21) was significantly longer than the others (marked by *, and **).

MUA showed significant (t-test, $p<0.05$) increase during the peak of the initial spike component, while it decreased below baseline during the late wave component in the somatic region ($p<0.05$). iERSP analysis revealed significantly increased ($p<0.01$) broad band spectral activity (10-200Hz) during the spike, and later decrease ($p<0.01$) mostly in the 15-100Hz range during the wave in the somatic region (Figure 14.).

Type 2 discharges showed greater inter- and intra-subject variability (Figure 13.). In essence, the initial spike component (HW: 40 ±22ms) was accompanied by sources in the somatic and sinks in the dendritic region followed by another fast, but lower amplitude sink-source pair concluding with a slow source-sink pair contributing to the wave component (range: 50-500ms) of the discharge. Initial spike component related MUA in the somatic layer was significantly smaller than in Type 1 discharge (t-test, $p<0.05$, data not shown), but still significantly greater than the baseline activity ($p<0.05$, Figure 14.). The late, wave component associated MUA decrease was also detectable, but substantial variations occurred. It was either not changed compared to Type 1 MUA or it was significantly smaller or larger depending on the subject the data was recorded from. Type 2 event iERSP analysis showed significantly smaller (t-test, $p<0.05$, data not shown) initial activation increase in higher frequency activity (100-200Hz), than in the case of Type 1 spike. The wave component associated later spectral activity decrease was present, but mostly in the higher frequencies (Figure 14.).

Comparing the different types of discharges we found that the amplitude of initial sinks was lower in the type 1 discharge than in the type 2 ($81.2\mu V \pm 46.12\mu V$ vs. $103.8\mu V \pm 55.1\mu V$ $p=0.03$). The previously mentioned relationship was true for three cases (P22, P33 $p<0.01$, P25 $p>0.05$), with the exception of one case (P10) where we found opposite relationship. (Figure 15.) The duration of the initial sink was longer in the Type 1 discharge than in the Type 2 (25 ±7ms vs. 40 ±22ms HW, as seen above), which relationship was true again for three cases (P22, P25 $p<0.01$; P33 $p>0.05$), except the P10 case.

Intrasubicular and temporal lobe interactions

In order to further characterize intra-subicular (n=3) and subiculum-temporal lobe (n=2) discharge relationships, FPG, CSD and ECoG was analyzed. Spike time delay, synchrony index and spike amplitude correlation was computed using data obtained from spatially distinct subicular locations. In addition, spike onset and peak time delays and peri-event time histograms (PETH) were calculated using data obtained from simultaneous subicular and temporal lobe ECoG recordings.

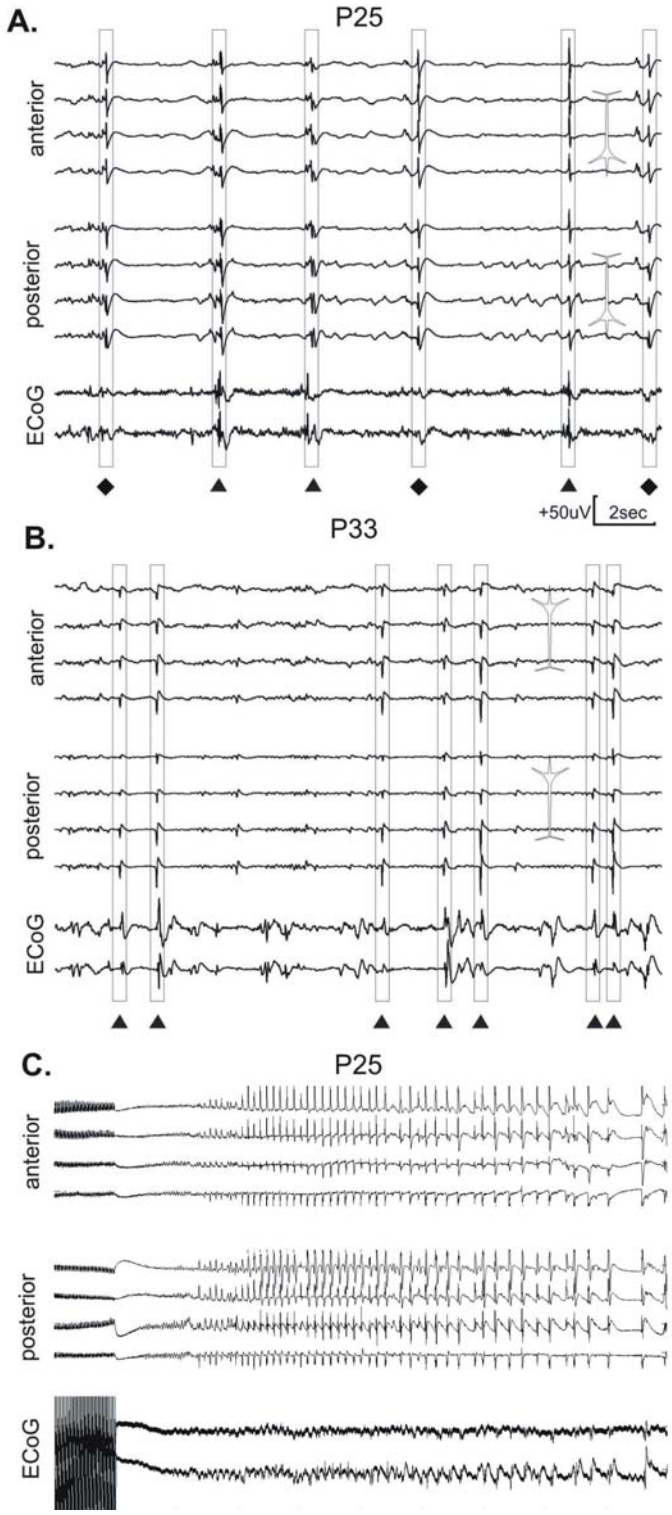

Figure 16.

Relationship of subicular and temporal lobe spiking. **(A)** Simultaneous dual laminar and ECoG strip electrode recordings from the anterior and posterior Sub, and temporal lobe in patient 25 in a somatically oriented penetration. Continuous, non averaged data. Temporal lobe strip electrode contacts were localized at the base of the temporal lobe, lateral to the inferotemporal sulcus. Four representative subicular traces separated by 400μm are shown from both anterior and posterior regions, while two representative ECoG traces are shown from the strip recordings. Type 1 (triangles) and Type 2 (diamonds) spikes arise synchronously at both subicular locations. Temporal lobe interictal spikes with a sharp initial component show a close timing relationship with Type 1 subicular discharges, while much less activity was seen in the temporal lobe during Type 2 (diamonds) spikes. **(B)** Similar recordings from patient 33. In this case the penetration was oriented dendritically as depicted by the inverted pyramidal cell. Each detected Type 1 (triangle) subicular spike was accompanied by a temporal lobe interictal spike. Local generation of temporal lobe spikes is highly possible, since in most cases the initial component of the ECoG spike inverted between strip contacts 5 and 6. Of note, smaller (not detected) subicular spikes were not clearly associated with temporal lobe spikes, in addition, several temporal lobe spikes lack corresponding subicular spikes **(C)** Typical after-discharge pattern in patient 25. The initial 50 Hz train stimulus elicited recurring afterdischarges lasting for 10 sec with average 3.5 Hz repetition rate. Note the close synchrony between ECoG and subicular spikes at both recording sites.
ECoG: Elecrocorticogram,

In both single (Figure 11.) and dual (Figure 12., Figure 16) multielectrode experiments, reaching distinct subicular locations, high degree of spike synchrony was observed. Detailed analysis revealed that synchronous subicular discharges were almost exclusively of the same type. Intra-subicular spike time delays in dual multielectrode experiments were estimated from the event triggered CSD to eliminate volume conduction effects. The largest amplitude sink (in the case of Type 1 event) and source (in the case of Type 2 event) peak at a given multielectrode was chosen as triggering base for the averages. We found, that a certain discharge type emerge at anterior and posterior subicular locations separated by 6mm with an average absolute sink or source peak time delay of 2.3ms (values: -3ms, 0ms and 4ms) with no clear association, which location produces the leader of follower event (Figure 17 / A). In cases when a single multielectrode covered both the proximal and distal part of the Sub in one track (Figure 11), the initial sink and/or source was not concurrently available due to positioning problems, thus discharge timing was estimated from FPG threshold crossing. Absolute time delays between the proximal and distal subicular locations were in the range of 0-10ms. Next we examined how often the spikes emerged in such a close temporal relationship at distinct subicular locations. We found that a large proportion (89-100%) of similar type spikes occurred concurrently (within a ±10ms window) between anterior-posterior and proximal-distal sites, expressed by the synchrony index (Figure 17 / B), suggesting strong functional coupling within the Sub. Correlation between spike peak FPG amplitudes measured at different locations was moderate to high, and it was significant in all except one case (Figure 17 / B), indicating strong linear relationship between activities at distinct subicular locations.

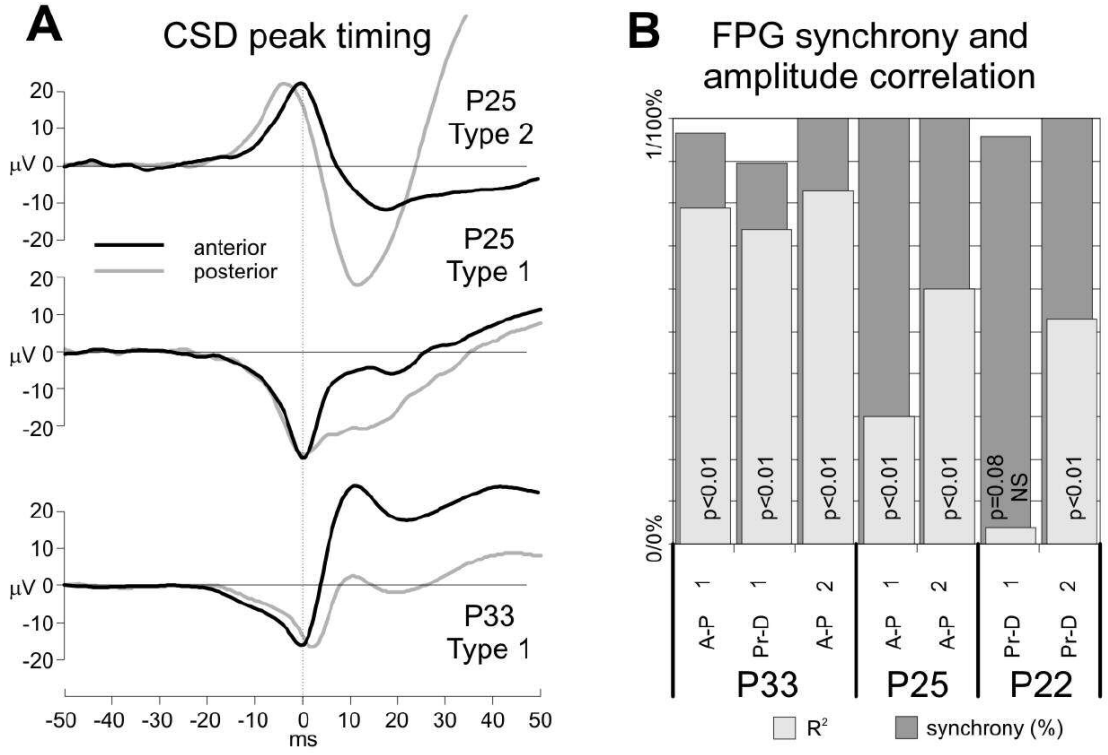

Figure 17.

(A) Examples of event triggered CSD averages at different subicular locations. Upper superimposed traces show Type 2 spike CSD derived from the pyramidal layer. Event triggering was based on the anterior Sub electrode (dark trace). The resulting CSD peak at the posterior Sub (light grey trace) preceded the anterior Sub CSD peak by 4ms. Middle superimposed traces show Type 1 spike CSD derived from the pyramidal layer of the same patient (P25). In this case event triggered CSD peaks were concurrent, with no delay. Lower superimposed traces depict spike Type 1 event (anterior Sub peak) triggered CSD from patient 33. In this case, the posterior Sub (light grey trace) follows the anterior (black trace) Sub CSD peak by 2ms delay. **(B)** FPG synchrony index and amplitude correlation. Correlation coefficient (Pearson's r^2) and its significance is shown with light grey bars between the peak FPG amplitude at distinct subicular locations in three patients (P22, P25, P33) with proximal-distal and/or anterior-posterior penetrations for separate spike types (1 and 2). Synchrony index is shown with dark grey bars.

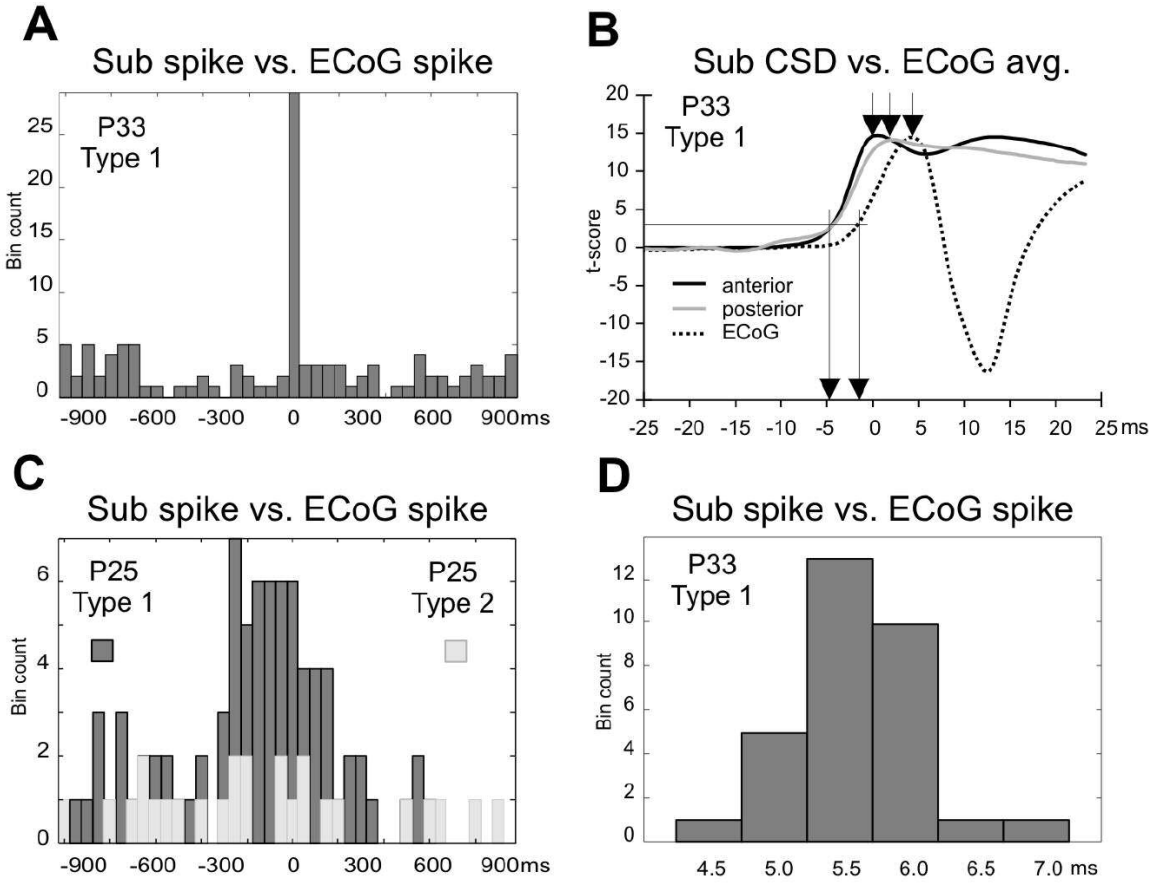

Figure 18.

(A) Timing relationship between Type 1 subicular spikes and temporal lobe ECoG spikes (P33); peri-event time histogram, -1000ms to 1000ms, 50ms bins. **(B)** Onsets and peaks of averaged, event triggered (based on the anterior spike peak) subicular CSD and temporal lobe ECoG spike, t-score plots (P33). The CSD of Type 1 spikes derived from the pyramidal layer was inverted in order to illustrate onset and peak differences compared to the ECoG. Anterior Sub CSD: dark line; posterior Sub CSD: light grey line; temporal lobe ECoG: dashed line. Long arrows indicate the onset (t-test: $p<0.05$) of activity. The onset of subicular activation is followed by the onset of the temporal cortex spike by 4ms. Short arrows indicate the peak of the activity. Both Sub CSD peaks are earlier the than ECoG spike peak by 3 to 5ms. **(C)** Timing relationship between Type 1 (dark grey) and Type 2 (light grey) subicular spikes, and temporal lobe ECoG spikes (P25); peri-event time histogram, -1000ms to 1000ms, 50ms bins. **(D)** Short time peri-event histogram (bin size: 0.5ms) of Sub CSD peak (time zero) and temporal lobe ECoG spike initial peak. All of the detected Sub spikes preceded temporal lobe spikes with a median latency of 5.5ms.

In addition to intra-subicular discharge synchronization, we found that temporal lobe spiking was clearly associated in time with the subicular events (Figure 16Figure 18). Long time scale PETH revealed close temporal spike coupling between Sub and temporal lobe in P25 and P33 (Figure 16, Figure 18 / A, B). This association was strong for Type 1 event in P33, weaker and broader in P25 for the same type, and virtually absent in P25 for Type 2 discharges (Figure 18 / C). To investigate temporal

directionality between Sub and temporal lobe in the P33 case, spike onset and peak timing was further analyzed. The timing of the initial sink peak and the earliest initial ECoG positive peak was correlated. Short time scale PETH showed that the earliest ECoG positivity follows the subicular sink peak with a 5.5ms ±1ms delay (Figure 18). The delay was further confirmed by event triggered averaging based on the sink peak. On Figure 8B t-scores (compared to baseline period) of CSD (multiplied by -1 for better visualization) from the anterior and posterior Sub and the t-score of temporal lobe ECoG is shown. It is evident, that both the onset and peak activity is earlier in the Sub, than in the temporal lobe, suggesting possible subicular driving role.

Evoked after-discharges

We applied electrical train stimuli (15mA, 50Hz, 2 sec duration) to the temporo-basal region that elicited spontaneously recurring after-discharges (AD) in the subiculum. Six AD sequences in three cases were involved in the analysis with 114 events. The average repetition rate of the individual ADs in the AD sequence was 3.51 Hz. (Figure 16 / C)
The spikes in the AD sequence had complex morphology. (Figure 19 / B) The spike and wave sequence was preserved but the spike had biphasic morphology. The initial sink was located in the somatic region resembling Type 1 discharge, which was followed by a somatic source contributing to the biphasic initial activation. This second component usually resembled the laminar distribution of the Type 2 discharge. The wave differed from the waves of interictal spikes since contained always somatic sinks that was not observed under spontaneous condition.
The initial biphasic spike of AD was associated with MUA enhancement and increased HFO activity. The spike was higher in amplitude (-318.6 ± 114uV vs. 81.2µV ± 46.12µV $p<0.01$) but shorter in duration (19.3 ± 6.2ms vs. 25 ±7ms $p<0.01$) compared to the same parameter of Type 1 discharge.

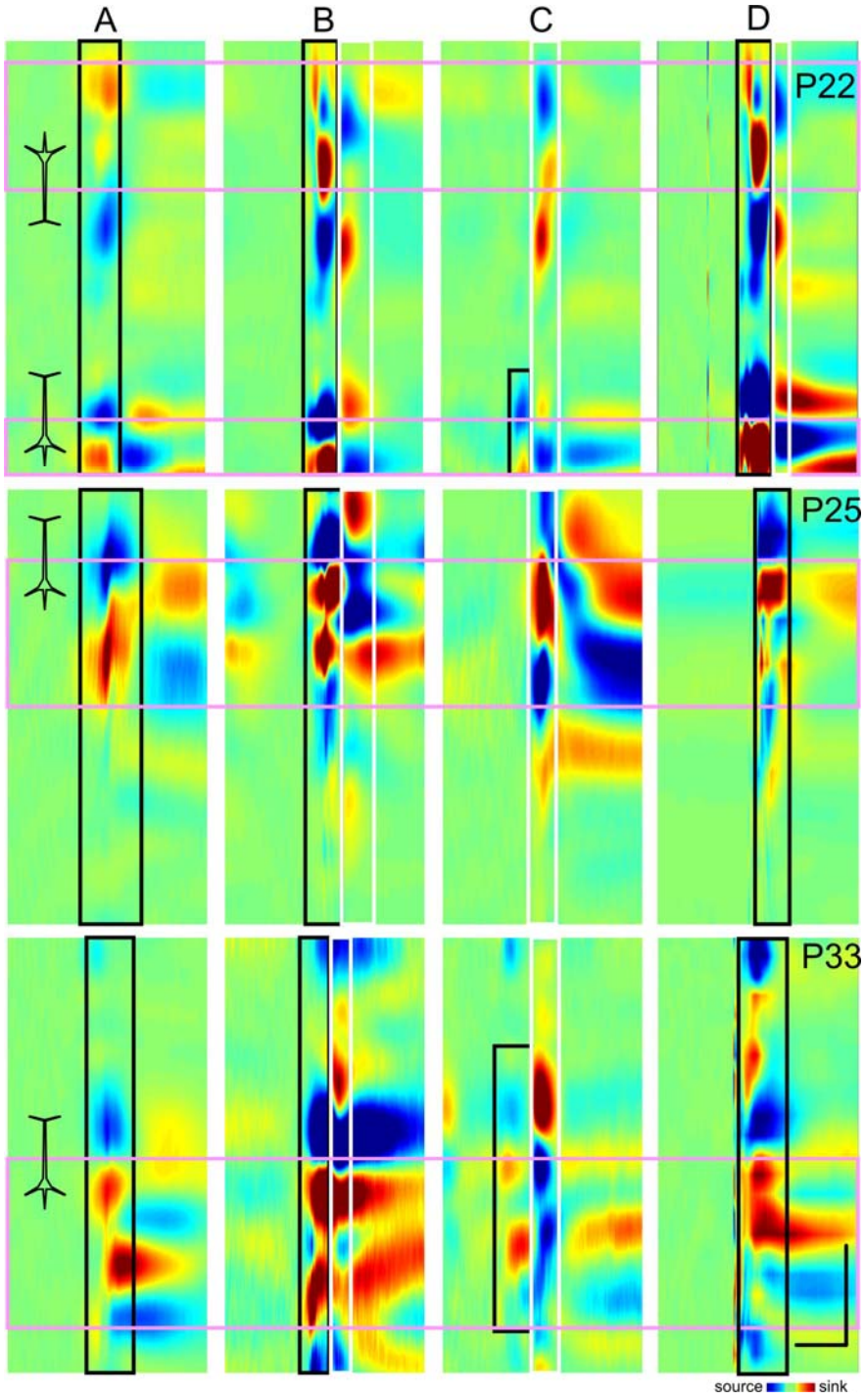

Figure 19.

Complex CSD pattern comparisons in 2 representative cases. Averaged CSD maps. **(A)** Type 1 spikes. **(B)** Evoked afterdischarges (AD). **(C)** Type 2 spikes. **(D)** Single shot stimulus evoked potentials (EP).
Black boxes indicate type 1 excitation with somatic sink, and white boxes type 2 excitation components with somatic source. The sink-source distribution was nearly opposite in several cases (P22, P33 A vs. C). Note the combination of type 1 and type 2 components in AD **(B)** sequences in all the cases. This sequential co-activation during EP **(D)** is visible only in P22 case. Note also the occasional low amplitude type 1 somatic sink preceding type 2 spike **(C)** in P22 and P33.
Pink box indicate cell layers. Schematic neurons show the orientation of pyramidal cells.

The HFO content of the AD spike was significantly higher than in the regular IIS. (Figure 20) The detailed spectral analysis of the HFOs associated to the initial sink revealed the existence of both ripples and fast ripples. The peak frequency was 106.4 ± 18.26Hz for ripples, and 192 ± 88.74Hz for fast ripples.

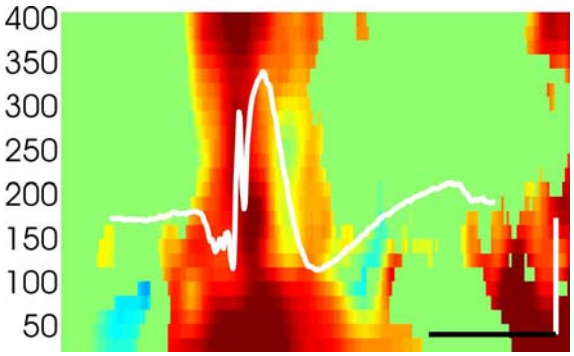

Figure 20.

Comparison of high frequency content of AD vs. type 1 spike. Red colors indicate the area that correspond the superiority of AD. Only significant values (Kruskal-Wallis ANOVA) are plotted, non significant values are homogeneously green. The white waveform in the middle represent averaged AD spike centered in the highest ripple peak. Scale bar: 50 μV white vertical, 50 ms black horizontal. Values on left represent Hz.
AD: after-discharge

Evoked responses in the Subiculum

To examine the effect of temporo-basal stimuli on the Sub we applied 25 or 50 single electrical current pulses with 2 sec interstimulus interval between the adjacent contacts of the strip electrode in five cases. The evoked potentials (EP) were later averaged in the Sub. During the electrical cortical mapping we tested every possible adjacent electrode pairs. In four cases we used different stimulus strengths (5, 10 and 15mA) in order to describe the stimulus site and strength dependence of the EPs.

Complex CSD and MUA characterization

The EPs started with an initial sharp sink in the somatic layer (range: 40-60 ms), followed by a wave (range: 100-500 ms). (Figure 19 / D) The CSD distribution resembled the Type 1 IIS because the initial sink was located in the somatic layer. A representative case is illustrated on Figure 21. The whole reconstructed CSD map is shown.

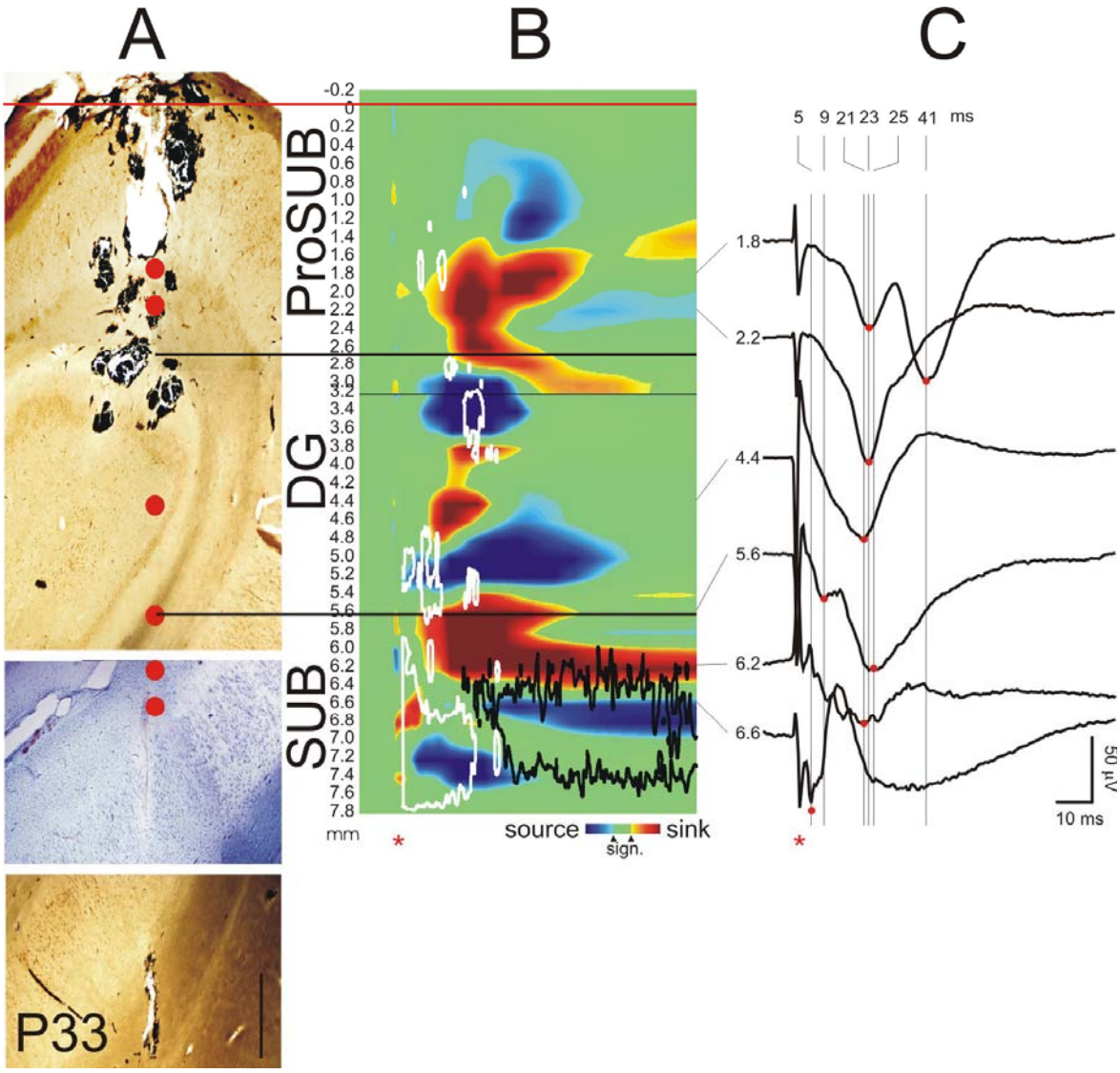

Figure 21.

Averaged evoked response from 3-4cm apart from the temporal pole, with 15mA (A) Histological reconstruction of the electrode track. Red dots indicate selected recording sites in (C) Scale bar 1 mm. **(B)** Reconstructed CSD map. Red colors are significant sinks, blue colors sources. The red line indicates the ependymal surface; the black lines indicate the borders between DG and Sub. The white line delineates significant MUA increase, the black line MUA decrease in space and time. X axis: time, scale is the same as in (C). **(C)** CSD traces from selected depths (values on the left represent mm). Vertical lines are correspondent to peak latencies in different depths. Red stars show stimulus artifact.
CSD: current source density; MUA: multiple unit activity; Prosub: prosubiculum; DG: dentate gyrus; Sub: subiculum;

In order to investigate the activity of input volleys we analyzed the initial sinks that represent feed forward excitation (Liu and Bilkey, 1997; Vida et al., 1995).

A clearly visible sink pair was found around the fissura hippocampi (indicated by the black lines in Figure 21./ B both when the electrode entered (2.2 mm) and exited (5.6 mm) the DG. Between the sinks there were sources in the granule cell layer and the hilus. These cell rich zones (between 3.2-3.6 and around 5 mm) were highlighted by MUA increase (white line). Bellow the DG the Sub is present with more complex evoked potential. Different sublayers activated in the Sub. The order of the sinks is illustrated in Figure 21./C. The earliest sink appeared in the deeper located pyramidal sublayer of the Sub (6.6-6.8 mm). The onset latency was less than 5 ms. (Note that the decay of the stimulus artefact took app. 4-5 ms, thus 5 ms was the minimum detectable onset latency for any responses.) The peak latency was 5 ms (Figure 21. / B). A sink around the fissura hippocampi under the ventral blade of the DG (5.6 mm) was the following with 9 ms peak latency. Multiple sinks were activated at 21-23 ms including the fissura hippocampi (both 2.6 and 5.6 mm) the superficial pyramidal layer of the Sub (6.2 mm) and prosubiculum dendritic layer (1.8 mm). The later structure produced a late sink with a peak at 41 ms.

Very early MUA increase was associated with the EP. The unit activation showed similar biphasic pattern as Type 1 spike. The initial somatic sink went hand in hand with the MUA increase, as shown on Figure 21. / A between 5 and 20ms, which decayed rapidly under baseline during the wave that lasted more than 100 ms.

Electrical cortical mapping

The Figure 22. illustrates the result of the electrical mapping of the same case discussed previously. The particular EP that was plotted on Figure 21. can be found in the black frame. The stimulus sites are named according to their distance from the temporal pole measured in centimetres.

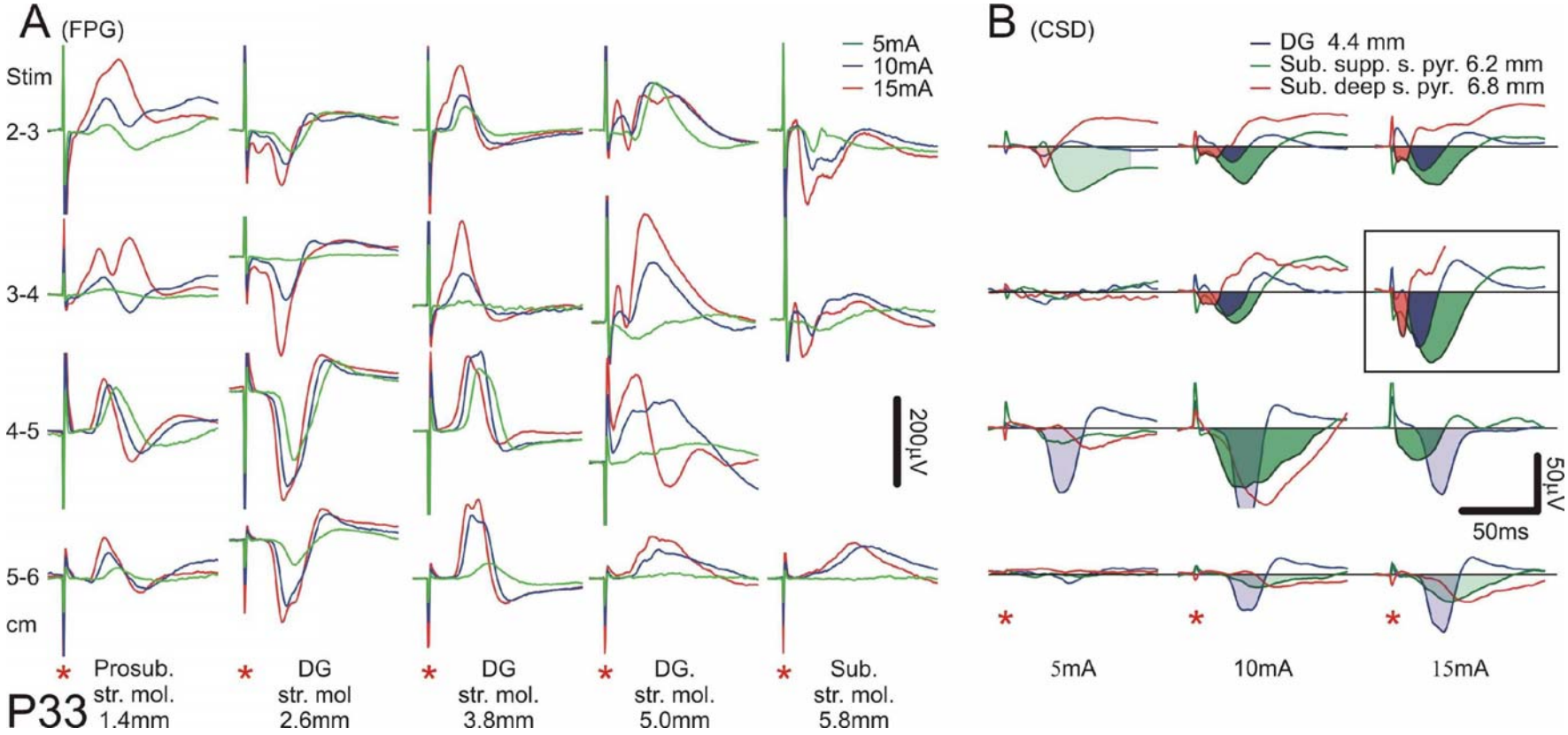

Figure 22.

Cortical mapping of evoked responses (A) Field potential gradients. Different stimulus strengths can be compared from different recording depths and stimulus site**s.** Note the advancement of response in parallel with the increased amplitude corresponding to higher and higher stimulus strengths. **(B)** CSD traces from different recording depths in the Sub and DG depending on stimulus site and strength. Red shaded area represent deeper - , green shaded area superficial pyramidal layer sink. Blue shading indicate sinks in the DG corresponding to perforant path activation. Note the early somatic sinks before perforant path sinks. The light shaded areas represent longer delay responses in the same depths. The black frame indicates EP in Figure 21. The recording depths are correspondent to Figure 21./ A.

Red stars indicate stimulus artifacts.
FPG: field potential gradient; CSD: current source density; DG: dentate gyrus; Sub : subiculum; str. mol: stratum moleculare; str. pyr: stratum pyramidale; supp.: superficial prosub: prosubiculum. Stim stimulus

The CSD distribution of EPs showed significant differences among stimulus sites. The earliest sink in this experiment was found in the deeper pyramidal layer of the Sub (shaded red). This sink was elicited only from stimulus sites 2-3 cm and 3-4 cm with 10 and 15mA. The superficial layer sink (shaded green) was elicited from a wider area but the onset latency was variable. From 4-5 cm this sink was the earliest activation. The fissura sink (shaded blue) showed opposite modulation than the somatic ones, from 4-5 and 5-6 cm it was higher in amplitude and from 5-6 cm it preceded the somatic sink, while from sites 2-3 and 3-4 slower amplitude was present.

We analyzed the amplitude of largest initial sink relative to the stimulus location and stimulus strength. The CSD amplitudes were taken into account to eliminate any volume conducted components of the cortical and adjacent hippocampal activation. We calculated the relative amplitude compared to the maximum amplitude CSD in each particular recording position to exclude the differences in CSD amplitude stemming from the different insertion angle of the cases. This ratio was used for any statistics of EP amplitudes.

The onset latencies of EPs correlated negatively with amplitude, resulting that the faster responses were higher in amplitude ($r=-0.63$, $p<0.001$). (Figure 23. / A3). The progressive change in the EP amplitude, and the advancement of higher amplitude responses are illustrated in Figure 22. / A. The amplitude of evoked responses correlated with stimulus strength (Pearson's $r=0.51$, $p=0.001$), even if the stimulus site was not taken into account (Figure 23. / A2). The Figure 23./ A1 illustrates the amplitude saturation curves in the Sub in eleven trials of three successfully tested patients. In two trials the response threshold was above 10mA, in three trials it was between 5 and 10mA, and in the other (six trials) the response threshold was below 5mA. The mean response curve was linear (red line). Extrapolating this finding, Sub probably can produce even higher responses that we were able to evoke by 15mA stimulation. In average, 5mA stimulus evoked 27%, 10mA stimulus 54 %, and 15mA 85 % of maximal amplitude response (reachable by 15mA).

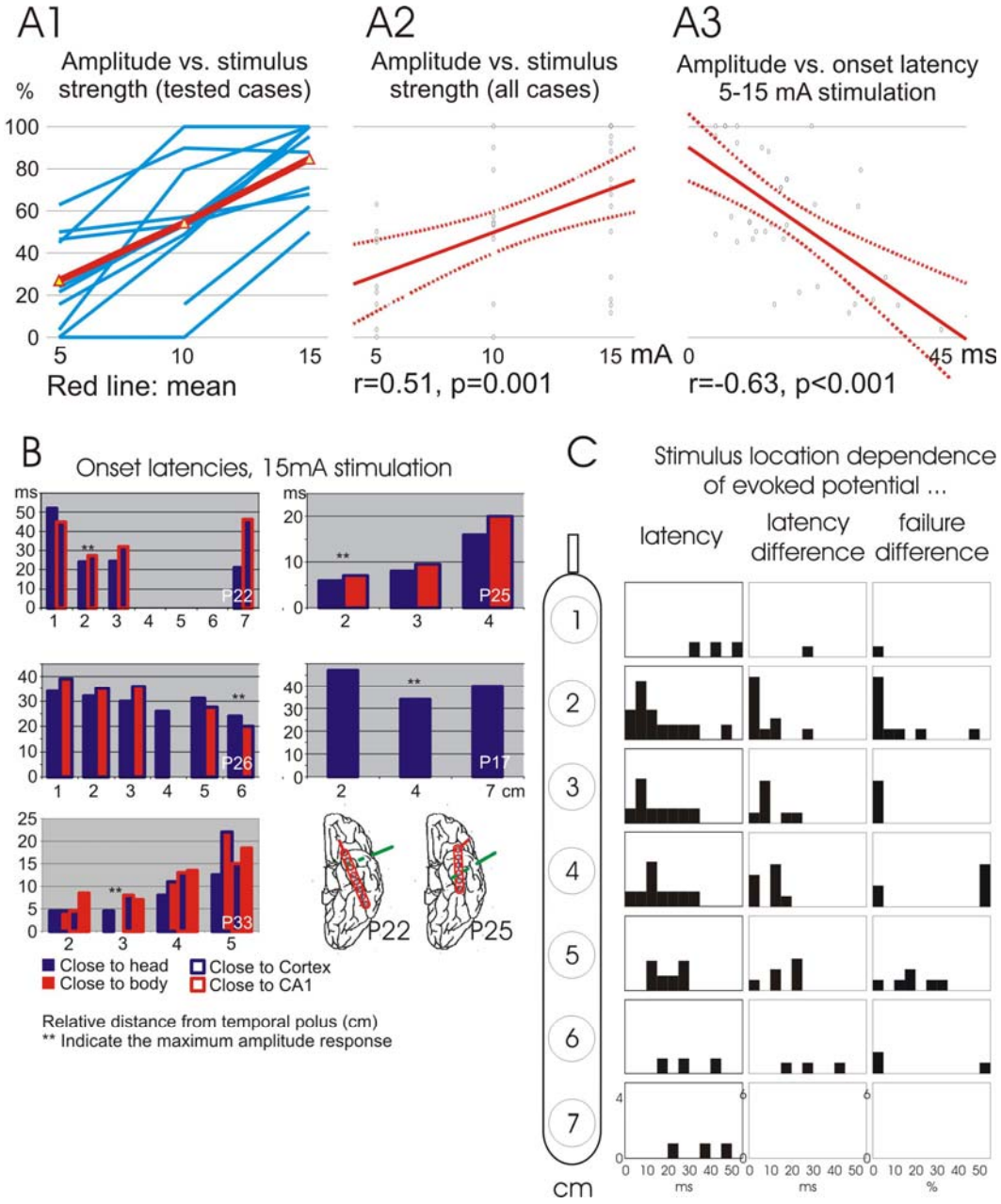

Figure 23.

Evoked response statistics (CSD amplitudes are given in percent of the largest amplitude recorded from the particular position of the electrode.) **(A1)** Response characteristics depending on stimulus strength. Only those cases and stimulus sites were involved that different stimulus strengths were applied. (Blue lines: individual cases; red line with yellow triangles: average. **(A2)** The average interdependence of amplitude and stimulus strength irrespective of stimulus site. **(A3)** Relationship between onset latency and the response amplitude. Dotted line: 95% confidence interval. **(B)** Case by case comparison of onset latencies following 15 mA stimuli. Note the short latency response surrounded by longer latency or absence (P22) of responses. **(C)** Onset latency and synchrony between recording sites. Note that short latency <5ms stimuli are restricted to 2-4 cm from the temporal pole. From this site the recording sites were reliably (low failure difference) synchronous (low onset latency difference).

We analyzed the onset latencies of the largest initial sinks relative to the stimulus location. It varied between 4.5 and 50 ms, implying the existence of single and multiple synaptic connections between the temporo-basal regions and the Sub. (Figure 23. / B, C column 1). There was a 2 cm range between 2-4 cm apart from the temporal pole that evoked the fastest and highest amplitude EPs. This "hot spot" was surrounded by progressively higher onset latency sites both anterior, and posterior. The case by case analysis of the same parameter revealed the same result. (Figure 23. / B). There was only 1 exception, case P22, where the same kinetics was followed but there was a 3-4 cm gap from where no EP could be elicited. From more posterior stimulus locations the EP reoccurred. In this case a relatively different position of the stimulating electrode was recorded, compared to the other cases. The strip electrode deviated from medial to lateral while distanced backward from the temporal pole. Probably this silent region was located more lateral to the measured areas in the other experiments.

The co-activation of different portions of the Sub was analyzed in those cases where antero-posterior or proximo-distal portions of the Sub were recorded. The synchrony between recording sites was determined by the difference of onset latencies, and the difference of the failure rates between EPs recorded in different portions of the Sub. The failure rate was calculated by the ratio of those stimuli that failed to evoke response, and the difference of this measure between the Sub sites gave an additional parameter to the synchrony. (Figure 23. / C). The fast and high amplitude EPs elicited from the above mentioned "hot spot" reflected in high degree of synchrony in the Sub, with less than 5 ms onset latency difference, and around zero failure rate difference. From farther stimulus sites, this synchrony broke down and up to 45ms onset latency difference occurred.

Spectral content of evoked potentials

Abundant high frequency oscillation (HFO) was found during the early excitation, which was followed by HFO decrease during the wave. The averaged waveforms are shown in Figure 24./ B. The red and green curves illustrate the band-pass filtered traces. The co-occurrence of slower and faster ripple activities is visible during the negatively deviating initial spike component.

The power spectrum analysis of EPs yielded usually 2 or 3 peak frequencies. One peak was recorded in the ripple range at 80-100Hz. This peak was much higher in power compared to that peak measured in spontaneous conditions. (Figure 24./ C). In all the three cases we detected activity in the fast ripple range. There was a peak at 150 Hz in every case and an additional peak at 200-250Hz in two cases (P25, P22). The presence of 150Hz fast ripple peak was unique for EPs. Both in spontaneous and in evoked AD conditions only the higher frequency peak appeared.

We were able to record CSD for both types of ripples. (Figure 24./ A). These oscillations were built up of alternating sinks and sources in the somatic layer of the Sub. The transition zone between the sinks and the sources differed slightly from that of the low frequency components of the EP. This suggests different synaptic contribution to the low frequency components and ripples in the human Sub. The fast ripples were detectable at 4-5 consecutive electrodes along the dME meantime that is correspondent to approximately 1 mm spatial extent. This was comparable to the cell layer thickness of the Subiculum. The fast ripple oscillation consisted of 5-6 complete cycles which was similar to the observation of previous authors in awake patients (Staba et al., 2002). (Figure 24./ B)

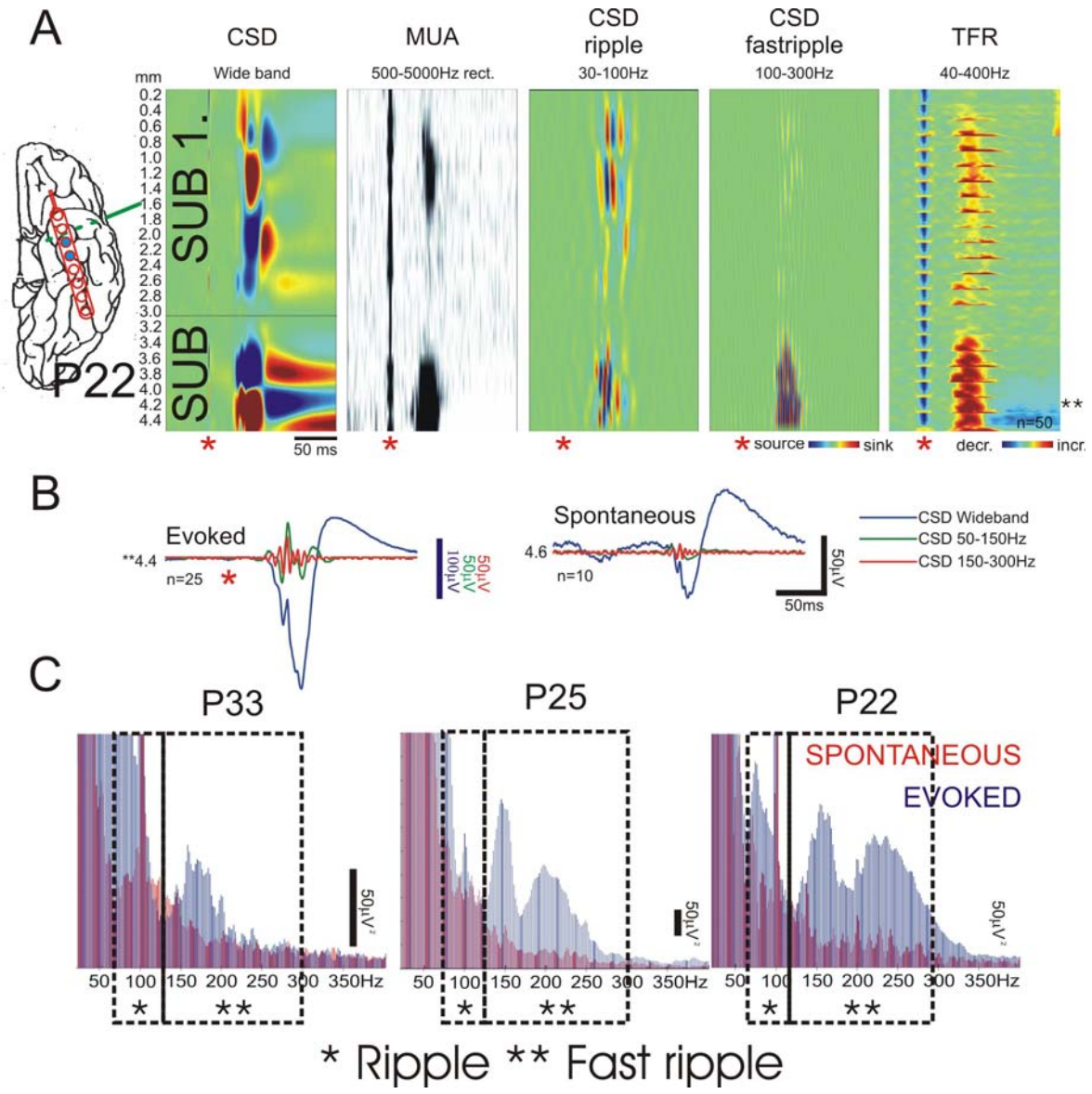

Figure 24.

Spontaneous and evoked high frequency oscillations (A) Layer specific comparison of CSD, MUA of EP, and CSD of EP related ripple and fast ripple oscillations. Broad band spectral distribution is also plotted. The ripple and fast ripple oscillations occurred in the MUA activation zone (str. pyramidale) mostly in the distal Sub. **(B)** Averaged ripple and fast ripple waveforms in spontaneous and evoked conditions. **(C)** FFT comparison of spontaneous and evoked potentials. Note the superiority of evoked response in every frequency range, and the unique 150 Hz peak recorded independently in multiple cases.

Sub: Subiculum; Sub1: proximal potion of the subiculum; CSD: current source density; rect.: rectified; TFR: time-frequency analysis; decr.: decrement; incr.: increment;

Discussion

We measured the interictal activity in eleven mTLE patients during anterior temporal lobectomy under general anaesthesia. Detailed FPG, CSD, MUA and spectral analysis of subicular electrical activity was performed on six patients. In two of the six cases, ECoG spikes were simultaneously obtained from the temporal lobe and were correlated with the subicular events.

In parallel with the multiple functions of Sub playing roles in a number of normal and pathologic processes, we have found multiple and complex spike generation mechanisms. The appearance of the subicular spikes closely resembled to the shape of the well known spike-wave discharges (de Curtis and Avanzini, 2001).

Based on the waveform morphology, two distinct discharge types were classified.

Type 1 event (73.5% of all) initial component started with brief inward current (sink) accompanied by cell firing rate and broad band spectral activity increase in the somatic layer with simultaneous outward current (source) in the dendrites. Increased cell firing rate with local inward current in the pyramidal layer strongly suggests active depolarizing, excitatory mechanisms at the soma of principal cells with passive, electrotonic return currents (source) drawn from the dendrites. Based on previous studies, the time course and localization of the early depolarizing current is at least partially compatible with the presence of fast glutamatergic excitation (Menendez de la Prida and Gal, 2004) in the pyramidal cell layer delivered through the local recurrent excitatory network (Harris and Stewart, 2001a; Witter, 2006). The wave component was characterized by longer lasting outward currents together with firing rate and spectral activity decrease in the somatic layer and simultaneous inward currents in the dendritic region. Decreased firing rate together with local outward current in the pyramidal layer strongly suggests active hyperpolarizing, inhibitory mechanisms at the soma of principal cells with passive, electrotonic return currents (sink) drawn from the dendrites. Membrane conductances underlying the late hyperpolarizing current cannot be clearly identified from extracellular measurements.

The rapid decay of the initial excitation is compatible with local circuit GABA-ergic inhibition (Cohen et al., 2002), while the later hyperpolarizing component is most likely to be a mixture of other synaptic (Cohen et al., 2006) and intrinsic (Alger and Nicoll,

1980) membrane currents, such as different kinds of potassium currents (Fernandez de Sevilla et al., 2006) or even disfacilitation (Gigg et al., 2000).

Resembling to Type 1 human spike activation sequence, electrical stimulation of CA1 in animals resulted in broad subicular excitation pattern including the pyramidal layer (Cappaert et al., 2007) with increased initial pyramidal cell firing followed by later action potential decrease (Gigg et al., 2000) and hyperpolarizing currents (Behr et al., 1998). Similar activation sequence was observed in human in vitro subicular slice preparations spontaneously or in response to electrical stimulation (Cohen et al., 2002; Wozny et al., 2005) suggesting that intrinsic activity can also be triggered by external input.

Type 2 event (26.5% of all) showed considerable spatio-temporal variability, which was in contrast to the more regular Type 1 event, suggesting more complex and/or less stable generator mechanisms. Its initial component started as a brief outward current in the somatic and inward current in the dendritic layer with relatively small firing rate and spectral power increase. In our opinion, one plausible interpretation of this pattern is the following. The flow of active excitatory, depolarizing currents located in the dendritic region cause passive return source linked by electrotonic conduction with the active dendritic sink (Uva and de Curtis, 2003; Wu and Leung, 2003). The following wave component emerged variably from the fading somatic source as a longer lasting outward current, while firing rate and spectral power decrease was present, although variable. Like in the case of Type 1 event wave component, its most probable generator mechanism is also a mixture of synaptic and intrinsic hyperpolarizing currents confined to the somatic layer. Cortical electrical stimulation in animals revealed initial apical dendritic excitation (Cappaert et al., 2007) with increased pyramidal firing and later action potential decrease (Gigg et al., 2000) accompanied by hyperpolarizing currents (Behr et al., 1998) in the Sub, which is in turn resembles to Type 2 in vivo human spike activation sequence. Whereas the role of subcortical inputs e.g. from the amygdala, anteroventral or reuniens nucleus of thalamus cannot be excluded (Witter, 2006).

Measured at long time scale, spike frequency was in the range of 9spike/min and 1spike/min for Type 1 and Type 2 event respectively. Type 1 discharge showed occasional bouts of rhythmic episodes in four patients with 0.3-1Hz recurrence rate. Interictal spike rate computed from long epochs in the human mesial temporal lobe

under in vivo conditions show large variability (Clemens et al., 2003). In general, the reported low average spike recurrence frequencies in the epilepsy literature are closer to our findings rather than to the in vitro works (Cohen et al., 2002; Wozny et al., 2003; Wozny et al., 2005), nonetheless bouts of rhythmic discharges at higher frequencies are not uncommon in vivo.

It has been hypothesized for more than 20 years that the timing of interictal spikes is regulated by the wave following the spike (Lebovitz, 1979). Lebovitz studied the effect of topically applied penicillin in the hippocampus of anaesthetized cats. They found rhythmic spiking with 2-10 sec interspike interval associated with long term decrease of excitability after each interictal spikes. In disinhibited whole brain preparation rhythmic interictal spikes developed with 8.81+/-4.47 sec interspike interval (de Curtis et al., 1999). The after-hiperpolarisation (AHP) occurring after individual spikes where blocked by GABA B receptor antagonists. Recently re-evaluated in disinhibited slice preparation GABA B blockers also inhibited pyramidal cell AHP and disrupted synchronization in the CA3 field of Hc. (Cohen et al., 2006). It is possible that the wave that we detected after the spike component at least partially reflects GABA B receptor dependent AHP-like process in the human brain, and it might be involved in the synchronization and timing of the interictal spikes.

Locally generated synchronous events emerged within ±10ms with high reliability, in a correlated fashion at different locations of the Sub regardless of its type. The spike frequency did not correlate with the level of HS, but significantly more Type 2 discharges were detected in sHS than in mHS patients. Although the number of patients is too small to formulate far reaching conclusions (4 sHS and 2 mHS patients), the reorganized input patterns of the subiculum due to the significant cell loss in the CA1 region might be in relation with this phenomenon. Besides the remarkable degree of intra-subicular synchrony, it was also closely associated with temporal lobe spiking. We have shown that Type 1 discharges reliably preceded temporal lobe spikes with a short but accurate (5.5ms ±1ms) delay. The analysis of the ECoG, CSD, MUA and spectral fingerprints of subicular and temporal lobe events in our study revealed multiple spike generator mechanisms suggesting complex network interplay between medial and lateral temporal lobe during epileptic activity. We have shown that spikes are generated locally and synchronously in the Sub, and that a subset of subicular discharges had close

timing association with temporal lobe spikes. These results support the hypothesis that a subicular focus might also take an active role in the distribution of epileptiform activity to other brain regions (de la Prida et al., 2006).

Opposing polarity spikes were observed in different phases of kindling in rats, dogs (Lopes da Silva et al., 1982; Wadman et al., 1983) and rabbits (Kogure, 1997). In humans, different laminar characteristics of de novo generated or propagated interictal discharges were distinguished in the neocortex (Ulbert et al., 2004) and opposing polarity spikes were shown in the entorhinal cortex (Bragin et al., 2002). The seizure protective or promoting nature of interictal spikes is under debate (de Curtis and Avanzini, 2001), however it seems to be clear, that some of the spikes are indubitably linked to seizures. Recent data bring evidence for the close relationship between interictal discharges and seizure generation, demonstrating that provoked spikes are good indicators of epileptogenic area in the frontal and temporal lobe including hippocampus (Valentin et al., 2005a; Valentin et al., 2005b; Valentin et al., 2002).

In line with this thinking, high frequency oscillations linked to spikes are proven to be epileptogenic in animal models of epilepsy (Bragin et al., 2004) and in humans (Staba et al., 2007; Staba et al., 2004). We have shown that greater amount of high frequency activity was associated with Type 1 spike vs. Type 2, which finding further extends the possibility that different spikes take a differential role in epileptogenesis.

In five of the eleven cases we applied electrical current pulses to the temporo-basal cortex in order to detect evoked potentials (EP) in the Subiculum. In three cases we evoked after-discharge (AD) sequences as well. The spontaneous IISs, EPs, and ADs were compared.

The Sub was able to follow the stimulation applied in a 2-3cm “hot spot” region at the temporo-basal structures in a reliable manner in a wide stimulation strength range starting below 5mA reaching maximum over 15mA. The evoked response onset latency progressively increased and amplitude decreased distancing off this region.

The cortico-hippocampal (Liu and Bilkey, 1997) and cortico-subicular (Behr et al., 1998) projections mainly targets the molecular layer. We were able to detect early – less than 10 ms – activation in the molecular layer of DG and Subiculum. However the earliest – occasionally less than 5ms latency – response was positioned to the somatic layer of the Sub. This early somatic sink was absent in the DG. Mainly the deep

portions of the subicular pyramidal layers were involved. Such an early response imply monosynaptic link to the Sub. The occurrence of this short latency response was stimulus site and strength dependent. One possible explanation for this observation is that there are cortical areas that project into the somatic layer of the Sub, the other is that the myelinated fibers in the deep white matter were stimulated on their way to the Sub. Functional differences between deep and superficial sublayers in the Sub pyramidal layer were reported earlier (Greene and Mason, 1996; Harris et al., 2001). Our findings are in line with these observations.

The evoked ADs consisted of a spike and a wave component similar to the IIS and EPs. The initial spike component of the AD had a biphasic shape however, which activation sequence was only occasionally observed during the IIS or the EP. This biphasic activation started with a somatic sink comparable with the pattern of type 1 IIS, which was followed by a type 2 like somatic source. Secondary afterdischarges related to interictal to ictal transition were observed in vitro preparation and was concluded as reverberation of activity between different subregions (Dzhala and Staley, 2003). The relationship of the different types of IISs to seizure genesis is still unknown but based on our observations it can be hypothesized that in the AD condition those neuronal processes become activated in an organized manner that are active also but relatively independently under interictal state.

We found abundant amount of ripple and fast ripple activities during ADs. Bragin et al. analyzed the CSD patterns of evoked after-discharges in rat. (Bragin et al., 1997) They found also robust HFO activity associated to ADs in response to commissural stimulation in the dentate gyrus, however the Sub was omitted in that study. Our finding further supports the hypothesis that in humans the Sub has an important role in seizure genesis.

To sum up the different ways of activation of the Sub (spontaneous, and the two evoked paradigms) three common features can be found. The most common activation pattern started with pyramidal layer sink with MUA increase. This activity was associated with prominent high frequency ripple activity. The initial activation was followed by longer lasting waves with decreased MUA and loss of high frequency spectral content.

The strength of high frequency ripples increased in the spontaneous, EP, AD condition order. The frequency of ripple changed also during these conditions. The fast ripple

frequencies occurred mainly in evoked conditions intermingled with ripple oscillation. This suggests that the neural networks responsible for fast ripple generation were spontaneously inactive under general anaesthesia but they can be activated by electrical stimuli. The current hypothesis on the epileptogenic nature of the high frequency oscillations, predominantly the fast ripples, was detailed in the introduction. See section "High frequency oscillations". Our results are in line with this observation since the most prominent HFO activity was recorded under seizure-like condition. Before us, Bragin et al recorded ripple and fast ripple activity from the EC of waking humans (Bragin et al., 2002). However they were able to record CSD activity for fast ripples only but failed to record it for ripples. This suggested that the ripples were generated elsewhere in the vicinity of their recording electrode but not in the EC. We were able to record CSD activity for ripple oscillation as well in the Sub that is located very close to the EC. (Figure 1.) Our results suggest that the ripples recorded by Bragin were generated in the Sub. Recently Clemens et al. reported ripples detected by foramen ovale electrodes associated to IIS (Clemens et al., 2007). The foramen ovale electrodes lie between the Sub and the EC that further supports the previous hypothesis.

The presence of fast ripple oscillation in the Sub was reported earlier (Staba et al., 2004). However, in their study the electrode position was verified by MRI imaging that was less accurate compared to our electrode localization technique. Our data provided direct evidence for fast ripple generation in the Sub that observation strengthen the possible epileptogenic role of Sub in temporal lobe epilepsy.

Beside the HFO activity, another common feature of different types of activities in the Sub was the presence of slow waves lasting from 100ms to 500ms. It was always associated with MUA and HFO decrease. This finding indicate that the strong feedback and feed-forward inhibitory system reported in rodents (Finch and Babb, 1980; Menendez de la Prida, 2003) may be present in humans as well.

Limitations

The major limitation of our acute intraoperative study was the unexplored effect of anaesthetics on the rate and morphology of different types of IISs. Chronically implanted laminar multielectrodes would provide comparative data between different states of vigilance and anaesthesia, in addition to revealing more completely the

relationship between spikes and seizures. Detailed evaluation of the spread of subicular activity requires implantation of more than one or two multielectrodes. Recent advances in silicone probe design may allow brain activity to be sampled in three-dimensions. The implantation of recording devices may itself have an unpredictable influence on brain activity. However, the size of our devices is a fraction of the conventionally used depth electrodes, probably inducing less damage, and thus improving the detection of pathological events.

Concerning for example the perisomatic inhibitory input of hippocampal principal cells, controversial results have been found in different rat models of epilepsy (Cossart et al., 2001; Morin et al., 1999) and in human studies (Wittner et al., 2005). These conflicting results require an extensive comparison and correlation of human and animal data to be able to extrapolate model predictions from animals to human.

Another disadvantage was that ten patients enrolled in the study, and all the six patients included the detailed analysis were females. Considering a 50-50% chance this observation is statistically significant (binomial distribution, $p=0.016$). The hypothesis that there are gender differences in the subiculum cannot be excluded.

Risks and benefits

Our investigations were done during the surgery of patients with therapy resistant epilepsy. The choice of the patients for resective surgery and the type of the operation were decisions made entirely for clinical purposes with no reference to the present study. The electrodes were implanted in the hippocampus of the seizure generating side. The surgeon followed the "en bloc" resection technique. The electrophysiological investigation did not required larger opening of the lateral ventricle that was necessary for "en bloc" resection. The electrodes were entered in tissue that had been previously decided to be removed. The additional time spent in anaesthesia was minimized and the patient was informed about the risks of prolonged anaesthesia and the consent agreement was obtained.

The risks caused by the surgery and the corticography consisted of cerebrospinal fluidum leakage, infection, bleeding, arterial occlusion caused by the damage of vessels during surgery and unexpected injury to the white matter that can cause additional neurological symptoms like paresis, hemianopia, acalculia, or different types of agnosia.

Common complications of temporal lobectomy are upper lateral quadrant anopia that may stem from the injury of Meyer loop near the lateral ventricle, memory and learning disorders including verbal or visuo-spatial modalities, and recurrence or even increase of seizures. The special electrodes used in this study are physically much smaller than the strip electrodes used during corticography thus expected to cause smaller risks. All materials in the microelectrode are widely used in standard clinical human diagnostics, and therapy, and are approved by the Food and Drug Administration (FDA) for human applications. The device can be entirely sterilized before usage.

The two main risks of invasive electrophysiological investigations are the haemorrhage caused by the electrode, and the ineffective surgery. The electrodes were implanted under visual control, therefore the risk of penetrating vessels were low. Furthermore if the haemorrhage would occur it could be immediately treated in the operating room. The effectiveness of the surgery was followed for each patient postoperatively. 64 % of our patients were seizure free at one year follow-up that is in the confidence interval of temporal lobectomies.

These considerations resulted that this device and experimental procedure were approved for clinical research as low risk at the OITI, and the MÁV Central Hospital.

The most important potential benefit of our investigations is the detailed insight into the activity of neuronal networks in the verified regions of epileptically transformed human hippocampus that preserved the functional connections to other brain regions. Based on our results the activity recorded in animal models of temporal lobe epilepsy can be compared to the activity obtained from in vitro from human materials, and the physiological relevance can be determined. Based on this knowledge the existing animal models may be validated according to the similarity of their interictal and ictal performance to humans.

In addition, elucidating the role of the Subiculum in the generation and spread of epileptic activity within the temporal lobe may also result in a less invasive and more selective treatment of TLE. Our results may also provide accurate templates for source localization procedures, which may further advance non-invasive diagnostic efforts.

Conclusions

We developed and reported a methodology, with which we have co-registered local EEG activity with the histological layers of subiculum (Sub) in anaesthetized humans in vivo. This method may bridge the gap of knowledge between the neuronal microcircuits of the animal models and human mesial temporal lobe epilepsy (mTLE).

We found that the Sub was active during anaesthesia, reflected in occasionally rhythmic interictal spikes (IIS) with high intrasubicular synchrony. The IISs occurred in close relationship to the spikes on the electrocorticogram above the temporo-basal neocortex (T-B). We characterized two major types of IISs both of which followed the known pattern of spike and wave complexes in mTLE. The more common type 1 originated in the cell layer, and the less frequent type 2 in the molecular layer of the subiculum. The occurrence of type 2 spike showed some relationship to the severity of the cell loss in the hippocampus. The electrically evoked afterdischarges in the Sub had more complex pattern, suggesting local and long range spatiotemporal synchronization of those neural networks that are also active but independently under the interictal state.

We recorded electrical stimulation evoked potentials (EP) with occasionally faster than 5 ms onset latency in the Sub suggesting monosynaptic link between T-B and the Sub. EPs originated in different subregions of the somatic layer of the Sub, the underlying pathways of which is not well known in humans. The potentials fitting the activation of the perforant pathway occurred later with peak latency between 9 and 22ms. Not only the response amplitude and onset latency, but the CSD distribution also varied depending on stimulus site, and strength suggesting multiple functional pathways to the Sub.

We found prominent ripple and fast ripple activity in the subiculum associated with the spontaneous IISs, evoked responses and afterdischarges with increasing strength in this order. Both types of oscillations were generated locally in Sub.

Our results further emphasize the role of the Sub in mTLE and can initiate studies investigating the contribution of different type interictal spikes in epileptogenesis. We demonstrated also that using new methods, detailed, reproducible and scientifically relevant electrophysiological data can be obtained from deep brain structures in humans.

Summary

Abundant data are available on the properties of neuronal microcircuits of mesial temporal lobe epilepsy (mTLE) from examinations of animal models including several studies using laminar multi-electrodes (ME). The activity of neuronal networks underlying human mTLE is however poorly understood. Recently emerging evidences support the idea that the subiculum (Sub) plays an important role in the epileptic human hippocampal formation. Currently high resolution MEs had been developed for local field potential (LFP), current source density (CSD), and multiple unit activity (MUA) measurements in humans.

Our aims were to adapt the existing ME system with which we were able to do LFP, CSD and MUA measurements in the Sub of mTLE patients during the temporal lobectomy in general anaesthesia. Using the adopted system we examined the spontaneous interictal spikes (IIS), electrically evoked potentials (EP) and after-discharges (AD), with special attention to its laminar organization, spectral properties and synchrony.

Based on our results we concluded that the co-registration of local electrical activity and the cell layers visualized by the histological processing of the tissue can be carried out in the Sub. The Sub was active under general anaesthesia and reflected in IISs with high intra-regional synchrony. We distinguished between two major types of IIS that agreed the well known spike and wave morphology. The more common type 1 originated in the somatic, the less frequent type 2 in the dendritic layer of the Sub.

The EPs and ADs in the Sub were generated in the somatic layer also, but reflected more complex spatio-temporal pattern than the IISs.

Occasionally the EPs appeared with less than 5 ms delay after the stimulus in the Sub that suggested mono-synaptic link between the temporo-basal neocortical areas and the Sub. The potentials fitting the activation of the perforant pathways occurred later with peak latency between 9 and 22 ms. Not only the amplitude, onset latency of the EPs depended on the site and strength of the stimulus, but the laminar organization also does. This suggests multiple functional pathways to the Sub.

Prominent ripple and fast ripple activity was attached to the IIS, EP and AD with increasing power in this order. Both type of ripples had intrasubicular generators.

Összefoglaló

A meziális temporális lebeny epilepszia (mTLE) neuron-hálózati tulajdonságairól sok adatot szolgáltattak az állati epilepszia-modellek vizsgálatai, beleértve számos rétegelektródás (ME) mérést is. Ugyanakkor az emberi mTLE – ban szerepet játszó neuron-hálózat aktivitása nagyrészt ismeretlen. A legújabb kutatások arra alapján a szubikulum (Sub) kiemelt szerepet játszik az emberi hippokampális-formáció epilepsziás működésében. Az elmúlt években nagy felbontású ME-kat fejlesztettek ki lokális mezőpotenciál (LFP) áramforrás-sűrűség (CSD) és soksejt-aktivitás (MUA) mérésének kivitelezésére emberben, amivel epilepsziás neuronhálózatok jobb megismerésére vált lehetővé.

Célunk az új ME technika intraszubikuláris adaptálása volt, melynek segítségével temporális lebeny eltávolításra kerülő mTLE betegek Sub-ából tudunk LFP, CSD, és MUA mérést végezni operáció alatt. A rendszerrel az interiktális tüskék (IIS) rétegek-szerinti szerveződését, spektrális tulajdonságát, szinkronitását, és temporo-bazálisan (T-B) alkalmazott egy-, és többszörös elektromos ingerek hatását vizsgáltuk a Sub-ban.

Eredményeink alapján megállapítottuk, hogy a lokális elektromos aktivitás korreláltatható a szövettani feldolgozással vizualizált sejtrétegekkel a Sub-ban. A Sub altatásban is aktív volt és erős régión belüli szinkronitást mutató IIS-okat generált. A Sub-ban 2 fő IIS típust különítettünk el, melyek a szokásos tüske-hullám morfológiának megfeleltek. A gyakoribb 1.-es típus a sejtrétegekben, a ritkább 2.-es tipus a dendritikus rétegben keletkezett.

Az ingerléssel kiváltott utókisülések (AD), és egyszeres kiváltott válaszok (EP) szintén a sejtrétegben keletkeztek, ám komplexebb időbeli lefutást mutattak mint az IIS-ok.

Az egyszeres ingerek alkalmanként 5 ms-on belüli késéssel váltottak ki választ (EP) a Sub-ban, ami felvetette a mono-szinaptikus kapcsolat meglétét a T-B kérgi területek és a Sub között. A potenciálok, amik megfeleltek a perforáns pálya aktivitásának, később, 9-22 ms csúcslatenciával érte el a Sub-ot. Nem csak a EP amplitúdója, és latenciája, de a rétegek szerinti szerveződése in függött az inger helyétől és erősségétől, ami funkcionálisan különböző pályák meglétére utal.

Az IIS-hoz, EP-hoz, AD-hez ripple, és gyors ripple aktivitás társult erősség szerint ebben a sorrendben. Mindkét féle ripple lokálisan a Sub-ban generálódott.

Acknowledgements

I thank to Péter Halász and István Ulbert for their mentorship to the present thesis. I thank István Ulbert for the pleasant and intellectually exciting mood in the laboratory, and Péter Halász for his scientific and personal mentorship and clinical guidance throughout the study. I would like to thank Zsófia Maglóczky for her excellent scientific work, useful comments, and original ideas, to Loránd Erőss for his virtuosity in the operating room, to Lucia Wittner for her comments and help, to Tamás Freund for he had turned my interest toward hippocampus, and to György Karmos that he provided place and time for this work in the MTA-PKI. I thank László Papp and the anaesthetic team in the OITI for their excellent technical assistance. I would like also thank all the co-authors in OPNI †, OITI, MÁV Central Hospital and "Szent István" Hospital for their support to this work. I thank my family for the infinite patience.

Supported by

ETT 135/2006, OTKA T049122, NeuroProbes IP 027017, EPICURE LSH-037315, NS44623, and János Szentágothai Knowledge Centre RET 05/2004.

Reference list

Aggleton JP, Vann SD, Saunders RC. Projections from the hippocampal region to the mammillary bodies in macaque monkeys. Eur J Neurosci 2005; 22: 2519-30.

Alarcon G, Garcia Seoane JJ, Binnie CD, Martin Miguel MC, Juler J, Polkey CE, et al. Origin and propagation of interictal discharges in the acute electrocorticogram. Implications for pathophysiology and surgical treatment of temporal lobe epilepsy. Brain 1997; 120 (Pt 12): 2259-82.

Alger BE, Nicoll RA. Epileptiform burst afterhyperolarization: calcium-dependent potassium potential in hippocampal CA1 pyramidal cells. Science 1980; 210: 1122-4.

Amaral DG. A Golgi study of cell types in the hilar region of the hippocampus in the rat. J Comp Neurol 1978; 182: 851-914.

Amaral DG, Dolorfo C, Alvarez-Royo P. Organization of CA1 projections to the subiculum: a PHA-L analysis in the rat. Hippocampus 1991; 1: 415-435.

Amaral DG, Witter MP. Hippocampal formation. In: Paxinos G, editor. The Rat Nervous System. San Diego: Academic Press, Inc., 1985: 443-494.

Arellano JI, Munoz A, Ballesteros-Yanez I, Sola RG, DeFelipe J. Histopathology and reorganization of chandelier cells in the human epileptic sclerotic hippocampus. Brain 2004; 127: 45-64.

Babb TL. Synaptic reorganizations in human and rat hippocampal epilepsy. Adv Neurol 1999; 79: 763-79.

Babb TL, Carr E, Crandall PH. Analysis of extracellular firing patterns of deep temporal lobe structures in man. Electroencephalogr Clin Neurophysiol 1973; 34: 247-57.

Babb TL, Pretorius JK, Kupfer WR, Crandall PH. Glutamate decarboxylase-immunoreactive neurons are preserved in human epileptic hippocampus. J Neurosci 1989; 9: 2562-74.

Bancaud J, Angelergues R, Bernouilli C, Bonis A, Bordas-Ferrer M, Bresson M, et al. Functional stereotaxic exploration (SEEG) of epilepsy. Electroencephalogr Clin Neurophysiol 1970; 28: 85-6.

Barsi P, Kenez J, Solymosi D, Kulin A, Halasz P, Rasonyi G, et al. Hippocampal malrotation with normal corpus callosum: a new entity? Neuroradiology 2000; 42: 339-45.

Bartesaghi R, Gessi T. Hippocampal output to the subicular cortex: an electrophysiological study. Exp Neurol 1986; 92: 114-33.

Bartolomei F, Wendling F, Bellanger JJ, Regis J, Chauvel P. Neural networks involving the medial temporal structures in temporal lobe epilepsy. Clin Neurophysiol 2001; 112: 1746-60.

Behr J, Gloveli T, Heinemann U. The perforant path projection from the medial entorhinal cortex layer III to the subiculum in the rat combined hippocampal-entorhinal cortex slice. European Journal of Neuroscience 1998; 10: 1011-1018.

Behr J, Heinemann U. Low Mg2+ induced epileptiform activity in the subiculum before and after disconnection from rat hippocampal and entorhinal cortex slices. Neuroscience Letters 1996; 205: 25-28.

Ben-Ari Y, Cossart R. Kainate, a double agent that generates seizures: two decades of progress. Trends Neurosci 2000; 23: 580-7.

Benini R, Avoli M. Rat subicular networks gate hippocampal output activity in an in vitro model of limbic seizures. J Physiol 2005; 566: 885-900.

Berkovic SF, Andermann F, Olivier A, Ethier R, Melanson D, Robitaille Y, et al. Hippocampal sclerosis in temporal lobe epilepsy demonstrated by magnetic resonance imaging. Ann Neurol 1991; 29: 175-82.

Blumcke I, Pauli E, Clusmann H, Schramm J, Becker A, Elger C, et al. A new clinico-pathological classification system for mesial temporal sclerosis. Acta Neuropathol (Berl) 2007; 113: 235-244.

Bragin A, Csicsvari J, Penttonen M, Buzsaki G. Epileptic afterdischarge in the hippocampal-entorhinal system: current source density and unit studies. Neuroscience 1997; 76: 1187-203.

Bragin A, Wilson CL, Almajano J, Mody I, Engel J, Jr. High-frequency oscillations after status epilepticus: epileptogenesis and seizure genesis. Epilepsia 2004; 45: 1017-23.

Bragin A, Wilson CL, Staba RJ, Reddick M, Fried I, Engel J, Jr. Interictal high-frequency oscillations (80-500 Hz) in the human epileptic brain: entorhinal cortex. Ann Neurol 2002; 52: 407-15.

Buhl EH, Otis TS, Mody I. Zinc-induced collapse of augmented inhibition by GABA in a temporal lobe epilepsy model. Science 1996; 271: 369-73.

Buzsaki G. Theta oscillations in the hippocampus. Neuron 2002; 33: 325-40.

Canteras NS, Swanson LW. Projections of the ventral subiculum to the amygdala, septum, and hypothalamus: A PHAL anterograde tract-tracing study in the rat. Journal of Comparative Neurology 1992; 324: 180-194.

Cappaert NL, Wadman WJ, Witter MP. Spatiotemporal analyses of interactions between entorhinal and CA1 projections to the subiculum in rat brain slices. Hippocampus 2007.

Cavazos JE, Jones SM, Cross DJ. Sprouting and synaptic reorganization in the subiculum and CA1 region of the hippocampus in acute and chronic models of partial-onset epilepsy. Neuroscience 2004; 126: 677-688.

Chatrian G, Bergamini L, Dondey M, Klass E, Lennox-Buchtal M, Petersen I. A glossary of terms most commonly used by clinical electroencephalographers. Electroencephalogr Clin Neurophysiol 1974; 37: 538–548.

Clemens Z, Janszky J, Szucs A, Bekesy M, Clemens B, Halasz P. Interictal epileptic spiking during sleep and wakefulness in mesial temporal lobe epilepsy: a comparative study of scalp and foramen ovale electrodes. Epilepsia 2003; 44: 186-92.

Clemens Z, Molle M, Eross L, Barsi P, Halasz P, Born J. Temporal coupling of parahippocampal ripples, sleep spindles and slow oscillations in humans. Brain 2007; 130: 2868-78.

Cobb SR, Buhl EH, Halasy K, Paulsen O, Somogyi P. Synchronization of neuronal activity in hippocampus by individual GABAergic interneurons. Nature 1995; 378: 75-8.

Cohen I, Huberfeld G, Miles R. Emergence of disinhibition-induced synchrony in the CA3 region of the guinea pig hippocampus in vitro. J Physiol 2006; 570: 583-94.

Cohen I, Navarro V, Clemenceau S, Baulac M, Miles R. On the origin of interictal activity in human temporal lobe epilepsy in vitro. Science 2002; 298: 1418-21.

Colino A, Fernandez de Molina A. Inhibitory response in entorhinal and subicular cortices after electrical stimulation of the lateral and basolateral amygdala of the rat. Brain Res 1986; 378: 416-9.

Cossart R, Dinocourt C, Hirsch JC, Merchan-Perez A, De Felipe J, Ben-Ari Y, et al. Dendritic but not somatic GABAergic inhibition is decreased in experimental epilepsy. Nat Neurosci 2001; 4: 52-62.

Cross DJ, Cavazos JE. Synaptic reorganization in subiculum and CA3 after early-life status epilepticus in the kainic acid rat model. Epilepsy Research 2007; 73: 156-165.

Dawodu S, Thom M. Quantitative neuropathology of the entorhinal cortex region in patients with hippocampal sclerosis and temporal lobe epilepsy. Epilepsia 2005; 46: 23-30.

de Curtis M, Avanzini G. Interictal spikes in focal epileptogenesis. Prog Neurobiol 2001; 63: 541-67.

de Curtis M, Radici C, Forti M. Cellular mechanisms underlying spontaneous interictal spikes in an acute model of focal cortical epileptogenesis. Neuroscience 1999; 88: 107-17.

de Guzman P, Inaba Y, Biagini G, Baldelli E, Mollinari C, Merlo D, et al. Subiculum network excitability is increased in a rodent model of temporal lobe epilepsy. Hippocampus 2006; 16: 843-860.

de la Prida LM, Totterdell S, Gigg J, Miles R. The subiculum comes of age. Hippocampus 2006; 16: 916-23.

de Lanerolle NC, Kim JH, Williamson A, Spencer SS, Zaveri HP, Eid T, et al. A retrospective analysis of hippocampal pathology in human temporal lobe epilepsy: evidence for distinctive patient subcategories. Epilepsia 2003; 44: 677-87.

Delorme A, Makeig S. EEGLAB: an open source toolbox for analysis of single-trial EEG dynamics including independent component analysis. J Neurosci Methods 2004; 134: 9-21.

Dudek FE, Yasumura T, Rash JE. 'Non-synaptic' mechanisms in seizures and epileptogenesis. Cell Biol Int 1998; 22: 793-805.

Duvernoy HM. The human hippocampus. Berlin: Springer-Verlag, 1998.

Dzhala VI, Staley KJ. Transition from interictal to ictal activity in limbic networks in vitro. J Neurosci 2003; 23: 7873-80.

Engel J, Jr. Mesial temporal lobe epilepsy: what have we learned? Neuroscientist 2001a; 7: 340-52.

Engel J, Jr. A proposed diagnostic scheme for people with epileptic seizures and with epilepsy: report of the ILAE Task Force on Classification and Terminology. Epilepsia 2001b; 42: 796-803.

Engel JJ, Van Ness PC, Rasmussen TB, Ojemann LM. Outcome with respect to epileptic seizures. In: Engel Jr. J, editor. Surgical treatment of the epilepsies. New York: Raven Press, 1993: 609-21.

Engel Jr. J, Williamson P, Wieser HG. Mesial Temporal Lobe Epilepsy. In: Engel JJ and T.A. P, editors. Epilepsy: A Comprehensive Textbook. Vol 13. Philadelphia: Lipincott-Raven, 1997: 2417-2426.

Falconer MA, Meyer A, Hill D, Mitchell W, Pond DA. Treatment of temporal-lobe epilepsy by temporal lobectomy; a survey of findings and results. Lancet 1955; 268: 827-35.

Fernandez de Sevilla D, Garduno J, Galvan E, Buno W. Calcium-activated afterhyperpolarizations regulate synchronization and timing of epileptiform bursts in hippocampal CA3 pyramidal neurons. J Neurophysiol 2006; 96: 3028-41.

Finch DM, Babb TL. Inhibition in subicular and entorhinal principal neurons in response to electrical stimulation of the fornix and hippocampus. Brain Res 1980; 196: 89-98.

Finch DM, Tan AM, Isokawa-Akesson M. Feedforward inhibition of the rat entorhinal cortex and subicular complex. J Neurosci 1988; 8: 2213-26.

Fisher PD, Sperber EF, Moshe SL. Hippocampal sclerosis revisited. Brain Dev 1998; 20: 563-73.

Freeman JA, Nicholson C. Experimental optimization of current source-density technique for anuran cerebellum. J Neurophysiol 1975; 38: 369-82.

Freund TF, Buzsaki G. Interneurons of the hippocampus. Hippocampus 1996; 6: 347-470.

Gabrieli JD, Brewer JB, Desmond JE, Glover GH. Separate neural bases of two fundamental memory processes in the human medial temporal lobe. Science 1997; 276: 264-6.

Gaitatzis A, Johnson AL, Chadwick DW, Shorvon SD, Sander JW. Life expectancy in people with newly diagnosed epilepsy. Brain 2004; 127: 2427-32.

Geisler C, Robbe D, Zugaro M, Sirota A, Buzsaki G. Hippocampal place cell assemblies are speed-controlled oscillators. Proc Natl Acad Sci U S A 2007; 104: 8149-54.

Gigg J, Finch DM, O'Mara SM. Responses of rat subicular neurons to convergent stimulation of lateral entorhinal cortex and CA1 in vivo. Brain Res 2000; 884: 35-50.

Gloor P. Contributions of electroencephalography and electrocorticography to the neurosurgical treatment of the epilepsies. Adv Neurol 1975; 8: 59-105.

Greene JR, Mason A. Neuronal diversity in the subiculum: correlations with the effects of somatostatin on intrinsic properties and on GABA-mediated IPSPs in vitro. J Neurophysiol 1996; 76: 1657-66.

Greene JR, Totterdell S. Morphology and distribution of electrophysiologically defined classes of pyramidal and nonpyramidal neurons in rat ventral subiculum in vitro. J Comp Neurol 1997; 380: 395-408.

Halasz P, Vajda J, Czirjak S. [Surgical treatment of epilepsy]. Ideggyogy Sz 2004; 57: 189-205.

Halgren E, Wang C, Schomer DL, Knake S, Marinkovic K, Wu J, et al. Processing stages underlying word recognition in the anteroventral temporal lobe. Neuroimage 2006; 30: 1401-13.

Hampson RE, Deadwyler SA. Temporal firing characteristics and the strategic role of subicular neurons in short-term memory. Hippocampus 2003; 13: 529-41.

Harris E, Stewart M. Intrinsic connectivity of the rat subiculum: II. Properties of synchronous spontaneous activity and a demonstration of multiple generator regions. Journal of Comparative Neurology 2001a; 435: 506-518.

Harris E, Stewart M. Propagation of synchronous epileptiform events from subiculum backward into area CA1 of rat brain slices. Brain Research 2001b; 895: 41-49.

Harris E, Witter MP, Weinstein G, Stewart M. Intrinsic connectivity of the rat subiculum: I. Dendritic morphology and patterns of axonal arborization by pyramidal neurons. J Comp Neurol 2001; 435: 490-505.
Hauser WA. Incidence and prevalence. In: Engel JJ and T.A. P, editors. Epilepsy: A Comprehensive Textbook. Vol 13. Philadelphia: Lipincott-Raven, 1997: 47-58.
Hauser WA, Annegers JF, Kurland LT. Incidence of epilepsy and unprovoked seizures in Rochester, Minnesota: 1935-1984. Epilepsia 1993; 34: 453-68.
Heit G, Ulbert II, Halgren E, Karmos G, Shuer L. Current source density analysis of synaptic generators of human interictal spike. Stereotact Funct Neurosurg 1999; 73: 116.
Helmstaedter C. Neuropsychological aspects of epilepsy surgery. Epilepsy Behav 2004; 5 Suppl 1: S45-55.
Hermann BP, Wyler AR, Somes G, Berry AD, 3rd, Dohan FC, Jr. Pathological status of the mesial temporal lobe predicts memory outcome from left anterior temporal lobectomy. Neurosurgery 1992; 31: 652-6; discussion 656-7.
Huberfeld G, Wittner L, Clemenceau S, Baulac M, Kaila K, Miles R, et al. Perturbed chloride homeostasis and GABAergic signaling in human temporal lobe epilepsy. J Neurosci 2007; 27: 9866-73.
Insausti R, Amaral DG. Hippocampal formation. In: G. P, editor. The Human Nervous System. San Diego: Academic Press, Inc., 1990: 711-755.
Ishizuka N. Laminar organization of the pyramidal cell layer of the subiculum in the rat. Journal of Comparative Neurology 2001; 435: 89-110.
Isokawa-Akesson M, Wilson CL, Babb TL. Inhibition in synchronously firing human hippocampal neurons. Epilepsy Res 1989; 3: 236-47.
Jackson H. On the anatomical, physiological and pathological investigation of epilepsies. West Riding Lunatic Assylum Medical Reports 1873; 3: 315-339.
Janszky J, Janszky I, Schulz R, Hoppe M, Behne F, Pannek HW, et al. Temporal lobe epilepsy with hippocampal sclerosis: predictors for long-term surgical outcome. Brain 2005; 128: 395-404.
Janszky J, Ollech I, Jokeit H, Kontopoulou K, Mertens M, Pohlmann-Eden B, et al. Epileptic activity influences the lateralization of mesiotemporal fMRI activity. Neurology 2004; 63: 1813-7.
Jasper H. EEG and cortical electrograms in patients with temporal lobe seizures. AMA Arch Neurol Psychiatry 1951; 65: 272.
Kelemen A, Rasonyi G, Szucs A, Fabo D, Halasz P. [Predictive factors of temporal lobe surgery]. Ideggyogy Sz 2006; 59: 353-9.
Khalilov I, Le Van Quyen M, Gozlan H, Ben-Ari Y. Epileptogenic actions of GABA and fast oscillations in the developing hippocampus. Neuron 2005; 48: 787-96.
Kloosterman F, van Haeften T, Lopes da Silva FH. Two reentrant pathways in the hippocampal-entorhinal system. Hippocampus 2004; 14: 1026-39.
Knopp A, Kivi A, Wozny C, Heinemann U, Behr J. Cellular and network properties of the subiculum in the pilocarpine model of temporal lobe epilepsy. J Comp Neurol 2005; 483: 476-88.
Kogure S. Properties of interictal discharges induced by hippocampal kindling. Epilepsy Res 1997; 27: 139-48.
Kosel KC, Van Hoesen GW, Rosene DL. A direct projection from the perirhinal cortex (area 35) to the subiculum in the rat. Brain Research 1983; 269: 347-351.

Kwan P, Brodie MJ. Early identification of refractory epilepsy. N Engl J Med 2000; 342: 314-9.

Lange HH, Lieb JP, Engel J, Jr., Crandall PH. Temporo-spatial patterns of pre-ictal spike activity in human temporal lobe epilepsy. Electroencephalogr Clin Neurophysiol 1983; 56: 543-55.

Le Van Quyen M, Khalilov I, Ben-Ari Y. The dark side of high-frequency oscillations in the developing brain. Trends Neurosci 2006; 29: 419-27.

Lebovitz RM. Autorhythmicity of spontaneous interictal spike discharge at hippocampal penicillin foci. Brain Res 1979; 172: 35-55.

Lehericy S, Semah F, Hasboun D, Dormont D, Clemenceau S, Granat O, et al. Temporal lobe epilepsy with varying severity: MRI study of 222 patients. Neuroradiology 1997; 39: 788-96.

Lehmann TN, Gabriel S, Eilers A, Njunting M, Kovacs R, Schulze K, et al. Fluorescent tracer in pilocarpine-treated rats shows widespread aberrant hippocampal neuronal connectivity. Eur J Neurosci 2001; 14: 83-95.

Lehmann TN, Gabriel S, Kovacs R, Eilers A, Kivi A, Schulze K, et al. Alterations of neuronal connectivity in area CA1 of hippocampal slices from temporal lobe epilepsy patients and from pilocarpine-treated epileptic rats. Epilepsia 2000; 41 Suppl 6: S190-4.

Lerche H, Jurkat-Rott K, Lehmann-Horn F. Ion channels and epilepsy. Am J Med Genet 2001; 106: 146-59.

Lhatoo SD, Johnson AL, Goodridge DM, MacDonald BK, Sander JW, Shorvon SD. Mortality in epilepsy in the first 11 to 14 years after diagnosis: multivariate analysis of a long-term, prospective, population-based cohort. Ann Neurol 2001; 49: 336-44.

Lim C, Mufson EJ, Kordower JH, Blume HW, Madsen JR, Saper CB. Connections of the hippocampal formation in humans: II. The endfolial fiber pathway. J Comp Neurol 1997; 385: 352-71.

Liu P, Bilkey DK. Current source density analysis of the potential evoked in hippocampus by perirhinal cortex stimulation. Hippocampus 1997; 7: 389-96.

Lopes da Silva FH, Wadman WJ, Leung LS, Van Hulten K. Common aspects of the development of a kindling epileptogenic focus in the prepyriform cortex of the dog and in the hippocampus of the rat: spontaneous interictal transients with changing polarities. Electroencephalogr Clin Neurophysiol Suppl 1982; 36: 274-87.

Lopes da Silva FH, Witter MP, Boeijinga PH, Lohman AH. Anatomic organization and physiology of the limbic cortex. Physiol Rev 1990; 70: 453-511.

Lorente de Nó R. Studies on the structure of the cerebral cortex - II. Continuation of the study of the ammonic system. J.Psychol.Neurol 1934; 46: 113-177.

Lux HD, Heinemann U. Ionic changes during experimentally induced seizure activity. Electroencephalogr Clin Neurophysiol Suppl 1978: 289-97.

Magloczky Z, Freund TF. Impaired and repaired inhibitory circuits in the epileptic human hippocampus. Trends Neurosci 2005; 28: 334-40.

Magloczky Z, Halasz P, Vajda J, Czirjak S, Freund TF. Loss of Calbindin-D28K immunoreactivity from dentate granule cells in human temporal lobe epilepsy. Neuroscience 1997; 76: 377-85.

Magloczky Z, Wittner L, Borhegyi Z, Halasz P, Vajda J, Czirjak S, et al. Changes in the distribution and connectivity of interneurons in the epileptic human dentate gyrus. Neuroscience 2000; 96: 7-25.

Marco P, DeFelipe J. Altered synaptic circuitry in the human temporal neocortex removed from epileptic patients. Exp Brain Res 1997; 114: 1-10.

Margerison JH, Corsellis JA. Epilepsy and the temporal lobes. A clinical, electroencephalographic and neuropathological study of the brain in epilepsy, with particular reference to the temporal lobes. Brain 1966; 89: 499-530.

McIntosh AM, Wilson SJ, Berkovic SF. Seizure outcome after temporal lobectomy: current research practice and findings. Epilepsia 2001; 42: 1288-307.

Meencke HJ, Veith G. Hippocampal sclerosis in epilepsy. In: Luders HO, editor. Epilepsy surgery. New York: Raven Press Ltd, 1991: 705-715.

Mehta AD, Ulbert I, Schroeder CE. Intermodal selective attention in monkeys. II: physiological mechanisms of modulation. Cereb Cortex 2000; 10: 359-70.

Menendez de la Prida L. Control of bursting by local inhibition in the rat subiculum in vitro. Journal of Physiology 2003; 549: 219-230.

Menendez de la Prida L, Gal B. Synaptic contributions to focal and widespread spatiotemporal dynamics in the isolated rat subiculum in vitro. J Neurosci 2004; 24: 5525-36.

Morin F, Beaulieu C, Lacaille JC. Alterations of perisomatic GABA synapses on hippocampal CA1 inhibitory interneurons and pyramidal cells in the kainate model of epilepsy. Neuroscience 1999; 93: 457-67.

Naber PA, Witter MP. Subicular efferents are organized mostly as parallel projections: a double-labeling, retrograde-tracing study in the rat. J Comp Neurol 1998; 393: 284-97.

Nicholson C, Freeman JA. Theory of current source-density analysis and determination of conductivity tensor for anuran cerebellum. J Neurophysiol 1975; 38: 356-68.

Nusser Z, Hajos N, Somogyi P, Mody I. Increased number of synaptic GABA(A) receptors underlies potentiation at hippocampal inhibitory synapses. Nature 1998; 395: 172-7.

Ojemann G, Sutherling W, Lesser R, Dinner D, Jayakar P, Saint Hilaire J-M. Cortical stimulations. In: Engel Jr. J, editor. Surgical Treatment of the Epilepsies. New York: Raven Press, 1992: 399-414.

O'Mara S. Controlling hippocampal output: The central role of subiculum in hippocampal information processing. Behavioural Brain Research 2006; 174: 304-312.

O'Mara SM, Commins S, Anderson M, Gigg J. The subiculum: A review of form, physiology and function. Progress in Neurobiology 2001; 64: 129-155.

Palma E, Amici M, Sobrero F, Spinelli G, Di Angelantonio S, Ragozzino D, et al. Anomalous levels of Cl- transporters in the hippocampal subiculum from temporal lobe epilepsy patients make GABA excitatory. Proc Natl Acad Sci U S A 2006; 103: 8465-8.

Penfield W, Jasper H. Epilepsy and the Functional Anatomy of the Brain. Boston, Mass: Little Brown & Co, 1954.

Pfander M, Arnold S, Henkel A, Weil S, Werhahn KJ, Eisensehr I, et al. Clinical features and EEG findings differentiating mesial from neocortical temporal lobe epilepsy. Epileptic Disord 2002; 4: 189-95.

Ramón y Cajal S. Histologie du systeme nerveux de l'homme et des vertébrés. Paris: Maloine, 1909-1911.
Ramón y Cajal S. The structure of Ammon's horn: Springfield, 1968.
Rampp S, Stefan H. Fast activity as a surrogate marker of epileptic network function? Clin Neurophysiol 2006; 117: 2111-7.
Rappelsberger P, Pockberger H, Petsche H. Current source density analysis: methods and application to simultaneously recorded field potentials of the rabbit's visual cortex. Pflugers Arch 1981; 389: 159-70.
Reynolds E. Todd, Hughlings Jackson, and the electrical basis of epilepsy. Lancet 2001; 358: 575-7.
Rivera C, Voipio J, Payne JA, Ruusuvuori E, Lahtinen H, Lamsa K, et al. The K+/Cl- co-transporter KCC2 renders GABA hyperpolarizing during neuronal maturation. Nature 1999; 397: 251-5.
Rogawski MA, Loscher W. The neurobiology of antiepileptic drugs. Nat Rev Neurosci 2004; 5: 553-64.
Roger J, Dreifuss FE, Martinez-Lage M, Munari C, Porter RJ, Seino M, et al. Proposal for revised classification of epilepsies and epileptic syndromes. Epilepsia 1989; 30: 389-399.
Rose DF, Sato S, Smith PD, Porter RJ, Theodore WH, Friauf W, et al. Localization of magnetic interictal discharges in temporal lobe epilepsy. Ann Neurol 1987; 22: 348-54.
Rosene DL, Van Hoesen GW. Hippocampal efferents reach widespread areas of cerebral cortex and amygdala in the rhesus monkey. Science 1977; 198: 315-7.
Salin P, Tseng GF, Hoffman S, Parada I, Prince DA. Axonal sprouting in layer V pyramidal neurons of chronically injured cerebral cortex. J Neurosci 1995; 15: 8234-45.
Samar VJ, Bopardikar A, Rao R, Swartz K. Wavelet analysis of neuroelectric waveforms: a conceptual tutorial. Brain Lang 1999; 66: 7-60.
Sammaritano M, Gigli GL, Gotman J. Interictal spiking during wakefulness and sleep and the localization of foci in temporal lobe epilepsy. Neurology 1991; 41: 290-7.
Scoville WB, Milner B. Loss of recent memory after bilateral hippocampal lesions. J Neurol Neurosurg Psychiatry 1957; 20: 11-21.
Semah F, Picot MC, Adam C, Broglin D, Arzimanoglou A, Bazin B, et al. Is the underlying cause of epilepsy a major prognostic factor for recurrence? Neurology 1998; 51: 1256-62.
Seress L. Interspecies comparison of the hippocampal formation shows increased emphasis on the regio superior in the Ammon's horn of the human brain. J Hirnforsch 1988; 29: 335-40.
Sloviter RS. Permanently altered hippocampal structure, excitability, and inhibition after experimental status epilepticus in the rat: the "dormant basket cell" hypothesis and its possible relevance to temporal lobe epilepsy. Hippocampus 1991; 1: 41-66.
Sommer W. Erkrankung des Ammonshornes als Aetiologisches Moment der Epilepsie. Arch. Psychiat. NervKrankh 1880; 10: 631-675.
Spencer DD, Spencer SS. Surgery for epilepsy. Neurol Clin 1985; 3: 313-30.
Sperling MR, Schnur JK. Temporal lobectomy. Arch Neurol 2002; 59: 482-4.

Staba RJ, Frighetto L, Behnke EJ, Mathern GW, Fields T, Bragin A, et al. Increased Fast ripple to ripple Ratios Correlate with Reduced Hippocampal Volumes and Neuron Loss in Temporal Lobe Epilepsy Patients. Epilepsia 2007.

Staba RJ, Wilson CL, Bragin A, Fried I, Engel J, Jr. Quantitative analysis of high-frequency oscillations (80-500 Hz) recorded in human epileptic hippocampus and entorhinal cortex. J Neurophysiol 2002; 88: 1743-52.

Staba RJ, Wilson CL, Bragin A, Jhung D, Fried I, Engel J, Jr. High-frequency oscillations recorded in human medial temporal lobe during sleep. Ann Neurol 2004; 56: 108-15.

Stafstrom CE. The role of the subiculum in epilepsy and epileptogenesis. Epilepsy Curr 2005; 5: 121-9.

Swanson LW, Cowan WM. An autoradiographic study of the organization of the efferent connections of the hippocampal formation in the rat. J Comp Neurol 1977; 172: 49-84.

Swartz BE. The advantages of digital over analog recording techniques. Electroencephalogr Clin Neurophysiol 1998; 106: 113-7.

Tamamaki N, Abe K, Nojyo Y. Columnar organization in the subiculum formed by axon branches originating from single CA1 pyramidal neurons in the rat hippocampus. Brain Research 1987; 412: 156-160.

Tamamaki N, Nojyo Y. Projection of the entorhinal layer II neurons in the rat as revealed by intracellular pressure-injection of neurobiotin. Hippocampus 1993; 3: 471-80.

Taube JS. Electrophysiological properties of neurons in the rat subiculum in vitro. Experimental Brain Research 1993; 96: 304-318.

Toth K, Wittner L, Urban Z, Doyle WK, Buzsaki G, Shigemoto R, et al. Morphology and synaptic input of substance P receptor-immunoreactive interneurons in control and epileptic human hippocampus. Neuroscience 2007; 144: 495-508.

Townsend G, Peloquin P, Kloosterman F, Hetke JF, Leung LS. Recording and marking with silicon multichannel electrodes. Brain Res Brain Res Protoc 2002; 9: 122-9.

Ulbert I. Investigation of the evoked and spontaneous intracortical electrical activity with multielectrodes in humans. Doctoral School. Budapest: Semmelweis University, 2002: 100.

Ulbert I, Halgren E, Heit G, Karmos G. Multiple microelectrode-recording system for human intracortical applications. J Neurosci Methods 2001a; 106: 69-79.

Ulbert I, Heit G, Madsen J, Karmos G, Halgren E. Laminar analysis of human neocortical interictal spike generation and propagation: current source density and multiunit analysis in vivo. Epilepsia 2004; 45 Suppl 4: 48-56.

Ulbert I, Karmos G, Heit G, Halgren E. Early discrimination of coherent versus incoherent motion by multiunit and synaptic activity in human putative MT+. Hum Brain Mapp 2001b; 13: 226-38.

Urrestarazu E, Jirsch JD, LeVan P, Hall J, Avoli M, Dubeau F, et al. High-frequency intracerebral EEG activity (100-500 Hz) following interictal spikes. Epilepsia 2006; 47: 1465-76.

Uva L, de Curtis M. Propagation pattern of entorhinal cortex subfields to the dentate gyrus in the guinea-pig: an electrophysiological study. Neuroscience 2003; 122: 843-51.

Valentin A, Alarcon G, Garcia-Seoane JJ, Lacruz ME, Nayak SD, Honavar M, et al. Single-pulse electrical stimulation identifies epileptogenic frontal cortex in the human brain. Neurology 2005a; 65: 426-35.

Valentin A, Alarcon G, Honavar M, Garcia Seoane JJ, Selway RP, Polkey CE, et al. Single pulse electrical stimulation for identification of structural abnormalities and prediction of seizure outcome after epilepsy surgery: a prospective study. Lancet Neurol 2005b; 4: 718-26.

Valentin A, Anderson M, Alarcon G, Seoane JJ, Selway R, Binnie CD, et al. Responses to single pulse electrical stimulation identify epileptogenesis in the human brain in vivo. Brain 2002; 125: 1709-18.

Van Groen T, Van Haren FJ, Witter MP, Groenewegen HJ. The organization of the reciprocal connections between the subiculum and the entorhinal cortex in the cat: I. A neuroanatomical tracing study. Journal of Comparative Neurology 1986; 250: 485-497.

Van Hoesen GW, Rosene DL, Mesulam MM. Subicular input from temporal cortex in the rhesus monkey. Science 1979; 205: 608-10.

Van Roost D, Solymosi L, Schramm J, van Oosterwyck B, Elger CE. Depth electrode implantation in the length axis of the hippocampus for the presurgical evaluation of medial temporal lobe epilepsy: a computed tomography-based stereotactic insertion technique and its accuracy. Neurosurgery 1998; 43: 819-26; discussion 826-7.

Vanhatalo S, Voipio J, Kaila K. Full-band EEG (FbEEG): an emerging standard in electroencephalography. Clin Neurophysiol 2005; 116: 1-8.

Vida I, Czopf J, Czeh G. A current-source density analysis of the long-term potentiation in the hippocampus. Brain Res 1995; 671: 1-11.

Vreugdenhil M, Hoogland G, Van Veelen CWM, Wadman WJ. Persistent sodium current in subicular neurons isolated from patients with temporal lobe epilepsy. European Journal of Neuroscience 2004; 19: 2769-2778.

Wadman WJ, Da Silva FH, Leung LW. Two types of interictal transients of reversed polarity in rat hippocampus during kindling. Electroencephalogr Clin Neurophysiol 1983; 55: 314-9.

Wallace RH, Wang DW, Singh R, Scheffer IE, George AL, Jr., Phillips HA, et al. Febrile seizures and generalized epilepsy associated with a mutation in the Na+-channel beta1 subunit gene SCN1B. Nat Genet 1998; 19: 366-70.

Wang C, Ulbert I, Schomer DL, Marinkovic K, Halgren E. Responses of human anterior cingulate cortex microdomains to error detection, conflict monitoring, stimulus-response mapping, familiarity, and orienting. J Neurosci 2005; 25: 604-13.

Ward AA, Jr., Schmidt RP. Some properties of single epileptic neurons. Arch Neurol 1961; 5: 308-13.

Wellmer J, Su H, Beck H, Yaari Y. Long-lasting modification of intrinsic discharge properties in subicular neurons following status epilepticus. Eur J Neurosci 2002; 16: 259-66.

Wiebe S, Blume WT, Girvin JP, Eliasziw M. A randomized, controlled trial of surgery for temporal-lobe epilepsy. N Engl J Med 2001; 345: 311-8.

Wieser HG. Temporal lobe epilepsy, sleep and arousal: stereo-EEG findings. Epilepsy Res Suppl 1991; 2: 97-119.

Wieser HG. ILAE Commission Report. Mesial temporal lobe epilepsy with hippocampal sclerosis. Epilepsia 2004; 45: 695-714.

Wieser HG, Elger CE, Stodieck SR. The 'foramen ovale electrode': a new recording method for the preoperative evaluation of patients suffering from mesio-basal temporal lobe epilepsy. Electroencephalogr Clin Neurophysiol 1985; 61: 314-22.
Wieser HG, Ortega M, Friedman A, Yonekawa Y. Long-term seizure outcomes following amygdalohippocampectomy. J Neurosurg 2003; 98: 751-63.
Witter MP. Connections of the subiculum of the rat: Topography in relation to columnar and laminar organization. Behavioural Brain Research 2006; 174: 251-264.
Witter MP, Groenewegen HJ. The subiculum: Cytoarchitectonically a simple structure, but hodologically complex. Progress in Brain Research 1990; 83: 47-58.
Wittner L, Eross L, Czirjak S, Halasz P, Freund TF, Magloczky Z. Surviving CA1 pyramidal cells receive intact perisomatic inhibitory input in the human epileptic hippocampus. Brain 2005; 128: 138-52.
Wittner L, Eross L, Szabo Z, Toth S, Czirjak S, Halasz P, et al. Synaptic reorganization of calbindin-positive neurons in the human hippocampal CA1 region in temporal lobe epilepsy. Neuroscience 2002; 115: 961-78.
Wittner L, Magloczky Z, Borhegyi Z, Halasz P, Toth S, Eross L, et al. Preservation of perisomatic inhibitory input of granule cells in the epileptic human dentate gyrus. Neuroscience 2001; 108: 587-600.
Worrell GA, Parish L, Cranstoun SD, Jonas R, Baltuch G, Litt B. High-frequency oscillations and seizure generation in neocortical epilepsy. Brain 2004; 127: 1496-506.
Wozny C, Kivi A, Lehmann TN, Dehnicke C, Heinemann U, Behr J. Comment on "On the origin of interictal activity in human temporal lobe epilepsy in vitro". Science 2003; 301: 463; author reply 463.
Wozny C, Knopp A, Lehmann T-N, Heinemann U, Behr J. The subiculum: A potential site of ictogenesis in human temporal lobe epilepsy. Epilepsia 2005; 46: 17-21.
Wu K, Leung LS. Enhanced but fragile inhibition in the dentate gyrus in vivo in the kainic acid model of temporal lobe epilepsy: a study using current source density analysis. Neuroscience 2001; 104: 379-96.
Wu K, Leung LS. Increased dendritic excitability in hippocampal ca1 in vivo in the kainic acid model of temporal lobe epilepsy: a study using current source density analysis. Neuroscience 2003; 116: 599-616.
Yasargil MG, Wieser HG, Valavanis A, von Ammon K, Roth P. Surgery and results of selective amygdala-hippocampectomy in one hundred patients with nonlesional limbic epilepsy. Neurosurg Clin N Am 1993; 4: 243-61.
Ylinen A, Bragin A, Nadasdy Z, Jando G, Szabo I, Sik A, et al. Sharp wave-associated high-frequency oscillation (200 Hz) in the intact hippocampus: network and intracellular mechanisms. J Neurosci 1995; 15: 30-46.
Zhu L, Lovinger D, Delpire E. Cortical neurons lacking KCC2 expression show impaired regulation of intracellular chloride. J Neurophysiol 2005; 93: 1557-68.
Zilles K, Qu MS, Kohling R, Speckmann EJ. Ionotropic glutamate and GABA receptors in human epileptic neocortical tissue: quantitative in vitro receptor autoradiography. Neuroscience 1999; 94: 1051-61.
Zola-Morgan S, Squire LR, Amaral DG. Human amnesia and the medial temporal region: enduring memory impairment following a bilateral lesion limited to field CA1 of the hippocampus. J Neurosci 1986; 6: 2950-67.

Author's Publication List

Connected with the present thesis

Fabó D., Maglóczky Zs., Wittner L., Pék Á., Erőss L., Czirják S., Vajda J., Sólyom A., Rásonyi Gy., Szűcs A., Kelemen A., Juhos V., Grand L., Dombovári B., Halász P., Freund TF., Halgren E., Karmos Gy. and Ulbert I. Properties of in vivo interictal spike generation in the human subiculum. Brain 2008; 131(Pt 2):485-99.

Ulbert, I., Magloczky, Z., Eross, L., Czirjak, S., Vajda, J., Bognar, L., Toth, S., Szabo, Z., Halasz, P., Fabo, D., Halgren, E., Freund, T. F., Karmos, G. In vivo laminar electrophysiology co-registered with histology in the hippocampus of patients with temporal lobe epilepsy. Exp Neurol 2004; 187: 310-8.

Kelemen A., Rasonyi G., Szucs A., Fabo D., Halasz P. A temporalis epilepszia műtétek kimenetelét előre jelző tényezők vizsgálata. Ideggyogy Sz 2006; 59: 353-9.

Not connected with the present thesis

Clemens Z., Fabo D., Halasz P. Twenty-four hours retention of visuospatial memory correlates with the number of parietal sleep spindles. Neurosci Lett 2006; 403: 52-6.

Clemens Z., Fabo D., Halasz P. Overnight verbal memory retention correlates with the number of sleep spindles. Neuroscience 2005; 132: 529-35.

Borhegyi Z., Varga V., Szilagyi N., Fabo D., Freund TF. Phase segregation of medial septal GABAergic neurons during hippocampal theta activity. J Neurosci 2004; 24: 8470-9.